
Quasiclassical methods for spin-charge coupled dynamics in low-dimensional systems

Cosimo Gorini

Lehrstuhl für Theoretische Physik II
Universität Augsburg



Augsburg, April 2009

Supervisors

Priv.-Doz. Dr. Peter Schwab
Institut für Physik
Universität Augsburg

Prof. Roberto Raimondi
Dipartimento di Fisica
Università degli Studi di Roma Tre

Prof. Dr. Ulrich Eckern
Institut für Physik
Universität Augsburg

Referees: Prof. Dr. Ulrich Eckern
Prof. Roberto Raimondi

Oral examination: 12/6/2009

*Mi scusi, dei tre telefoni qual è quello con il tarapiotapioco che avverto la
supercazzola? ... Dei tre ...*

Conte Mascetti

Mario Monicelli, *Amici Miei*, 1975

*Gib Acht auf dich, wenn du durch Deutschland kommst,
die Wahrheit unter dem Rock.*

Galileo Galilei

Bertolt Brecht, *Leben des Galilei*, 1943

God might have mercy, he won't!

Colonel Trautmann on John J. Rambo

Rambo III, 1988

Contents

1	Introduction	7
1.1	Spintronics	7
1.2	The theoretical tools	10
1.3	Outline	12
2	Enter the formalism	13
2.1	Green's functions, contours and the Keldysh formulation	13
2.1.1	Closed-time contour Green's function and Wick's theorem	15
2.1.2	The Keldysh formulation	18
2.2	From Dyson to Eilenberger	19
2.2.1	Vector potential and gauge invariance	26
3	Quantum wells	31
3.1	2D systems in the real world	31
3.2	The theory: effective Hamiltonians	34
4	Quasiclassics and spin-orbit coupling	43
4.1	The Eilenberger equation	43
4.1.1	The continuity equation	46
4.2	ξ -integration vs. stationary phase	48
4.3	Particle-hole symmetry	56
5	Spin-charge coupled dynamics	57
5.1	The spin Hall effect	57
5.1.1	Experiments	58
5.1.2	Bulk dynamics: the direct spin Hall effect	59

5.1.3	Confined geometries	68
5.1.4	Voltage induced spin polarizations and the spin Hall effect in finite systems	70
5.2	Spin relaxation in narrow wires	79
6	Epilogue	85
A	Time-evolution operators	89
B	Equilibrium distribution	91
C	On gauge invariant Green's functions	93
D	The self energy	97
E	Effective Hamiltonians	99
E.1	The $\mathbf{k} \cdot \mathbf{p}$ expansion	99
E.2	Symmetries and matrix elements	101
E.3	The Löwdin technique	102
F	The Green's function ansatz	105
F.1	The stationary phase approximation	105
G	Matrix form of the Eilenberger equation and boundary conditions	109
G.1	The matrix form	109
G.2	Boundary conditions	114
	Bibliography	116
	Acknowledgements	129

Chapter 1

Introduction

1.1 Spintronics

The word “spintronics” refers to a new field of study concerned with the manipulation of the spin degrees of freedom in solid state systems [1–4]. The realization of a new generation of devices capable of making full use of, besides the charge, the electronic – and possibly nuclear – spin is one of its main goals. Ideally, such devices should consist of only semiconducting materials, making for a smooth transition from the present *electronic* technology to the future *spintronic* one. More generally though metals, both normal and ferromagnetic, are part of the game.

Besides in its name, which was coined in the late nineties, the field is “new” mainly in the sense of its approach to the solid state problems it tackles, as it tries to establish novel connections between the older subfields it consists of – e.g. magnetism, superconductivity, the physics of semiconductors, information theory, optics, mesoscopic physics, electrical engineering.

Typical spintronics issues are

1. how to polarize a system, be it a single object or an ensemble of many;
2. how to keep it in the desired spin configuration longer than the time required by a device to make use of the information so encoded;
3. how to possibly transport such information across a device and, finally, accurately read it.

The field is broad in scope and extremely lively. Without any attempt at generality, we now delve into some more specific problems and refer the interested reader to the literature. The reviews [2, 4] could be a good starting point.

When dealing with III-V (e.g. GaAs, InAs) and II-VI (e.g. ZnSe) semiconductors optical methods have been successfully used both for the injection and detection of spin in the systems [5]. Basically, circularly polarized light is shone on a sample and, via angular-momentum transfer controlled by some selection rules, polarized electron-hole pairs with a certain spin direction are excited. These can be used to produce spin-polarized currents. Vice versa, as in [6–9], when previously polarized electrons (holes) recombine with unpolarized holes (electrons), polarized light is emitted and detected – this is the principle behind the so-called spin light emitting diodes (spin LEDs).

All-electrical means of spin injection and detection would however be preferable for practical spintronic devices. Resorting to ferromagnetic contacts is quite convenient, at least for metals. Roughly, the idea is to run a current first through a ferromagnet, so that the carriers will be spin polarized, and then into a normal metal. Actually, relying on a cleverly designed non-local device based on the scheme of Johnson and Silsbee [10], Valenzuela and Tinkham [11] were able to inject a pure spin current – in contrast to a polarized charge current – into an Al strip and, moreover, to use this for the observation of the inverse spin Hall effect.¹ Similar experiments followed [12–15].

In semiconducting systems things are complicated by the so-called “mismatch problem” one runs into as soon as a ferromagnetic metal-semiconductor interface shows up. As it turns out, the injection is efficient only if $\sigma_F \leq \sigma$, where σ_F is the conductivity in the ferromagnetic metal and σ that in the material it is in contact with, which is not the case when this is a semiconductor [16, 17]. Workarounds are subtle but possible, and revolve around the use of tunnel barriers between the ferromagnetic metal and the semiconducting material [8, 9], or the substitution of the former with a magnetic semiconductor [6, 7, 18]. Whereas in the second case results are limited to low temperatures, the first approach has led to efficient injection even at room temperature [9]. Finally, a successful all-electrical injection-detection scheme in a semiconductor has been recently demonstrated [19].

On the other hand, the already mentioned spin Hall effect could itself be a

¹More on this shortly and in Chapter 5.

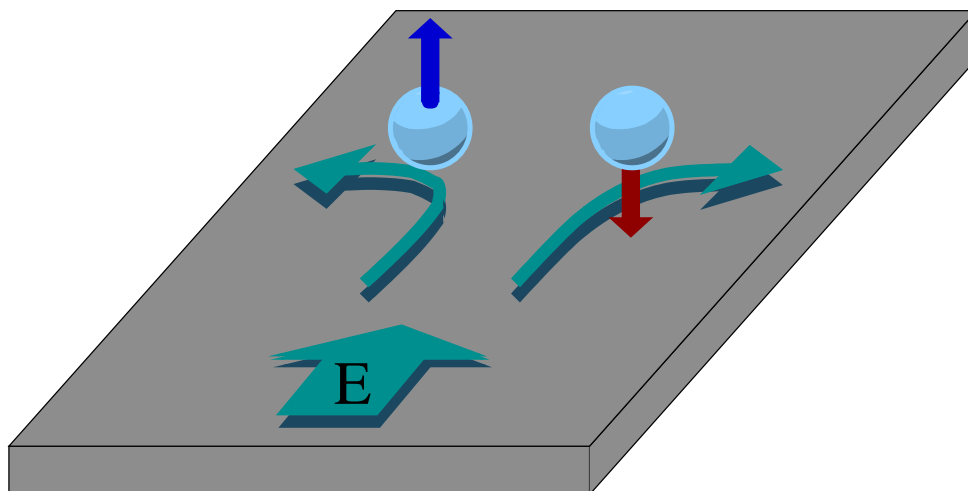


Figure 1.1: The direct spin Hall effect. The gray layer is a two-dimensional electron (hole) gas, abbreviated 2DEG (2DHG), to which an in-plane electric field is applied. Because of spin-orbit interaction in the system, spin-up and spin-down fermions are deflected in opposite directions, creating a pure spin current in the direction orthogonal to the driving field. Spin accumulation at the boundaries of the sample is the quantity usually observed in experiments and taken as a signature of the effect.

method for generating pure spin currents without the need for ferromagnetic contacts. Perhaps even more importantly, it could allow for the manipulation of the spin degrees of freedom inside a device by means of electrical fields only. It is an eminent example of what Awschalom calls a “coherent spintronic property” [4], as opposed to the “non-coherent” ones on which older devices are based.² Originally proposed in 2003 for a two-dimensional hole gas by Murakami et al. [20], and soon after for a two-dimensional electron gas by Sinova et al. [21], it has attracted much attention and is still being actively debated. Rather simply, it is the appearance of a pure spin current orthogonal to an applied electric field, as shown in Fig. 1.1, in the absence of any magnetic field. Its inverse counterpart is, most obviously, the generation of a charge current by a spin one, both flowing orthogonal

²For example, giant-magnetoresistance-based hard drives. Roughly, non-coherent devices are able to distinguish between “blue” (spin up) and “red” (spin down) electrons, but cannot deal with “blue-red” mixtures, that is, coherences.

to each other – in [11], for example, the injected spin current produced a measurable voltage drop in the direction transverse to its flow. They are two of a group of closely related and quite interesting phenomena which, induced by spin-orbit coupling, present themselves as potential electric field-controlled handles on the spin degrees of freedom of carriers. They will be discussed extensively in Chapter 5, and represent the main motivation behind our present work.

1.2 The theoretical tools

Out-of-equilibrium systems are ubiquitous in the physical world. Examples could be a body in contact with reservoirs at different temperatures, electrons in a conductor driven by an applied electric field or a stirred fluid in turbulent motion. Indeed, the abstraction of an isolated system in perfect equilibrium is more often than not just that, an abstraction, and a convenient starting point for a quantitative treatment of its physical properties. However, we do not wish to discuss in general terms nonequilibrium statistical mechanics [22–24]. More modestly, we want to focus on an approximate quantum-field theoretical formulation, the quasiclassical formalism [24–27], constructed to deal with nonequilibrium situations and which has the virtues of

- having, by definition, a solid microscopic foundation;
- being perfectly suited for dealing with mesoscopic systems, i.e. systems whose size, though much bigger than the microscopic Fermi wavelength λ_F , can nevertheless be comparable to that over which quantum interference effects extend [28, 29];
- bearing a resemblance to standard Boltzmann transport theory that makes for physical transparency.

In particular, we will be dealing with disordered fermionic gases in the presence of spin-orbit coupling.

The established language in which the quasiclassical theory is expressed is that of the real-time formulation of the Keldysh technique [24–26, 30, 31]. The latter is a powerful formalism which generalizes the standard perturbative approach typical of equilibrium quantum field theory [24, 32–34] to nonequilibrium problems

and stems from Schwinger's ideas [35]. Its range of applications goes from particle physics to solid state and soft condensed matter.

Quasiclassics, on the other hand, was historically born to deal with transport phenomena in electron-phonon systems [27], and was originally formulated according to the work of Kadanoff and Baym [36]. It was later extended, highly successfully, to deal with superconductivity.³ Its main assumption is that all energy scales involved – external fields, interactions, disorder, call this $\hbar\omega$ – be small compared to the Fermi energy ϵ_F . Thanks to the diagrammatic formalism inherited from the underlying Keldysh structure, a systematic expansion in $\hbar\omega/\epsilon_F$ is possible. This way quantum corrections due to weak localization and electron-electron interaction can also be included [26]. More generally though, the theory is built so as to naturally take into account coherences, and has the great merit of making Boltzmann-like kinetic equations available also for systems in which the standard definition of quasiparticles – i.e. excitations sharply defined in energy space thanks to a delta-like momentum-energy relation – is not possible. Of course, it has shortcomings too. A rather important one is its relying on perfect particle-hole symmetry. In other words, the quasiclassical equations are obtained neglecting any sort of dependence on the modulus of the momentum of the density of states N and of the velocity \mathbf{v} , which are simply fixed at their values at the Fermi surface, N_0 and \mathbf{v}_F . This turns out to be a problem whenever different folds of the Fermi surface exist – e.g. when spin-orbit coupling is considered – across which variations of N and \mathbf{v} are necessary in order to catch the physics of some particular phenomena. Examples of these are a number of spin-electric effects in two-dimensional fermionic systems very promising for potential applications in the field of spintronics, like the voltage induced spin accumulation and the anomalous and spin Hall effects [20, 21, 37–40]. It is such phenomena that motivated us to generalize the quasiclassical formalism to situations in which particle-hole symmetry, at least in the sense now described, is broken. More precisely, to situations in which new physics arises because the charge and spin degrees of freedom of carriers are coupled due to spin-orbit interaction.

³For a more detailed overview see [25], where a number of additional references can be found.

1.3 Outline

Chapter 2 introduces the general formalism we rely on, the Keldysh technique and the quasiclassical theory, and is complemented by the Appendices A–D.

Chapter 3 is dedicated to the low-dimensional systems in which the physics we focus on takes place: their main characteristics, how they are realized, what kind of Hamiltonians describe them. Additional material is given in Appendix E.

In Chapter 4 we present original results regarding the generalization of the quasiclassical equations to the case in which spin-orbit coupling is present. Some additional technical details can be found in Appendix F.

Chapter 5 starts with a rather general discussion of the spin Hall effect and related phenomena, giving also a brief overview of the experimental scene, and then moves on to treat some specific aspects of the matter, like

- the details of the direct intrinsic spin Hall effect in the two-dimensional electron gas, with focus on the Rashba model;
- the influence of different kinds of disorder – non-magnetic long-range, magnetic short-range – on spin-charge coupled dynamics in two-dimensional electron systems;
- the effects of boundaries and confined geometries on the aforementioned phenomena and on the more general issue of spin relaxation.

Original results are presented. Additional technical material is given in Appendix G.

The closing Chapter 6 provides with a brief summary and an overview of the current work in progress and of possible future research.

Finally, if not otherwise specified, units of measure will be chosen so that $\hbar = k_B = c = 1$ throughout the whole text.

Chapter 2

Enter the formalism

As its title suggests, this Chapter is mostly a technical one. The main objects of the discussion are the Keldysh formulation of nonequilibrium problems and the quasiclassical formalism. This presentation, though only introductory, is supposed to be self-contained. For details we refer the interested reader to the fairly rich literature [24–26, 30, 32, 35, 36, 41–44]. We will mainly move along the lines of [25, 26]. A further reference for the basic background is [45].

2.1 Green’s functions, contours and the Keldysh formulation

The Green’s function, or propagator, lies at the core of quantum field theory. It represents a powerful and convenient way of encoding information about a given system, and lets one calculate the expectation values of physical observables. For a system in thermodynamical equilibrium described by a Hamiltonian H the definition of the one-particle propagator reads¹

$$G(1, 1') \equiv -i \langle T \{ \psi_H(1) \psi_H^\dagger(1') \} \rangle \quad (2.1)$$

where $\langle \dots \rangle$ indicates the grandcanonical ensemble average, $T \{ \dots \}$ the time-ordering operator, and $\psi_H(1), \psi_H^\dagger(1')$ are the field operators in the Heisenberg picture. We

¹In the following “1” will indicate the space-time point (\mathbf{x}_1, t_1) . Additional degrees of freedom, for example pertaining to the spin, can also be included in a “generalized” space coordinate.

write

$$H = H_0 + H^i, \quad (2.2)$$

where H_0 represents the diagonalizable part of H while H^i contains the possibly complicated interactions between particles, and move from the Heisenberg to the interaction picture. Thanks to Wick's theorem [33, 45] it is possible to obtain a perturbative expansion of $G(1, 1')$ in powers of H^i , which can be pictorially represented by connected Feynman diagrams. A crucial step in this procedure is the so-called adiabatic switching on, in the “far” past, and off, in the “far” future, of interactions, which assures that at $t \rightarrow \pm\infty$ the system lies in *the same* eigenstate of the noninteracting H_0 .

One can go a little further, and in the case of an additional weak and time-dependent external perturbation being turned on at time $t = t_0$

$$\mathcal{H} = H + H^{ext}(t), \quad H^{ext}(t) = 0 \text{ for } t < t_0, \quad H^{ext} \ll H \quad (2.3)$$

it is possible to calculate the response of the system to linear order in $H^{ext}(t)$, since this is determined by its equilibrium properties only.² To tackle real nonequilibrium problems $G(1, 1')$ given above, Eq. (2.1), is however not enough. The reason is the following. Let us assume that the external perturbation $H^{ext}(t)$, not necessarily small, is switched on and off not adiabatically at times $t = t_i$ and $t = t_f > t_i$

$$\mathcal{H}(t) = \begin{cases} H & t \in (-\infty, t_i) \cup (t_f, +\infty) \\ H + H^{ext}(t) & t \in [t_i, t_f] \end{cases}, \quad (2.4)$$

where possibly $t_i \rightarrow -\infty$ and $t_f \rightarrow +\infty$ – indeed this is what will happen in Sec. 2.1.2. If the system was lying in a given eigenstate of the unperturbed Hamiltonian at $t < t_i$, nothing guarantees that after $H^{ext}(t)$ had driven it out of equilibrium it will go back to the same initial state. Schwinger suggested [35] to avoid referring to the final state at $t > t_f$, and rather to stick to the initial one only, i.e. to define a Green's function on the closed time contour c shown in Fig. 2.1 (since from now on the only reference time will be the “switch on” time t_i , we will call this t_0)

$$G(1, 1') \equiv -i \langle T_c \{ \psi_{\mathcal{H}}(1) \psi_{\mathcal{H}}^\dagger(1') \} \rangle. \quad (2.5)$$

Here $T_c \{ \dots \}$ is the contour time-ordering operator

²This statement corresponds to the fluctuation-dissipation theorem [32, 45].

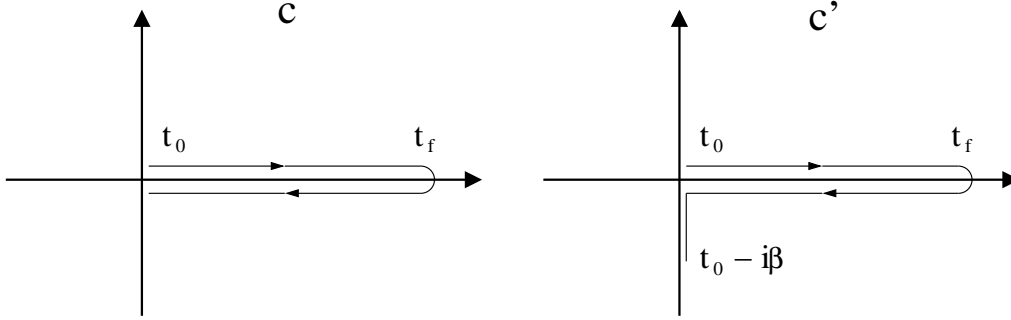


Figure 2.1: The closed-time contours c (left) and c' (right). The downward-pointing branch of c' , describing evolution in the imaginary time interval $(0, -i\beta)$, corresponds to the thermodynamical ensemble average.

$$T_c \left\{ \psi_{\mathcal{H}}(1) \psi_{\mathcal{H}}^\dagger(1') \right\} = \begin{cases} \psi_{\mathcal{H}}(1) \psi_{\mathcal{H}}^\dagger(1') & t_1 >_c t_{1'} \\ \pm \psi_{\mathcal{H}}^\dagger(1') \psi_{\mathcal{H}}(1) & t_1 <_c t_{1'}, \end{cases} \quad (2.6)$$

where the \pm sign corresponds to bosons and fermions. The meaning of the symbol $\langle \dots \rangle$ is now that of a weighted average with respect to some density operator ρ , which to all effects plays the role of a boundary condition imposed on $G(1, 1')$ – i.e. it does *not* influence the dynamics of the field operators. If one assumes that for $t < t_0$ the system lies in thermal equilibrium with a reservoir at temperature T then (we use the grandcanonical ensemble, so energies are measured from the chemical potential μ)

$$\rho(H) = \frac{e^{-\beta H}}{\text{Tr}[e^{-\beta H}]}, \quad \beta = \frac{1}{T}. \quad (2.7)$$

To explicitly show how to manipulate Eq. (2.5) in order to see the structure of $G(1, 1')$, and to obtain its perturbative expansion, we will assume Eq. (2.7) to hold. We emphasize that such an assumption is by no means necessary, as the functional derivative method shows [36, 41–44].

2.1.1 Closed-time contour Green's function and Wick's theorem

Our goal is to write down $G(1, 1')$ in a way that will let us use Wick's theorem to generate its perturbative expansion in both H^i and $H^{ext}(t)$, exactly as done in

ordinary equilibrium theory.

We start by considering the Hamiltonian

$$\mathcal{H}(t) = H + H^{ext}(t), \quad H = H_0 + H^i, \quad H^{ext}(t) = 0 \text{ for } t < t_0 \quad (2.8)$$

and the Green's function as defined in Eq. (2.5)

$$G(1, 1') \equiv \langle T_c \{ \psi_{\mathcal{H}}(1) \psi_{\mathcal{H}}^\dagger(1') \} \rangle, \quad (2.9)$$

with, thanks to Eq. (2.7),

$$\langle \dots \rangle = \text{Tr}[\rho(H)\dots] = \frac{\text{Tr}[e^{-\beta H} \dots]}{\text{Tr}[e^{-\beta H}]}. \quad (2.10)$$

For a given operator $\mathcal{O}_{\mathcal{H}}(t)$ in the Heisenberg picture one has

$$\mathcal{O}_{\mathcal{H}}(t) = \mathcal{U}^\dagger(t, t_0) \mathcal{O}(t_0) \mathcal{U}(t, t_0) \quad (2.11)$$

where t_0 is the reference time at which the Heisenberg and Schrödinger pictures coincide, and $\mathcal{U}(t, t_0)$ is the full time-evolution operator³

$$\mathcal{U}(t, t_0) \equiv T \left\{ \exp \left(-i \int_{t_0}^t dt' \mathcal{H}(t') \right) \right\}, \quad (2.12)$$

$T\{\dots\}$ indicating the usual time ordering. This can be factorized as

$$\begin{aligned} \mathcal{U}(t, t_0) &= \mathcal{U}_0(t, t_0) \mathcal{S}(t, t_0) \\ &= e^{-iH_0(t-t_0)} \mathcal{S}^i(t, t_0) \mathcal{S}^{ext}(t, t_0) \end{aligned} \quad (2.13)$$

where

$$\mathcal{S}^i(t, t_0) = T \left\{ \exp \left[-i \int_{t_0}^t dt' H_{H_0}^i(t') \right] \right\}, \quad (2.14)$$

$$\mathcal{S}^{ext}(t, t_0) = T \left\{ \exp \left[-i \int_{t_0}^t dt' H_{H_0}^{ext}(t') \right] \right\}. \quad (2.15)$$

From Eq. (2.11), using that $\mathcal{S}^\dagger(t, t') = \mathcal{S}(t', t)$

$$\begin{aligned} \psi_{\mathcal{H}}(t) \psi_{\mathcal{H}}^\dagger(t') &= \mathcal{U}^\dagger(t, t_0) \psi(t_0) \mathcal{U}(t, t_0) \mathcal{U}^\dagger(t', t_0) \psi^\dagger(t_0) \mathcal{U}(t', t_0) \\ &= \mathcal{S}(t_0, t) \psi_{H_0}(t) \mathcal{S}(t, t') \psi_{H_0}^\dagger(t') \mathcal{S}(t, t_0). \end{aligned} \quad (2.16)$$

³For details regarding \mathcal{U} and its manipulations see Appendix A.

The thermodynamical weight factor $e^{-\beta H}$ can be regarded as an evolution operator in imaginary time from t_0 to $t_0 - i\beta$ and thus similarly decomposed

$$e^{-\beta H} = e^{-\beta H_0} \mathcal{S}^i(t_0 - i\beta, t_0). \quad (2.17)$$

This way the numerator of Eq. (2.9) reads

$$\begin{aligned} & \text{Tr} \left[e^{-\beta H} T_c \left\{ \psi_{\mathcal{H}}(t) \psi_{\mathcal{H}}^\dagger(t') \right\} \right] = \\ & \text{Tr} \left[e^{-\beta H_0} \mathcal{S}^i(t_0 - i\beta, t_0) T_c \left\{ \mathcal{S}(t_0, t) \psi_{H_0}(t) \mathcal{S}(t, t') \psi_{H_0}^\dagger(t') \mathcal{S}(t, t_0) \right\} \right] = \\ & \text{Tr} \left[e^{-\beta H_0} T_c \left\{ \mathcal{S}_{c'}^i \mathcal{S}_c^{ext} \psi_{H_0}(t) \psi_{H_0}^\dagger(t') \right\} \right]. \end{aligned} \quad (2.18)$$

In the above we wrote $\mathcal{S}_{c'}^i$ (\mathcal{S}_c^{ext}) for the time evolution operator generated by H^i ($H^{ext}(t)$) on the contour c' (c) of Fig. 2.1, and we let $T_c \{ \dots \}$ take care of rearranging the various terms in the correct time order.

To rewrite the denominator of Eq. (2.9) we exploit that a unitary time evolution along the closed-time contour c is simply the identity

$$T_c \left\{ \mathcal{S}_{c'}^i \mathcal{S}_c^{ext} \right\} = 1 \quad (2.19)$$

and thus obtain

$$\begin{aligned} \text{Tr} \left[e^{-\beta H} \right] &= \text{Tr} \left[e^{-\beta H_0} \mathcal{S}^i(t_0 - i\beta, t_0) T_c \left\{ \mathcal{S}_{c'}^i \mathcal{S}_c^{ext} \right\} \right] \\ &= \text{Tr} \left[e^{-\beta H_0} T_c \left\{ \mathcal{S}_{c'}^i \mathcal{S}_c^{ext} \right\} \right]. \end{aligned} \quad (2.20)$$

From Eqs. (2.18) and (2.20) we end up with

$$\begin{aligned} G(1, 1') &= -i \frac{\langle T_c \left\{ \mathcal{S}_{c'}^i \mathcal{S}_c^{ext} \psi_{H_0}(t) \psi_{H_0}^\dagger(t') \right\} \rangle_0}{\langle T_c \left\{ \mathcal{S}_{c'}^i \mathcal{S}_c^{ext} \right\} \rangle_0} \\ &\equiv -i \frac{\text{Tr} \left[e^{-\beta H_0} T_c \left\{ \mathcal{S}_{c'}^i \mathcal{S}_c^{ext} \psi_{H_0}(t) \psi_{H_0}^\dagger(t') \right\} \right]}{\text{Tr} \left[e^{-\beta H_0} T_c \left\{ \mathcal{S}_{c'}^i \mathcal{S}_c^{ext} \right\} \right]}. \end{aligned} \quad (2.21)$$

As anticipated, Eq. (2.21) is formally identical to the expression one would obtain in equilibrium. The only difference is the appearance of the contours c, c' , which take the place of the more usual real-time axis $(-\infty, +\infty)$. Wick's theorem can now be applied, and perturbation theory formulated in terms of connected Feynman diagrams.⁴ The algebraic structure of $G(1, 1')$ is however a little more complicated than in an equilibrium situation. We deal with it in the next section.

⁴Looking at Eq. (2.21) one could think that the denominator is responsible for the cancellation of the non connected diagrams. Actually, in contrast to the equilibrium case, these are automatically "canceled", since the evolution operator S on the closed-time contour is 1.

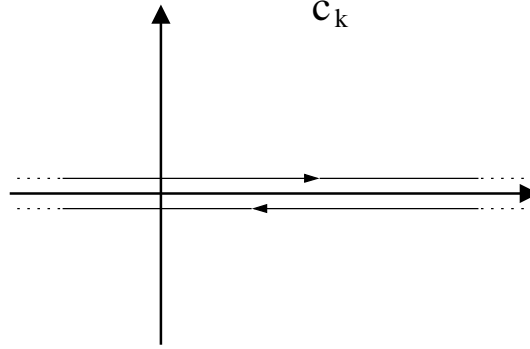


Figure 2.2: The Keldysh contour in the complex t -plane.

2.1.2 The Keldysh formulation

To obtain the Keldysh contour c_K [31] shown in Fig. 2.2 we first neglect initial correlations⁵ and send $t_0 \rightarrow -\infty$, then extend the right “tip” of c to $+\infty$ by using the unitarity of the time-evolution operator. The Green's function $G(1, 1')$, now defined on c_K , can be mapped onto a matrix in the so-called Keldysh space

$$G_{c_K}(1, 1') \mapsto \hat{G} \equiv \begin{pmatrix} \hat{G}_{11} & \hat{G}_{12} \\ \hat{G}_{21} & \hat{G}_{22} \end{pmatrix}. \quad (2.22)$$

A matrix element \hat{G}_{ij} corresponds to $t \in c_i, t' \in c_j$. Explicitly

$$\hat{G}_{11}(1, 1') = -i \langle T \{ \psi_{\mathcal{H}}(1) \psi_{\mathcal{H}}^\dagger(1') \} \rangle, \quad (2.23)$$

$$\hat{G}_{12}(1, 1') = G^<(1, 1') = \mp i \langle \psi_{\mathcal{H}}^\dagger(1') \psi_{\mathcal{H}}(1) \rangle, \quad (2.24)$$

$$\hat{G}_{21}(1, 1') = G^>(1, 1') = -i \langle \psi_{\mathcal{H}}(1) \psi_{\mathcal{H}}^\dagger(1') \rangle, \quad (2.25)$$

$$\hat{G}_{22}(1, 1') = -i \langle \tilde{T} \{ \psi_{\mathcal{H}}(1) \psi_{\mathcal{H}}^\dagger(1') \} \rangle, \quad (2.26)$$

where $\tilde{T} \{ \dots \}$ is the anti-time-ordering operator. A convenient representation was introduced by Larkin and Ovchinnikov [46]:

$$\check{G} \equiv L \sigma_3 \hat{G} L^\dagger \quad (2.27)$$

⁵In our language this means neglecting the part of c' extending from t_0 to $t_0 - i\beta$. In the functional derivative method this corresponds to considering as boundary condition a noncorrelated state.

with $L = 1/\sqrt{2}(\sigma_0 - i\sigma_2)$ and σ_i , $i = 0, 1, 2, 3$, the Pauli matrices. This way the Green's function reads

$$\check{G} = \begin{pmatrix} G^R & G^K \\ 0 & G^A \end{pmatrix}. \quad (2.28)$$

G^R and G^A are the usual retarded and advanced Green's functions

$$G^R(1, 1') = -i\theta(t - t')\langle\{\psi_{\mathcal{H}}(1), \psi_{\mathcal{H}}^\dagger(1')\}\rangle, \quad (2.29)$$

$$G^A(1, 1') = i\theta(t' - t)\langle\{\psi_{\mathcal{H}}(1), \psi_{\mathcal{H}}^\dagger(1')\}\rangle, \quad (2.30)$$

with $\{\psi_{\mathcal{H}}(1), \psi_{\mathcal{H}}^\dagger(1')\} = \psi_{\mathcal{H}}(1)\psi_{\mathcal{H}}^\dagger(1') + \psi_{\mathcal{H}}^\dagger(1')\psi_{\mathcal{H}}(1)$, while G^K , the Keldysh component of \check{G} , is

$$G^K(1, 1') = -i\langle\{\psi_{\mathcal{H}}(1), \psi_{\mathcal{H}}^\dagger(1')\}\rangle. \quad (2.31)$$

G^R, G^A carry information about the spectrum of the system, G^K about its distribution. The equation of motion for G^K , the quantum-kinetic equation, can be thought of as a generalization of the Boltzmann equation. In fact, in the semi-classical limit, and provided a quasiparticle picture is possible, it reduces to the Boltzmann result. The representation given by Eq. (2.28) is particularly convenient since its triangular structure is preserved whenever one deals with a string of (triangular) operators O_1, O_2, \dots, O_n (standard matrix multiplication is assumed)

$$O_1 O_2 \dots O_n = O' = \begin{pmatrix} (O')^R & (O')^K \\ 0 & (O')^A \end{pmatrix}. \quad (2.32)$$

Such a string is the kind of object Wick's theorem produces. In other words, in this representation the structure of the Feynman diagrams is the simplest possible. We will not discuss this in detail (see [25] for more), and will rather move on to study the equation of motion of \check{G} in the quasiclassical approximation. From now on spin-1/2 fermions will be considered.

2.2 From Dyson to Eilenberger

Thanks to \check{G} , a full quantum-mechanical description of our system is – formally – possible. In principle all one needs is the solution of the Dyson equation, i.e. the

equation of motion for the Green's function. Its right- and left-hand expressions in the general case read

$$[\check{G}_0^{-1}(1, 2) - \check{\Sigma}(1, 2)] \otimes \check{G}(2, 1') = \delta(1 - 1'), \quad (2.33)$$

$$\check{G}(1, 2) \otimes [\check{G}_0^{-1}(2, 1') - \check{\Sigma}(2, 1')] = \delta(1 - 1'), \quad (2.34)$$

where the symbol “ \otimes ” indicates convolution in space-time and matrix multiplication in Keldysh space

$$\check{A}(1, 2) \otimes \check{B}(2, 1') \equiv \int d2 \begin{pmatrix} A^R & A^K \\ 0 & A^A \end{pmatrix} (1, 2) \begin{pmatrix} B^R & B^K \\ 0 & B^A \end{pmatrix} (2, 1') \quad (2.35)$$

and the δ -function has to be interpreted as

$$\delta(1 - 1') = \begin{pmatrix} \delta(1 - 1') & 0 \\ 0 & \delta(1 - 1') \end{pmatrix}. \quad (2.36)$$

\check{G}_0^{-1} is the inverse of the free Green's function⁶

$$\check{G}_0^{-1}(1, 2) \equiv [i\partial_{t_1} - H_0(1)] \delta(1 - 2), \quad (2.37)$$

while the self-energy $\check{\Sigma}$ contains the effects due to interactions (electron-phonon, electron-electron and so on, but also disorder). Explicitly, for electrons in the presence of an electromagnetic field ($e = |e|$, μ is the chemical potential)

$$H_0(1) \equiv \frac{1}{2m} [-i\nabla_{x_1} + e\mathbf{A}(1)]^2 - e\Phi(1) - \mu. \quad (2.38)$$

The Dyson equation contains too much information for our purposes. What we are looking for is a kinetic equation with as clear and simple a structure as possible – that is, some sort of compromise between physical transparency and amount of information retained. The model is that of the already cited Boltzmann equation, which we aim at generalizing starting from the full microscopic quantum picture delivered by Eqs. (2.33) and (2.34). While physical quantities are written in terms of equal-time Green's functions, the Dyson equation cannot, and thus approximations are needed. With this in mind, we introduce the Wigner coordinates

$$\mathbf{R} = \frac{\mathbf{x}_1 + \mathbf{x}_{1'}}{2}, \quad T = \frac{t_1 + t_{1'}}{2}, \quad (2.39)$$

$$\mathbf{r} = \mathbf{x}_1 - \mathbf{x}_{1'}, \quad t = t_1 - t_{1'} \quad (2.40)$$

⁶External fields, like the electromagnetic one, can also be included. See below.

and Fourier-transform with respect to the relative ones

$$\check{G}(1, 1') \xrightarrow{FT} \check{G}(X, p) = \int dx e^{-ipx} \check{G}(X + x/2, X - x/2). \quad (2.41)$$

Here

$$\begin{aligned} X &= (T, \mathbf{R}), & x &= (t, \mathbf{r}), & p &= (\epsilon, \mathbf{p}), \\ \partial_X &= (-\partial_T, \nabla_{\mathbf{R}}), & \partial_x &= (-\partial_\epsilon, \nabla_{\mathbf{r}}) \end{aligned}$$

and the metric is such that

$$px = -\epsilon t + \mathbf{p} \cdot \mathbf{r}, \quad \partial_X \partial_p = -\partial_T \partial_\epsilon + \nabla_{\mathbf{R}} \cdot \nabla_{\mathbf{p}}. \quad (2.42)$$

The coordinates (X, p) define the so-called mixed representation. Physical quantities must be functions of the center-of-mass time T , not of the relative time t – or, in other words, must be functions of $(T, t = 0)$.

A convolution $A(1, 2) \otimes B(2, 1')$ in Wigner space can be written as [47]

$$(A \otimes B)(X, p) = e^{i(\partial_X^A \partial_p^B - \partial_p^A \partial_X^B)/2} A(X, p) B(X, p), \quad (2.43)$$

where the superscript on the partial derivative symbol indicates on which object it operates. We now subtract Eqs. (2.33) and (2.34) to obtain

$$[\check{G}_0^{-1}(1, 2) - \check{\Sigma}(1, 2) \circledast \check{G}(2, 1')] = 0, \quad (2.44)$$

then move to Wigner space and use Eq. (2.43) to evaluate the convolutions. If $A(X, p)$ and $B(X, p)$ are slowly varying functions of X the exponential in Eq. (2.43) can be expanded order by order in the small parameter $\partial_X \partial_p \ll 1$, thus generating from Eq. (2.44) an approximated equation. If possible, this is then integrated first over ϵ – i.e. written in terms of $t = 0$ quantities – to produce the kinetic equation, then over the momentum \mathbf{p} to deliver at last the dynamics of the physical observables.

To clarify the procedure we consider the simplest example possible: free electrons in a perfect lattice (no disorder) and in the presence of an electric field described by a scalar potential⁷

$$\check{G}_0^{-1}(1, 1') = \left[i\partial_{t_1} - \frac{(-i\nabla_{\mathbf{x}_1})^2}{2m} + e\Phi(1) + \mu \right] \delta(1 - 1'), \quad \check{\Sigma}(1, 1') = 0. \quad (2.45)$$

⁷The presence of a vector potential will be handled in the next Section.

We move to Wigner coordinates and Fourier-transform $x \rightarrow p$, so that

$$\check{G}_0^{-1} = \epsilon - \frac{\mathbf{p}^2}{2m} + e\Phi(X) + \mu. \quad (2.46)$$

Eq. (2.44) is then written expanding the convolution [Eq. (2.43)] to linear order in the exponent,⁸ since we make the standard semiclassical assumption that $\Phi(\mathbf{R})$ varies slowly in space and time on the scale set by $1/p_F, 1/\epsilon_F$

$$\begin{aligned} -i [\check{G}_0^{-1} \circledast \check{G}] &\approx \partial_T \check{G} - e\partial_T \Phi \partial_\epsilon G - \nabla_{\mathbf{p}} \check{G}_0^{-1} \cdot \nabla_{\mathbf{R}} \check{G} + \nabla_{\mathbf{R}} \check{G}_0^{-1} \cdot \nabla_{\mathbf{p}} \check{G} \\ &= \partial_T \check{G} - e\partial_T \Phi \partial_\epsilon G + \mathbf{v} \cdot \nabla_{\mathbf{R}} \check{G} + e\nabla_{\mathbf{R}} \Phi(\mathbf{R}) \cdot \nabla_{\mathbf{p}} \check{G} \end{aligned} \quad (2.47)$$

with $\check{G} = \check{G}(X, p)$ and $\mathbf{v} = \mathbf{p}/m$. At this point we define the distribution function $f(X, \mathbf{p})$

$$f(X, \mathbf{p}) \equiv \frac{1}{2} \left(1 + \int \frac{d\epsilon}{2\pi i} G^K(X, p) \right), \quad (2.48)$$

which in equilibrium reduces to the Fermi function (see Appendix B), and consider the Keldysh component of Eq. (2.47). Integrated over $\epsilon/2\pi i$ it reads

$$(\partial_T + \mathbf{v} \cdot \nabla_{\mathbf{R}} + e\nabla_{\mathbf{R}} \Phi(\mathbf{R}) \cdot \nabla_{\mathbf{p}}) f(X, \mathbf{p}) = 0, \quad (2.49)$$

that is, the collisionless Boltzmann equation. As known, there follows the standard continuity equation

$$\partial_T \rho(X) + \nabla_{\mathbf{R}} \cdot \mathbf{j}(X) = 0, \quad (2.50)$$

where the particle density and particle current are

$$\int \frac{d\mathbf{p}}{(2\pi)^3} f(X, \mathbf{p}) = \rho(X) \quad (2.51)$$

$$\int \frac{d\mathbf{p}}{(2\pi)^3} \mathbf{v} f(X, \mathbf{p}) = \mathbf{j}(X). \quad (2.52)$$

When $\Sigma(1, 1') \neq 0$ care is needed. The procedure sketched above goes through as shown only as long as the self-energy has a weak ϵ dependence. Otherwise the term $[\check{\Sigma} \circledast \check{G}]$ cannot be easily – if at all – ϵ -integrated.⁹ Such a requirement

⁸The gradient approximation, $e^{i(\partial_X^A \partial_p^B - \partial_p^A \partial_X^B)/2} \approx 1 + \frac{i}{2} (\partial_X^A \partial_p^B - i\partial_p^A \partial_X^B)$.

⁹Basically, if Σ has a weak ϵ -dependence the spectral weight $G^R - G^A$ has a delta-like profile in ϵ . This can be interpreted as defining quasiparticle excitations. Details can be found in [25, 27].

is avoided by the quasiclassical technique. Its idea is to “swap” the integration procedure

$$\int \frac{d\mathbf{p}}{(2\pi)^3} \int \frac{d\epsilon}{2\pi i} \approx N_0 \int \frac{d\hat{\mathbf{p}}}{4\pi} \int d\xi \int \frac{d\epsilon}{2\pi i} \rightarrow N_0 \int \frac{d\hat{\mathbf{p}}}{4\pi} \int \frac{d\epsilon}{2\pi i} \int d\xi. \quad (2.53)$$

Here, $\xi \equiv p^2/2m - \mu$ and N_0 is the density of states at the Fermi surface per spin and volume (for example in three dimensions $N_0 = mp_F/2\pi^2$). The crucial assumption of the quasiclassical approximation is that the all energy scales involved in the problem be much smaller than the Fermi energy. This means that the Green’s function, which in equilibrium is strongly peaked around the Fermi surface $|\mathbf{p}| = p_F$, will stay so even after the interactions have been turned on. In other words $\check{\Sigma}$ will be a slowly varying function of $|\mathbf{p}|$ when compared to \check{G} , and it will be possible to easily integrate (over $|\mathbf{p}|$) the commutator $[\check{\Sigma} \otimes \check{G}]$.

Let us then define the quasiclassical Green’s function \check{g} as

$$\check{g}(\mathbf{R}, \hat{\mathbf{p}}; t_1, t_2) \equiv \frac{i}{\pi} \int d\xi \check{G}(\mathbf{R}, \mathbf{p}; t_1, t_2). \quad (2.54)$$

As manifest, the quasiclassical approximation does not in general involve the time coordinates. Since $\check{G}(\mathbf{R}, \mathbf{p}; t_1, t_2)$ falls off as $1/\xi$ when $\xi \rightarrow \infty$ the integral does not converge, and high-energy contributions – i.e. far away from the Fermi surface – must be discarded. This can be achieved by introducing a physically sensible cutoff. The assumption that all energy scales be small compared to the Fermi energy ensures that only the low-energy region determines the dynamics of the system. In other words, introducing a cutoff cures the divergence of Eq. (2.54) and at the same time tells us that $\check{g}(\mathbf{R}, \hat{\mathbf{p}}; t_1, t_2)$ will carry the dynamical (nonequilibrium) information we are interested in. The discarded high-energy contributions¹⁰ can however be relevant: no matter what technical procedure is involved – that is, what kind of Boltzmann-like kinetic equation is obtained – Eq. (2.50) must in the end hold.

Still assuming for a moment $\check{\Sigma} = 0$, we go back to Eq. (2.47), take once again the Keldysh component and integrate it according to

$$\int \frac{d\mathbf{p}}{(2\pi)^3} \int \frac{d\epsilon}{2\pi i} \approx N_0 \int \frac{d\hat{\mathbf{p}}}{4\pi} \int \frac{d\epsilon}{2\pi i} \int d\xi. \quad (2.55)$$

¹⁰Far from the Fermi surface equilibrium sets in, so these are equivalently called “equilibrium” contributions.

After the ξ -integration we have

$$-i\pi [\partial_T + e\partial_T\phi(X)\partial_\epsilon + v_F\hat{\mathbf{p}} \cdot \nabla_{\mathbf{R}}] g^K(X, \epsilon, \hat{\mathbf{p}}) = 0, \quad (2.56)$$

the Eilenberger equation. The absence of a self-energy term lets us move to the mixed representation in time and perform a gradient expansion without worries, $\check{g}(t_1, t_2) \rightarrow \check{g}(T, \epsilon)$.

After comparing Eq. (2.56) with the Boltzmann equation (2.49) a couple of comments are in order.

1. The force term originating from the $\sim \nabla_{\mathbf{p}}\check{G}$ bit of Eq. (2.47) has been neglected in Eq. (2.56) because it is order ω/ϵ_F smaller than the others, ω being a typical energy scale of the problem (for example associated with an external field or with disorder). The driving effect of an applied electric field seems this way to be beyond the quasiclassical approximation. This is not the case, as will be shown in the next section.
2. The velocity is fixed in modulus at the Fermi surface.
3. The second term on the l.h.s. of Eq. (2.56) does not appear in Eq. (2.49). It carries the information coming from the high-energy region which is not included in the quasiclassical Green's function \check{g} – as already pointed out, the loss of such information has to do with the swapping procedure, Eq. (2.55), which requires the introduction of a cutoff in the definition (2.54).

The continuity equation is readily obtained from Eq. (2.56) and leads to the following relations between g^K and the physical quantities

$$\begin{aligned} \rho(X) &= -2N_0 \left[\frac{\pi}{2} \int \frac{d\epsilon}{2\pi} \int \frac{d\hat{\mathbf{p}}}{4\pi} g^K(X, \epsilon, \hat{\mathbf{p}}) - e\Phi(X) \right], \\ \mathbf{j}(X) &= -N_0\pi \int \frac{d\epsilon}{2\pi} \int \frac{d\hat{\mathbf{p}}}{4\pi} v_F\hat{\mathbf{p}} g^K(X, \epsilon, \hat{\mathbf{p}}). \end{aligned} \quad (2.57)$$

When $\check{\Sigma} \neq 0$ Eq. (2.47) is modified, and a gradient expansion is first performed in the space coordinates only. The self-energy term reads

$$\begin{aligned} -i [\check{\Sigma} \circledast \check{G}] &\approx -i [\check{\Sigma}(\mathbf{R}, \mathbf{p}; t_1, t_2) \circledast \check{G}(\mathbf{R}, \mathbf{p}; t_1, t_2)] + \\ &\quad + \frac{1}{2} \{ \nabla_{\mathbf{p}}\check{\Sigma} \circledast \cdot \nabla_{\mathbf{R}}\check{G} \} - \frac{1}{2} \{ \nabla_{\mathbf{R}}\check{\Sigma} \circledast \cdot \nabla_{\mathbf{p}}\check{G} \} \\ &\approx -i [\check{\Sigma}(\mathbf{R}, \mathbf{p}; t_1, t_2) \circledast \check{G}(\mathbf{R}, \mathbf{p}; t_1, t_2)], \end{aligned} \quad (2.58)$$

where the symbol \circ indicates convolution in time, and where only the leading order term has been kept, while for the rest one has

$$\begin{aligned}
 -i [G_0^{-1} \otimes \check{G}] &\approx -i [G_0^{-1} \circ \check{G}] + \frac{1}{2} \{ \nabla_{\mathbf{R}} G_0^{-1} \circ \cdot \nabla_{\mathbf{p}} \check{G} \} + \\
 &+ \frac{1}{2} \{ \nabla_{\mathbf{p}} G_0^{-1} \circ \cdot \nabla_{\mathbf{R}} \check{G} \}. \tag{2.59}
 \end{aligned}$$

Both Eq. (2.58) and Eq. (2.59) can be integrated over ξ exploiting the peaked nature of \check{G} , since thanks to the quasiclassical assumption – weak ξ -dependence of the self-energy – one has

$$\begin{aligned}
 -\frac{i}{\pi} \int d\xi [\check{\Sigma}(\mathbf{R}, \mathbf{p}; t_1, t_2) \circ \check{G}(\mathbf{R}, \mathbf{p}; t_1, t_2)] &\approx \\
 -[\check{\Sigma}(\mathbf{R}, \hat{\mathbf{p}}, p_F; t_1, t_2) \circ \check{g}(\mathbf{R}, \hat{\mathbf{p}}; t_1, t_2)]. \tag{2.60}
 \end{aligned}$$

We now assume external perturbations and the self-energy to be slowly varying in time, so that in Eqs. (2.58) and (2.59) the following gradient expansion can be performed

$$-i [A \circ B] \approx \partial_{\epsilon} A \partial_T B - \partial_T A \partial_{\epsilon} B. \tag{2.61}$$

The Eilenberger equation therefore reads

$$[\partial_T + e \partial_T \phi(X) \partial_{\epsilon} + v_F \hat{\mathbf{p}} \cdot \nabla_{\mathbf{R}}] \check{g}(X, \epsilon, \hat{\mathbf{p}}) + i [\check{\Sigma}(X, \epsilon, \hat{\mathbf{p}}, p_F), \check{g}(X, \epsilon, \hat{\mathbf{p}})] = 0. \tag{2.62}$$

We note that since the inhomogeneous term on the r.h.s. of the Dyson equation drops out of Eq. (2.44), the quasiclassical Green's function will be determined only up to a multiplicative constant. This is determined by the normalization condition

$$[\check{g} \circ \check{g}](t, t') = \delta(t - t'). \tag{2.63}$$

Such a condition can be directly established in equilibrium and thus be used as a boundary condition for the solution of the kinetic equation, which far from the perturbed region approaches its equilibrium form. For a detailed discussion see [24]. When the self-energy describes elastic short-range scattering in the Born approximation one has (see Appendix D)

$$\check{\Sigma}(X, \epsilon, \hat{\mathbf{p}}, p_F) = -\frac{i}{2\tau} \langle \check{g}(X, \epsilon, \hat{\mathbf{p}}) \rangle, \tag{2.64}$$

where $\langle \dots \rangle$ indicates the average over the momentum angle $\hat{\mathbf{p}}$ and τ is the quasi-particle lifetime. Then, taking the Keldysh component of Eq. (2.62) and exploiting Eq. (2.64) we finally obtain¹¹

$$[\partial_T + e\partial_T\phi(X)\partial_\epsilon + v_F\hat{\mathbf{p}} \cdot \nabla_{\mathbf{R}}] g^K(X, \epsilon, \hat{\mathbf{p}}) = -\frac{1}{\tau} [g^K(X, \epsilon, \hat{\mathbf{p}}) - \langle g^K(X, \epsilon, \hat{\mathbf{p}}) \rangle]. \quad (2.65)$$

In the following Chapters we will start from an equation with this same basic structure and modify it to allow for the description of various spin-related phenomena.

2.2.1 Vector potential and gauge invariance

So far only the coupling to an external scalar potential has been considered. We now treat the more general case of both electromagnetic potentials present, and see how to deal with gauge invariance at the quasiclassical level of accuracy. For simplicity the self-energy $\check{\Sigma}$ is taken to be zero, though its presence would not change the reasoning. Also for simplicity we assume to be in two dimensions, which means that Eq. (2.55) is modified according to

$$\int \frac{d\mathbf{p}}{(2\pi)^2} \int \frac{d\epsilon}{2\pi i} \approx N_0 \int \frac{d\hat{\mathbf{p}}}{2\pi} \int \frac{d\epsilon}{2\pi i} \int d\xi, \quad (2.66)$$

with $N_0 = m/2\pi$.

We start from the Dyson equation for the Hamiltonian (2.38), whose left-hand version reads

$$\left[i\partial_{t_1} + e\Phi(1) - \frac{1}{2m} (\mathbf{p} + e\mathbf{A}(1))^2 + \mu \right] \otimes G(1, 2) = \delta(1 - 2). \quad (2.67)$$

We then follow the standard procedure, just as done in the previous Section:

1. take the left- and right-hand Dyson equations and subtract the two;
2. move to Wigner coordinates;
3. expand the convolution to gradient expansion accuracy.

¹¹We use that in a normal state with no spin-orbit coupling $g^R(t, t') = -g^A(t, t') = \delta(t - t')$.

One obtains the equivalent of Eq. (2.47)

$$\begin{aligned}
 -i [G_0^{-1} \otimes G] &\rightarrow -i [G_0^{-1}, G]_p \\
 &\approx \partial_T G + \frac{1}{m} [p_i + eA_i(X)] \nabla_{R_i} G + \\
 &\quad + \left\{ -\partial_T \Phi(X) + \frac{1}{m} [p_i + eA_i(X)] \partial_T A_i(X) \right\} \partial_\epsilon G + \\
 &\quad + \left\{ e \nabla_{R_j} \Phi(X) - \frac{1}{m} [p_i + eA_i(X)] \nabla_{R_j} A_i(X) \right\} \nabla_{p_j} G \\
 &= 0, \quad i, j = x, y, z. \tag{2.68}
 \end{aligned}$$

Both here and below a sum over repeated indices is implied.

Before dealing with quasiclassics proper, it is instructive to try and derive from the above the Boltzmann equation. It is the easiest way to realize that the problem of gauge invariance is rather delicate. A distribution function $f(X, \mathbf{p})$ is defined as in Eq. (2.48) and the Keldysh component of Eq. (2.68) is integrated over $\epsilon/2\pi i$. The surface terms give no contribution

$$\int d\epsilon(\dots) \partial_\epsilon G^K = (\dots) [G^K(+\infty) - G^K(-\infty)] = 0, \tag{2.69}$$

therefore one ends up with

$$\begin{aligned}
 &\left(\partial_T + \frac{1}{m} [p_i + eA_i(X)] \nabla_{R_i} + \right. \\
 &\quad \left. + \left\{ e \nabla_{R_j} \Phi(X) - \frac{1}{m} [p_i + eA_i(X)] \nabla_{R_j} A_i(X) \right\} \nabla_{p_j} \right) f(X, \mathbf{p}) = 0.
 \end{aligned}$$

Such an expression is apparently *not* gauge invariant. In particular we would expect the term proportional to $\nabla_{p_j} f(X, \mathbf{p})$ to represent the Lorentz force, but this is not the case. The point is that the distribution function $f(X, \mathbf{p})$ is itself not gauge invariant. To obtain one that is – and to find its equation of motion – it is convenient to go one step back, to Eq. (2.68), and work directly on the Green's function. We refer to Appendix C for additional details on the following.

In the mixed representation and to the gradient expansion accuracy a gauge-

invariant Green's function $\tilde{G}(p, X)$ can be introduced

$$\begin{aligned}
 \tilde{G}(p, X) &= \int dx e^{-ipx} \tilde{G}(x, X) \\
 &\approx \int dx e^{-i[p - eA(X)]x} G(x, X) \\
 &= G(\epsilon - e\Phi(X), \mathbf{p} - e\mathbf{A}(X); X) \\
 &\approx G(p, X) - e\Phi(X)\partial_\epsilon G - e\mathbf{A}(X) \cdot \nabla_{\mathbf{p}} G.
 \end{aligned} \tag{2.70}$$

Its equation of motion is easily obtained and reads

$$[\partial_T + \mathbf{v} \cdot (\nabla_{\mathbf{R}} - e\mathbf{E}\partial_\epsilon) + \mathbf{F} \cdot \nabla_{\mathbf{p}}] \tilde{G}(\epsilon, \mathbf{p}; X) = 0, \tag{2.71}$$

where

$$\begin{aligned}
 \mathbf{v} &= \frac{\mathbf{p}}{m}, \\
 \mathbf{E}(X) &= -(\nabla_{\mathbf{R}}\Phi(X) + \partial_T\mathbf{A}(X)), \\
 \mathbf{B}(X) &= \nabla_{\mathbf{R}} \wedge \mathbf{A}(X), \\
 \mathbf{F}(X, p) &= -e(\mathbf{E}(X) + \mathbf{v} \wedge \mathbf{B}(X)).
 \end{aligned} \tag{2.72}$$

We now define the gauge invariant distribution function

$$\tilde{f}(X, \mathbf{p}) \equiv \frac{1}{2} \left(1 - \frac{i}{2\pi} \int d\epsilon \tilde{G}(X, p) \right), \tag{2.73}$$

take the Keldysh component of Eq. (2.71) and perform once more the ϵ -integration with the more satisfactory result

$$[\partial_T + \mathbf{v} \cdot \nabla_{\mathbf{R}} + \mathbf{F} \cdot \nabla_{\mathbf{p}}] \tilde{f}(X, \mathbf{p}) = 0. \tag{2.74}$$

The procedure to obtain a gauge invariant Eilenberger equation is similar but a little more delicate. We saw this already in the previous Section: to standard quasiclassical accuracy terms that in the Dyson equation are proportional to $\nabla_{\mathbf{p}}\tilde{G}$ get dropped after the ξ -integration. However, it is precisely these terms that allow one to construct a gauge invariant equation, and they cannot be discarded.

Knowing this, the ξ -integration of Eq. (2.71) leads to

$$\left[\partial_T + v_F \hat{\mathbf{p}} \cdot \nabla_{\mathbf{R}} - ev_F \mathbf{E} \cdot \hat{\mathbf{p}} \partial_\epsilon + e \frac{\mathbf{E} \cdot \hat{\mathbf{p}}}{p_F} + \frac{\mathbf{F}(p_F, \varphi) \cdot \hat{\boldsymbol{\varphi}}}{p_F} \partial_\varphi \right] \tilde{g}^K(\epsilon, \varphi; X) = 0. \tag{2.75}$$

Note that Φ is the scalar potential, while φ is the angle of the momentum, $\hat{\mathbf{p}} = (\cos \varphi, \sin \varphi)$, $\hat{\boldsymbol{\varphi}} = (-\sin \varphi, \cos \varphi)$. The last term in square brackets contains the Lorentz force. We note that to leading order accuracy the effect of an applied electric field is quasiclassically handled through the “minimal substitution” $\nabla_{\mathbf{R}} \rightarrow \nabla_{\mathbf{R}} - e\mathbf{E}\partial_\epsilon$.

Integrating Eq. (2.75) over the energy and averaging over the angle – taking now into account the prefactors given by Eqs. (2.66) and (2.54) – must lead to the continuity equation. This reads

$$\begin{aligned} \partial_T \left[-N_0\pi \langle \int d\epsilon \tilde{g}^K(\epsilon, \varphi; X) \rangle \right] + \nabla_{\mathbf{R}} \cdot \left[-N_0\pi \langle \int d\epsilon v_F \hat{\mathbf{p}} \tilde{g}^K(\epsilon, \varphi; X) \rangle \right] = \\ \partial_T \rho(X) + \nabla_{\mathbf{R}} \cdot \mathbf{j}(X) = 0. \end{aligned} \quad (2.76)$$

The observables $\rho(X)$ and $\mathbf{j}(X)$ are thus conveniently expressed in terms of the gauge-invariant \tilde{g}^K . Moreover, since from Eq. (2.70) one has

$$\begin{aligned} \tilde{g}(\epsilon, \hat{\mathbf{p}}) &= \frac{i}{\pi} \int d\xi \tilde{G}(\epsilon, \mathbf{p}) \\ &= \frac{i}{\pi} \int d\xi G(\epsilon - e\Phi(X), \mathbf{p} - e\mathbf{A}(X)) \\ &= \frac{i}{\pi} \int d\xi [G(\epsilon, \mathbf{p}) - e\Phi(X)\partial_\epsilon G - e\mathbf{A} \cdot \nabla_{\mathbf{p}} G] \\ &= \left[1 - e\Phi(X)\partial_\epsilon + e \frac{\mathbf{A}(X)}{p_F} (\hat{\mathbf{p}} - \hat{\boldsymbol{\varphi}}\partial_\varphi) \right] g(\epsilon, \mathbf{p}), \end{aligned} \quad (2.77)$$

then

$$\rho(X) = -2N_0 \left[\frac{\pi}{2} \langle \int \frac{d\epsilon}{2\pi} g^K(\epsilon, \varphi; X) \rangle - e\Phi(X) \right] \quad (2.78)$$

and

$$\mathbf{j}(X) = -N_0\pi \langle \int \frac{d\epsilon}{2\pi} \left[v_F \hat{\mathbf{p}} g^K(X, \epsilon, \hat{\mathbf{p}}) + \left(\frac{e\mathbf{A}(X) \cdot \hat{\boldsymbol{\varphi}}}{m} \right) \hat{\boldsymbol{\varphi}} g^K(\epsilon, \varphi; X) \right] \rangle. \quad (2.79)$$

The expression for the density is the same as in Section 2.2, whereas the one for the current is modified by a sub-leading contribution due to the transverse component of the vector potential.

A similar procedure can be followed in order to obtain a $SU(2)$ -covariant formulation of quasiclassics. This could prove very useful for systems in which spin-orbit interaction is present, as the latter can often be introduced via a $SU(2)$

gauge transformation, much in the same way as the electromagnetic field has now been introduced through the $U(1)$ gauge. We will briefly comment on this in Chapter 6.

Chapter 3

Quantum wells

Since our main goal is the description of spin-electric effects in low-dimensional systems, it is time to spend a few words answering the following questions:

1. what are these “low-dimensional systems” we talk about?
2. how do we model and describe them?

Let us see.

3.1 2D systems in the real world

The engineering of low-dimensional semiconductor-based structures is a vast and nowadays well established field of solid state physics. We refer the interested reader to [29, 48–50] and limit ourselves to an extremely succinct overview. Two-dimensional, one-dimensional (quantum wires) and zero-dimensional (quantum dots) systems can be realized, the first – which we will refer to as “quantum wells” – being the object of our interest. These are typically realized by growing layers of materials with different band structures, whose properties can then be fine-tuned exploiting strains – that is, effects due to mismatched lattice parameters in different layers – and doping, with the goal of creating a potential well for the conduction electrons (holes) of the desired characteristics. This is shown schematically in Fig. 3.1 for the typical example of a GaAs/GaAlAs modulation-doped heterostructure. More generally one speaks of III-V (e.g. GaAs-based) and II-VI (e.g. CdTe-based) heterostructures. A typical quantum well has a width in the

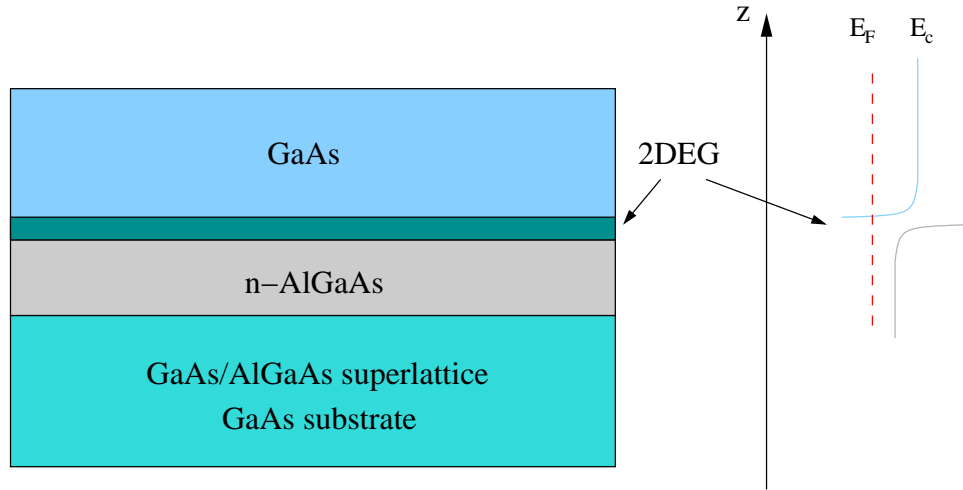


Figure 3.1: Scheme of a modulation-doped heterostructure based on the experimental setup from [51]. Of course, other types of structures exist, one popular example being the symmetric sandwich AlGaAs/GaAs/AlGaAs.

range $2 \div 20$ nm, and electron mobilities which can be as high as $10^6 \div 10^8 \text{ cm}^2/\text{Vs}$ – that is, roughly 4 orders of magnitude higher than high purity bulk GaAs – , which translate to mean free paths of more than $100 \mu\text{m}$ [52, 53]. Such high mobilities are achieved thanks to modulation doping (see Fig. 3.2). This spatially separates the conduction electrons from the donor impurities whence they come, the latter being instead a source of scattering in standard p-n junctions. Finally, its energy depth is usually in the range $0.2 \div 0.5$ eV, whereas the gap E_g , i.e. the difference between the conduction band minimum and the top of the valence band inside the well, is $1 \div 3$ eV.

For semiconductors, it is in low-dimensional systems of the kind now described that the spin Hall effect and its related phenomena mentioned in Chapter 1 have been observed, whereas experiments in metals have been based on thin films and nanowires with typical thicknesses of $4 \div 40$ nm. We will come back to this in Chapter 5.

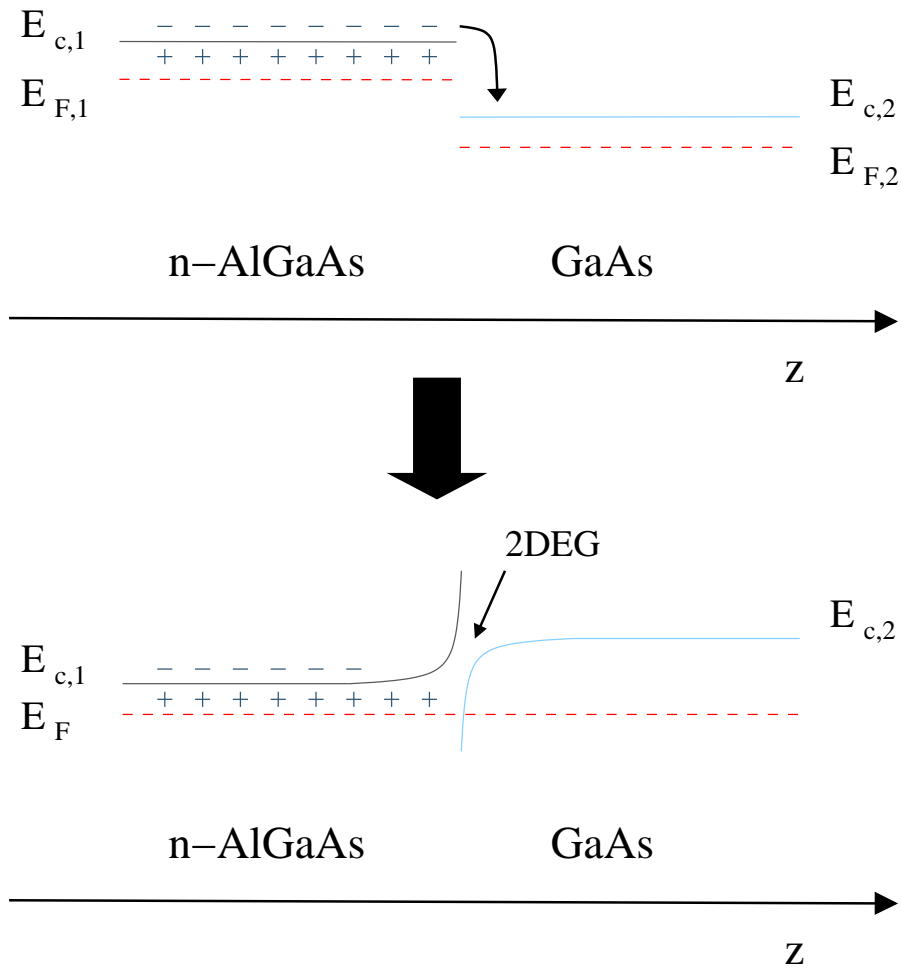


Figure 3.2: Schematic representation of the effect of modulation doping on the conduction band at an n-GaAlAs/GaAs interface. The Fermi level on the n-GaAlAs side is higher than on the GaAs one, the former having a bigger gap. Matching the two sides means that the electrons released by the donor impurities, e.g. Si, move to the GaAs layer until equilibrium is reached and the Fermi levels are aligned. The electrons are thus trapped at the interface in an asymmetric quantum well, and at the same time separated from the donor impurities.

3.2 The theory: effective Hamiltonians

The motion of charge carriers in a quantum well is a rather complicated matter. The goal is to describe it in terms of an effective Hamiltonian which, obtained through various approximations, catches to leading order all the relevant physics one is interested in. In our case that means the effects due to the band structure of the system, to disorder, to the external fields and, most importantly, to spin-orbit coupling. This is achieved via the Luttinger-Kohn method [54], also called $\mathbf{k} \cdot \mathbf{p}$ model, which will be now briefly outlined without a proper discussion – some additional details are given in Appendix E, but for a thorough treatment see [40, 49, 54–59]. We start with a couple of basic considerations.

1. We are concerned with conduction band electrons in zincblende crystals, e.g. III-V and II-VI compounds. The zincblende structure has no inversion symmetry. Energy level degeneracies present in diamond-like materials like Ge and Si, which are due to the combined effect of time-inversion \mathcal{T} and space-inversion \mathcal{S} symmetry, can be lifted in zincblende crystals by spin-orbit interaction alone, that is, without the need for external magnetic fields. Indeed, given an energy level $E_{\pm}(\mathbf{k})$, $\pm \leftrightarrow$ spin up/down, one has

$$E_{\pm}(\mathbf{k}) \xrightarrow{\mathcal{T}} E_{\mp}(-\mathbf{k}) \xrightarrow{\mathcal{S}} E_{\mp}(\mathbf{k}) \Rightarrow E_{\pm}(\mathbf{k}) = E_{\mp}(\mathbf{k}) \quad (3.1)$$

only for inversion-symmetric materials. A similar degeneracy-lifting effect can be achieved in two-dimensional systems when the inversion symmetry along the growth direction, i.e. perpendicular to the system itself, is broken by the confining potential.

2. The carrier concentration in a two-dimensional system is typically $10^{15} \div 10^{16}/\text{m}^2$, that is, several orders of magnitude smaller than the number of available states in a given band [48]. Thus, only the states close to the band minimum (or the maximum in the case of holes) will be occupied.
3. We wish to treat the carriers as free particles with a renormalized mass, i.e. in the so-called effective mass approximation commonly used in solid state physics. This is of course sound in perfect crystals, and proves to be so as long as the spatial variations of the perturbing fields, due to impurities,

strains or external fields, are much slower than that of the lattice potential, and the energy of the carriers remains much smaller than the gap energy E_g .

The single-particle Schrödinger equation for an electron in a lattice described by the potential $U(\mathbf{x})$ and in the presence of spin-orbit coupling reads

$$\begin{aligned} H_0 \Psi_{\nu\mathbf{k}}(\mathbf{x}) &= \left[\frac{(-i\hbar\nabla)^2}{2m_0} + U(\mathbf{x}) + \frac{\hbar}{4m_0^2 c^2} \nabla U(\mathbf{x}) \wedge (-i\hbar\nabla) \cdot \boldsymbol{\sigma} \right] \Psi_{\nu\mathbf{k}}(\mathbf{x}) \\ &= \epsilon_{\nu\mathbf{k}} \Psi_{\nu\mathbf{k}}(\mathbf{x}), \end{aligned} \quad (3.2)$$

where ν is the band index, m_0 the bare electron mass, and where we momentarily reintroduced \hbar and c to be explicit, though these will now be dropped once more. According to Bloch's theorem, the translational symmetry of the problem requires the wave function to be of the form

$$\Psi_{\nu\mathbf{k}}(\mathbf{x}) = e^{i\mathbf{k}\cdot\mathbf{x}} u_{\nu\mathbf{k}}(\mathbf{x}) \quad (3.3)$$

with $u_{\nu\mathbf{k}}(\mathbf{x})$ a function with the periodicity of the lattice. In GaAs the bottom of the conduction band – and the maximum of the valence one, since it is a direct-gap semiconductor – lies at the Γ point $\mathbf{k} = 0$. Then (3.3) can be expanded in the basis¹ $u_{\nu 0}(\mathbf{x}) = \langle \mathbf{x} | u_{\nu 0} \rangle$

$$u_{\nu\mathbf{k}}(\mathbf{x}) = \sum_{\nu'} c_{\nu\nu'\mathbf{k}} u_{\nu'0}(\mathbf{x}). \quad (3.4)$$

In such a basis, and using ket notation, one obtains the matrix elements

$$\begin{aligned} [H_0]_{\nu\nu'} &= \langle u_{\nu 0} | H_0 | u_{\nu' 0} \rangle \\ &= \left(\epsilon_{\nu 0} + \frac{\hbar^2 k^2}{2m_0} \right) \delta_{\nu\nu'} + \frac{\hbar}{m_0} \mathbf{k} \cdot \boldsymbol{\pi}_{\nu\nu'}, \end{aligned} \quad (3.5)$$

where $\epsilon_{\nu 0}$ is the energy offset of the band at $\mathbf{k} = 0$

$$\left[\frac{(-i\nabla)^2}{2m_0} + U + \frac{\hbar}{4m_0} \nabla U \wedge (-i\nabla) \cdot \boldsymbol{\sigma} \right] |u_{\nu 0}\rangle = \epsilon_{\nu 0} |u_{\nu 0}\rangle \quad (3.6)$$

and

$$\begin{aligned} \boldsymbol{\pi}_{\nu\nu'} &= \langle u_{\nu 0} | (-i\nabla) + \frac{\hbar}{4m_0} \nabla U \wedge \boldsymbol{\sigma} | u_{\nu' 0} \rangle \\ &\approx \langle u_{\nu 0} | (-i\nabla) | u_{\nu' 0} \rangle. \end{aligned} \quad (3.7)$$

¹The Luttinger-Kohn machinery can equally well deal with situations in which the band minimum is at $\mathbf{k}_0 \neq 0$, or in which more minima are present – e.g. in Si. See [54].

From Eqs. (3.6) and (3.7) one sees that the spin-orbit coupling is taken into account in the diagonal terms $\epsilon_{\nu 0}$ only (see Appendix E). For the expansion (3.4) to be of any real use, the basis $u_{\nu 0}(\mathbf{x})$ has to be truncated, and only the bands closest to the gap are considered. This leads to the so-called 8×8 Kane model [56] when two degenerate s -wave conduction bands and 6 p -wave valence bands are taken into account.² The latter are partially split by spin-orbit coupling into two groups, the first made of four degenerate levels, the light and heavy hole bands, and the other of two so-called split-off levels. This is schematically shown in Fig. 3.3. The simple 8×8 model includes only three parameters, the gap and split-off energies, E_g and Δ , and the matrix element of the momentum operator between s - and p -wave states. It loses however accuracy with growing gap energy E_g , and is not sufficient for properly treating holes in the valence bands.

The inclusion of the effects due to perturbing potentials – i.e. anything other than the crystal potential U – is done straightforwardly. Let us consider the Hamiltonian

$$(H_0 + V) \psi = \epsilon \psi, \quad (3.8)$$

with V slowly varying as compared to U . One then assumes that the band structure of the problem is not appreciably modified, so that the functions $u_{\nu 0}$ can still be used as a basis, and factorizes the high- (“fast”) and low- (“slow”) energy modes of the wavefunction ψ . In ket notation

$$|\psi\rangle = \sum_{\nu} \phi_{\nu}(\mathbf{x}) |u_{\nu 0}\rangle, \quad (3.9)$$

where $\phi_{\nu}(\mathbf{x})$ are envelopes varying on a scale much bigger than the lattice spacing, and which encode all information pertaining to the low energy phenomena introduced by V . Their equation of motion reads

$$H_{\nu\nu'} \phi_{\nu'}(\mathbf{x}) = \epsilon \phi_{\nu}(\mathbf{x}). \quad (3.10)$$

To be explicit, considering the more general case of an applied electromagnetic field and taking for V the total non-crystal potential – e.g. arising from impurities, confinement, strains and, of course, the driving electric field – the matrix elements

²It is sometimes necessary to consider the coupling between a larger number of bands, leading to higher-dimensional models.

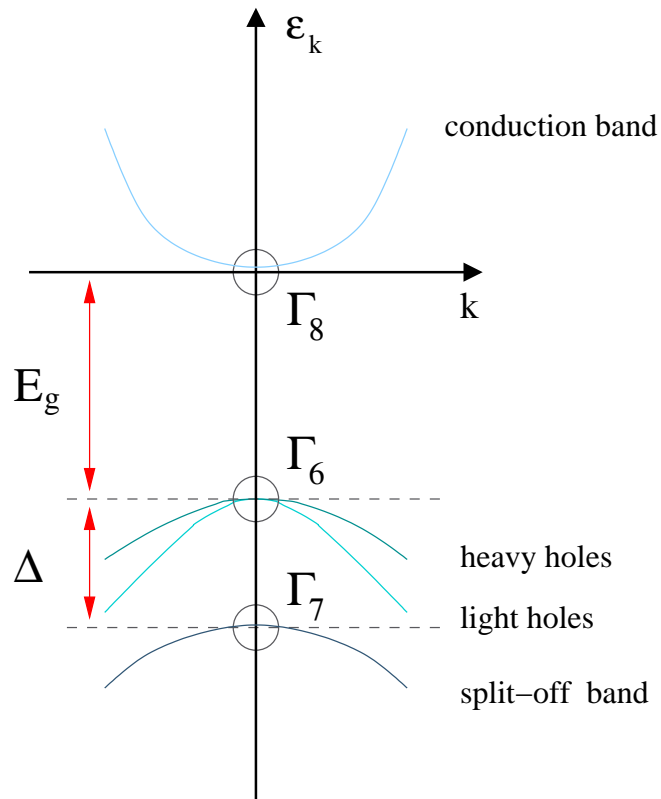


Figure 3.3: Schematic band structure at the Γ -point for the 8×8 Kane model. Spin-orbit interaction splits the six p -like valence levels into the light and heavy hole bands, with total angular momentum $J = 3/2$, and the split-off band, with $J = 1/2$. The circles identify the energy offsets $\epsilon_{\nu 0}$. The Γ 's indicate the symmetry properties of the levels (see Appendix E).

$H_{\nu\nu'}$ become

$$H_{\nu\nu'} = \left[\left(\epsilon_{\nu 0} + \frac{\tilde{k}^2}{2m} + V \right) \delta_{\nu\nu'} + \frac{1}{m_0} \tilde{\mathbf{k}} \cdot \boldsymbol{\pi}_{\nu\nu'} \right], \quad (3.11)$$

with $\tilde{\mathbf{k}} = -i\nabla + e\mathbf{A}$. We remark that, in line with the factorization (3.9), the offset energies $\epsilon_{\nu 0}$ are not modified, and thus the leading spin-orbit coupling term – actually the only such term retained – is left untouched.

As a final step in obtaining a lower-dimensional effective Hamiltonian describing the motion of electrons in the conduction band, the full Hamiltonian (3.11) is block-diagonalized using the Löwdin technique³ [60]. For clarity's sake we stick to the 8×8 model and write in explicit matrix notation

$$\begin{aligned} H \begin{pmatrix} \phi_c \\ \phi_v \end{pmatrix} &= \begin{pmatrix} [H_c]_{2 \times 2} & [H_{cv}]_{2 \times 6} \\ [H_{cv}^\dagger]_{6 \times 2} & [H_v]_{6 \times 6} \end{pmatrix} \begin{pmatrix} \phi_c \\ \phi_v \end{pmatrix} \\ &= \epsilon \begin{pmatrix} \phi_c \\ \phi_v \end{pmatrix}, \end{aligned} \quad (3.12)$$

with ϕ_c and ϕ_v respectively a two-dimensional and a six-dimensional spinor for the conduction and valence levels. If one assumes the energy separation between these two sets – i.e. $E_g \div E_g + \Delta$ – to be the biggest energy scale of the problem, or, in other words, that the two groups of states are far away from each other and thus weakly coupled, $H_{cv}, H_{cv}^\dagger \ll E_g \sim H_v$, it is possible to write a 2×2 equation

$$\mathcal{H}(\epsilon) \bar{\phi} = \epsilon \bar{\phi}, \quad (3.13)$$

with

$$\mathcal{H}(\epsilon) = H_c + H_{cv} (\epsilon - H_v)^{-1} H_{cv}^\dagger \quad (3.14)$$

and $\bar{\phi}$ a renormalized conduction band spinor. When (3.14) is expanded for energies close to the band minimum and inserted back into Eq. (3.13), the effective eigenvalue equation for $\bar{\phi}$ is obtained. All effects of the coupling with the valence bands are thus taken into account by a renormalization of the effective mass, the

³This is basically a reformulation of standard perturbation theory particularly well suited to treating degenerate states. See Appendix E.

g -factor, the spin-orbit coupling constant and the spinor ϕ . Explicitly⁴ [57]

$$\left\{ \frac{[(-i\nabla) + e\mathbf{A}]^2}{2m^*} + V - \frac{\mu_B g^*}{2} \boldsymbol{\sigma} \cdot \mathbf{B} + \lambda \boldsymbol{\sigma} \cdot [(-i\nabla) + e\mathbf{A}] \wedge \nabla V \right\} \bar{\phi} = \epsilon \bar{\phi}, \quad (3.15)$$

with μ_B the Bohr magneton, m^* and g^* the renormalized mass and g -factor, $\mathbf{B} = \nabla \wedge \mathbf{A}$ the magnetic field and λ the spin-orbit coupling constant. All of these quantities are explicitly written in terms of the matrix elements of the Hamiltonian in Appendix E, Eqs. (E.19)–(E.21). The quantity λ is of fundamental importance for our purposes. The spin-orbit term in the above has the very same structure of the Thomas term appearing in the Pauli equation,⁵ where, however, this is only a very small relativistic correction in which the vacuum constant λ_0 appears. On the contrary, in a solid λ can be as much as six orders of magnitude larger than λ_0 . Moreover

$$\lambda \sim \left(\frac{1}{E_g^2} - \frac{1}{(E_g + \Delta)^2} \right). \quad (3.16)$$

This simple equation, together with Eq. (3.15), shows how spin-orbit coupling in the band structure – i.e. in the diagonal offset energies $\epsilon_{\nu 0}$ where Δ appears – can induce spin-orbit effects in conduction band electrons as soon as these are subject to some non-crystalline potential V . One talks about *extrinsic* effects when V is due to impurities, and about *intrinsic* ones when it is due to an external potential like, say, the confining one in the case of a quantum well. The Hamiltonian appearing in Eq. (3.15) can be conveniently rewritten as

$$H = \frac{k^2}{2m^*} + V - \mathbf{b}'(\mathbf{k}) \cdot \boldsymbol{\sigma}, \quad (3.17)$$

where $\mathbf{k} = -i\nabla + e\mathbf{A}$ and $\mathbf{b}'(\mathbf{k})$ contains the contributions due to both the external field (\mathbf{B}) and the \mathbf{k} -dependent internal (spin-orbit induced) one,

$$\mathbf{b}'(\mathbf{k}) = \mathbf{b}_{ext} + \mathbf{b}(\mathbf{k}). \quad (3.18)$$

For the case of a two-dimensional system realized via an asymmetric confining potential $V = V(z)$ the Rashba model is obtained

$$\mathbf{b}(\mathbf{k}) \cdot \boldsymbol{\sigma} \rightarrow \mathbf{b}_R(\mathbf{k}) \cdot \boldsymbol{\sigma} = \alpha(k_x \sigma_y - k_y \sigma_x) = \alpha \hat{\mathbf{z}} \wedge \mathbf{k} \cdot \boldsymbol{\sigma}, \quad (3.19)$$

⁴We are not interested in the physics of the Darwin term ($\sim \nabla U \cdot (-i\nabla)$), so we neglect it. Also, the offset energy of the conduction band is set to zero, $\epsilon_{c0} = 0$.

⁵Formally, this is because both Eq. (3.15) and the Pauli equation are obtained using the same kind of perturbative expansion. In the second case the starting point is the 4×4 Dirac Hamiltonian.

with α a function of $V(z)$, and as such tunable via the gates. Of course, since the motion is two-dimensional, averaging over the growth direction \hat{z} should be performed, and is actually implied in the above definition of α . Since the z -average $\langle V \rangle$ is a constant we set it to zero, and the complete Rashba Hamiltonian reads

$$H = \frac{k^2}{2m^*} - \mathbf{b}_R(\mathbf{k}) \cdot \boldsymbol{\sigma}. \quad (3.20)$$

It is important to remember that other mechanisms which give rise to similar spin-orbit interaction terms are also possible, albeit in the context of more elaborate models. Indeed, in an extended 14×14 Kane model for zincblende crystals the following cubic-in-momentum term, called the cubic Dresselhaus term [61], is obtained [55]

$$\mathbf{b}_D(\mathbf{k}) \cdot \boldsymbol{\sigma} = \mathcal{C}k_x(k_z^2 - k_y^2)\sigma_x + \text{cyclic permutations}, \quad (3.21)$$

with \mathcal{C} a crystal-dependent constant. Once again, if we consider electrons in a two-dimensional quantum well, the average $\langle H_D \rangle$ along the growth direction \hat{z} – which we assume parallel to the [001] crystallographic direction – should be taken. k_z is quantized, with $\langle k_z^2 \rangle \sim (\pi/d)^2$, d being the width of the well. The main bulk-inversion-asymmetry contribution is then

$$[\mathbf{b}_D(\mathbf{k})]_{2d} \cdot \boldsymbol{\sigma} = \beta(k_x\sigma_x - k_y\sigma_y), \quad (3.22)$$

with $\beta \approx \mathcal{C}(\pi/d)^2$. Even though both (3.19) and (3.22) can be written in the same form, one should notice that in the second case the effective spin-orbit coupling constant β depends only on the crystal structure, whereas in the Rashba model α is different from zero only in the presence of the additional non-crystalline and asymmetric potential. The Rashba and Dresselhaus spin-orbit interactions can be of comparable magnitudes, the dominance of one or the other being determined by the specific characteristics of the system, and both give rise to an energy splitting which is usually much smaller than the Fermi energy,⁶ $|\mathbf{b}_R|, |\mathbf{b}_D| \ll \epsilon_F$.

With this we conclude the Chapter, and for more details about the material treated we refer to the literature. In all of the rest a general Hamiltonian of the form

$$H = \frac{p^2}{2m} - \mathbf{b}(\mathbf{p}) \cdot \boldsymbol{\sigma} + V_{imp} \quad (3.23)$$

⁶With typical densities in the range $10^{15} \div 10^{16} \text{ m}^{-2}$, one has $\epsilon_F \sim 10 \text{ meV}$ and $|\mathbf{b}_R|, |\mathbf{b}_D| \sim 10^{-1} \epsilon_F$. See for example [62–70].

will be considered, with $|\mathbf{b}| \ll \epsilon_F$ and V_{imp} the random impurity potential, possibly spin-dependent. The explicit form of both \mathbf{b} and V_{imp} will be specified whenever needed. Also, to adjust back to the notation of Chapter 2, we use \mathbf{p} , rather than \mathbf{k} , for the momentum. External fields will be introduced when necessary via the electromagnetic potentials (Φ, \mathbf{A}) .

Chapter 4

Quasiclassics and spin-orbit coupling

We present original material concerning the derivation of the Eilenberger equation for a two-dimensional fermionic system with spin-orbit coupling. Such a generalized equation will be applied to some problems of interest in Chapter 5. These results were published in [71] and [72], along whose lines we will move: Sections 4.1 and 4.1.1 are based on [71], Section 4.2 on [72].

4.1 The Eilenberger equation

We start from the Hamiltonian

$$H = \frac{p^2}{2m} - \mathbf{b}(\mathbf{p}) \cdot \boldsymbol{\sigma}, \quad (4.1)$$

where \mathbf{b} is the internal effective magnetic field due to spin-orbit coupling and $\boldsymbol{\sigma}$ is the vector of Pauli matrices. We are describing motion in a two-dimensional system, i.e. $\mathbf{p} = (p_x, p_y)$, and $\hat{\mathbf{z}}$ will from now on define the direction orthogonal to the plane. In the Rashba model for example $\mathbf{b} = \alpha \hat{\mathbf{z}} \wedge \mathbf{p}$. For a spin-1/2 particle one can write the spectral decomposition of the Hamiltonian in the form

$$H = \epsilon_+ |+\rangle\langle+| + \epsilon_- |-\rangle\langle-|, \quad (4.2)$$

where $\epsilon_{\pm} = p^2/2m \pm |\mathbf{b}|$ are the eigenenergies corresponding to the projectors

$$|\pm\rangle\langle\pm| = \frac{1}{2} \left(1 \mp \hat{\mathbf{b}} \cdot \boldsymbol{\sigma} \right), \quad (4.3)$$

$\hat{\mathbf{b}}$ being the unit vector in the \mathbf{b} direction. As explained in Chapter 2, to obtain the quasiclassical kinetic equation one has to sooner or later perform a ξ -integration. With this purpose we make for the Green's function the ansatz

$$\check{G} = \left(\begin{array}{cc} G^R & G^K \\ 0 & G^A \end{array} \right) = \frac{1}{2} \left\{ \left(\begin{array}{cc} G_0^R & 0 \\ 0 & -G_0^A \end{array} \right), \left(\begin{array}{cc} \check{g}^R & \check{g}^K \\ 0 & \check{g}^A \end{array} \right) \right\}, \quad (4.4)$$

where the curly brackets denote the anticommutator, $\check{G} = \check{G}_{t_1, t_2}(\mathbf{p}, \mathbf{R})$ and $\check{g} = \check{g}_{t_1, t_2}(\hat{\mathbf{p}}, \mathbf{R})$. $G_0^{R,A}$ are the retarded and advanced Green's functions in the absence of external perturbations,

$$G_0^{R(A)} = \frac{1}{\epsilon + \mu - p^2/2m + \mathbf{b} \cdot \boldsymbol{\sigma} - \Sigma^{R(A)}}, \quad (4.5)$$

and $\Sigma^{R(A)}$ are the retarded and advanced self-energies which will be specified below. The physical meaning of such an ansatz will become clear in the next Section. For now it suffices to see that it is such that in equilibrium \check{g} takes the form

$$\check{g} = \left(\begin{array}{cc} 1 & 2 \tanh(\epsilon/2T) \\ 0 & -1 \end{array} \right). \quad (4.6)$$

The main assumption for the following is that we can determine \check{g} such that it does not depend on the modulus of the momentum \mathbf{p} but only on the direction $\hat{\mathbf{p}}$. Under this condition \check{g} is directly related to the ξ -integrated Green's function \check{g} , as defined in Eq. (2.54)

$$\check{g} = \frac{i}{\pi} \int d\xi \check{G}, \quad \xi = p^2/2m - \mu. \quad (4.7)$$

For convenience we suppressed in the equations above spin and time arguments of the Green's function, $\check{g} = \check{g}_{t_1 s_1, t_2 s_2}(\hat{\mathbf{p}}, \mathbf{R})$. In some cases Wigner coordinates for the time arguments are more convenient, $\check{g} \rightarrow \check{g}_{s_1 s_2}(\hat{\mathbf{p}}, \epsilon; \mathbf{R}, T)$.

We evaluate the ξ -integral explicitly in the limit where $|\mathbf{b}|$ is small compared to the Fermi energy. Since the main contributions to the ξ -integral are from the region near zero, it is justified to expand \mathbf{b} for small ξ , $\mathbf{b} \approx \mathbf{b}_0 + \xi \partial_\xi \mathbf{b}_0$, with the final result

$$\check{g} \approx \frac{1}{2} \{1 + \partial_\xi \mathbf{b}_0 \cdot \boldsymbol{\sigma}, \check{g}\}, \quad (4.8)$$

$$\check{g} \approx \frac{1}{2} \{1 - \partial_\xi \mathbf{b}_0 \cdot \boldsymbol{\sigma}, \check{g}\}. \quad (4.9)$$

In the equation of motion we will also have to evaluate integrals of a function of \mathbf{p} and a Green's function. Assuming again that $|\mathbf{b}| \ll \epsilon_F$ we find

$$\frac{i}{\pi} \int d\xi f(\mathbf{p}) \check{G} \approx f(\mathbf{p}_+) \check{g}_+ + f(\mathbf{p}_-) \check{g}_-, \quad (4.10)$$

where \mathbf{p}_\pm is the Fermi momentum in the \pm -subband including corrections due to the internal field, $|\mathbf{p}_\pm| \approx p_F \mp |\mathbf{b}|/v_F$, and

$$\check{g}_\pm = \frac{1}{2} \left\{ \frac{1}{2} \mp \frac{1}{2} \hat{\mathbf{b}}_0 \cdot \boldsymbol{\sigma}, \check{g} \right\}, \quad \check{g} = \check{g}_+ + \check{g}_-. \quad (4.11)$$

Following the procedure presented in Chapter 2 one can derive the equation of motion for \check{g} . From the Dyson equation and after a gradient expansion one obtains for the Green's function \check{G}

$$\partial_T \check{G} + \frac{1}{2} \left\{ \frac{\mathbf{p}}{m} - \nabla_{\mathbf{p}}(\mathbf{b} \cdot \boldsymbol{\sigma}), \nabla_{\mathbf{R}} \check{G} \right\} - i[\mathbf{b} \cdot \boldsymbol{\sigma}, \check{G}] = -i[\check{\Sigma}, \check{G}]. \quad (4.12)$$

The ξ -integration of Eq. (4.12), retaining terms up to first order in $|\mathbf{b}|/\epsilon_F$, leads to an Eilenberger equation of the form

$$\sum_{\nu=\pm} (\partial_T \check{g}_\nu + \frac{1}{2} \left\{ \frac{\mathbf{p}_\nu}{m} - \nabla_{\mathbf{p}}(\mathbf{b}_\nu \cdot \boldsymbol{\sigma}), \nabla_{\mathbf{R}} \check{g}_\nu \right\} - i[\mathbf{b}_\nu \cdot \boldsymbol{\sigma}, \check{g}_\nu]) = -i[\check{\Sigma}, \check{g}]. \quad (4.13)$$

The self-energy depends on the kind of disorder considered, and is discussed in some detail in Appendix D. If not otherwise specified we will consider as a reference the simplest case, i.e. non-magnetic, elastic and short-range scatterers (δ -like impurities) in the Born approximation. In this case one has $\check{\Sigma} = -i\langle \check{g} \rangle / 2\tau$, $\langle \dots \rangle$ denoting the angular average over $\hat{\mathbf{p}}$.

To check the consistency of the equation we study at first its retarded component in order to verify that $\tilde{g}^R = 1$ solves the generalized Eilenberger equation. From Eq. (4.8) we find that

$$g^R = 1 + \partial_\xi(\mathbf{b}_0 \cdot \boldsymbol{\sigma}), \quad (4.14)$$

and using (4.11) we arrive at

$$g_\pm^R = (1 \mp \partial_\xi b) \left(\frac{1}{2} \mp \frac{1}{2} \hat{\mathbf{b}}_\mp \cdot \boldsymbol{\sigma} \right). \quad (4.15)$$

Both commutators, on the left and on the right hand side of the Eilenberger equation, are zero, at least to first order in the small parameter $\partial_\xi \mathbf{b}_0$, e.g. α/v_F in the

case of the Rashba model. Analogous results hold for the advanced component $g^A = -g^R$, and similar arguments may also be used to verify that the equilibrium Keldysh component of the Green's function, $g^K = \tanh(\epsilon/2T)(g^R - g^A)$, solves the equation of motion. Additionally, Eq. (4.14) shows how the normalization condition, Eq. (2.63), changes in the presence of spin-orbit coupling

$$\check{g}^2 = \check{1} \rightarrow \check{g}^2 = (1 + 2\partial_\xi \mathbf{b}_0 \cdot \boldsymbol{\sigma} + \mathcal{O}[(\partial_\xi \mathbf{b}_0)^2]) \check{1}, \quad (4.16)$$

where $\check{1}$ denotes the identity matrix in Keldysh space.

It is worthwhile to remark that the validity of Eq. (4.13) extends from the diffusive to the ballistic regime. These are defined by the relative strength of the disorder broadening $1/\tau$ compared to the spin-orbit energy $|\mathbf{b}_0|$

$$|\mathbf{b}_0|\tau \gg 1 \Rightarrow \text{weak disorder, "clean" system}, \quad (4.17)$$

$$|\mathbf{b}_0|\tau \ll 1 \Rightarrow \text{strong disorder, "dirty" system}. \quad (4.18)$$

Indeed, the quasiclassical technique does not fix the relation between $|\mathbf{b}_0|$ and $1/\tau$.

4.1.1 The continuity equation

In a system such as the one we are considering the spin is not conserved, so care is needed when talking about spin currents. We define these as

$$j_{s_k}^i = \frac{1}{2} \{ \mathbf{v}_i, s_k \}, \quad (4.19)$$

where $s_k, k = x, y, z$ is the spin-polarization, $i = x, y, z$ is the direction of the flow and $\mathbf{v} = -i[\mathbf{x}, H]$. Besides being the most used in the literature [21, 73–76], such a definition has a clear physical meaning. Moreover, it agrees with what one would obtain starting from an $SU(2)$ -covariant formulation of the Hamiltonian (4.1) [77]. However, it defines a non-conserved current, and therefore in the continuity equation for the spin there will appear source terms. When taking the angular average of the Eilenberger equation (4.13), the r.h.s. vanishes and we are left with a set of continuity equations for the charge and spin components of the

Green's function. With $\check{g}_{ss'} = \check{g}_0 \delta_{ss'} + \check{\mathbf{g}} \cdot \boldsymbol{\sigma}_{ss'}$ these read

$$\partial_t \langle \check{g}_0 \rangle + \partial_{\mathbf{x}} \cdot \check{\mathbf{J}}_c = 0, \quad (4.20)$$

$$\partial_t \langle \check{g}_x \rangle + \partial_{\mathbf{x}} \cdot \check{\mathbf{J}}_{s_x} = -2 \sum_{\nu=\pm} \langle \mathbf{b}_\nu \wedge \check{\mathbf{g}}_\nu \rangle_{s_x}, \quad (4.21)$$

$$\partial_t \langle \check{g}_y \rangle + \partial_{\mathbf{x}} \cdot \check{\mathbf{J}}_{s_y} = -2 \sum_{\nu=\pm} \langle \mathbf{b}_\nu \wedge \check{\mathbf{g}}_\nu \rangle_{s_y}, \quad (4.22)$$

$$\partial_t \langle \check{g}_z \rangle + \partial_{\mathbf{x}} \cdot \check{\mathbf{J}}_{s_z} = -2 \sum_{\nu=\pm} \langle \mathbf{b}_\nu \wedge \check{\mathbf{g}}_\nu \rangle_{s_z}, \quad (4.23)$$

with

$$\check{\mathbf{J}}_{c,s} = \sum_{\nu=\pm} \left\langle \frac{1}{2} \left\{ \frac{\mathbf{p}_\nu}{m} - \frac{\partial}{\partial \mathbf{p}} (\mathbf{b}_\nu \cdot \boldsymbol{\sigma}), \check{g}_\nu \right\} \right\rangle_{c,s}. \quad (4.24)$$

As known from Chapter 2, the densities and currents are related to the Keldysh components of $\langle \check{g} \rangle$ and of $\check{\mathbf{J}}_{c,s}$ integrated over ϵ . Explicitly the particle and spin current densities are given by

$$\mathbf{j}_c(\mathbf{x}, t) = -\pi N_0 \int \frac{d\epsilon}{2\pi} \mathbf{J}_c^K(\epsilon; \mathbf{x}, t), \quad (4.25)$$

$$\mathbf{j}_{s_k}(\mathbf{x}, t) = -\frac{1}{2} \pi N_0 \int \frac{d\epsilon}{2\pi} \mathbf{J}_{s_k}^K(\epsilon; \mathbf{x}, t), \quad (4.26)$$

where $N_0 = m/2\pi$ is the density of states of the two-dimensional electron gas. In the absence of spin-orbit coupling ($\mathbf{b} = 0$) one recovers the well known expressions

$$\mathbf{j}_c(\mathbf{x}, t) = -\frac{1}{2} N_0 \int d\epsilon \langle \mathbf{v}_F g_0^K \rangle, \quad (4.27)$$

$$\mathbf{j}_{s_k}(\mathbf{x}, t) = -\frac{1}{4} N_0 \int d\epsilon \langle \mathbf{v}_F g_k^K \rangle. \quad (4.28)$$

In the presence of the field \mathbf{b} things are in general more complex. For the Rashba model, for example, the particle current is given by

$$\begin{aligned} \mathbf{j}_c(\mathbf{x}, t) = & -\frac{1}{2} N_0 \int d\epsilon [v_F \langle \hat{\mathbf{p}} g_0^K \rangle \\ & + \alpha (\hat{\mathbf{z}} \wedge \langle \mathbf{g}^K \rangle - \langle \hat{\mathbf{p}} (\hat{\mathbf{p}} \cdot \hat{\mathbf{z}} \wedge \mathbf{g}^K) \rangle)]. \end{aligned} \quad (4.29)$$

In Chapter 5 we will make extensive use of Eqs. (4.21), (4.22) and (4.23) in specific cases.

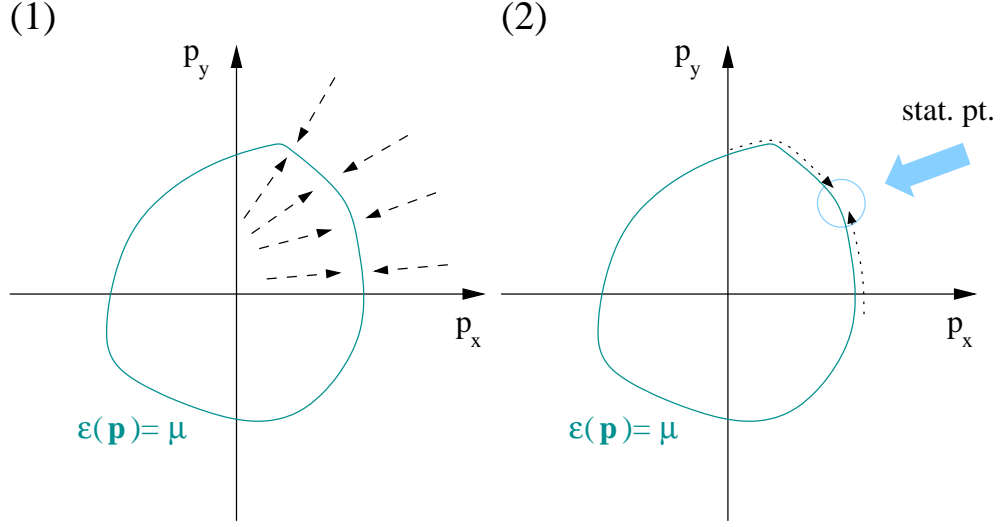


Figure 4.1: The idea behind the momentum integration. (1) Use the peak of $G(\mathbf{p}, \mathbf{R})$ to end up on the Fermi surface $\epsilon(\mathbf{p}) = \mu$. (2) Exploit the quick oscillations of $e^{i\mathbf{p}\mathbf{F}\cdot\mathbf{r}}$ to limit the integral to the stationary point region.

4.2 ξ -integration vs. stationary phase

Up to now we have rather mechanically relied on the ξ -integration procedure, as introduced in Chapter 2, to obtain quasiclassical expressions starting from the microscopic ones. To shed some light on the general physical meaning of such a procedure, and in particular on that of the ansatz used in Section 4.1, Eq. (4.4), we follow Shelankov's idea [78], which we aim at generalizing for spin-orbit coupled systems.

The idea itself can be stated as follows. The information carried by the Green's function pertaining to real space scales of the order of or smaller than the inverse Fermi momentum p_F^{-1} is quasiclassically not accessible. These “fast” – in the sense of high-momentum – components of the Green's function and its “slow” ones should then be factorized, with the goal of ending up with the kinetics of the latter only. The point is how to use the quasiclassical assumptions $p_F \gg |\mathbf{q}|$, $\epsilon_F \gg \omega$, with \mathbf{q}, ω the relevant momentum and energy scales of our problem, e.g. due to the presence of an external field, to obtain such a factorization. Indeed, as they imply that $G(\mathbf{p}, \mathbf{R})$ is peaked at the Fermi surface even when out of equilibrium,

they also suggest to handle the Wigner space momentum integration

$$G(\mathbf{r}, \mathbf{R}) = \int \frac{d\mathbf{p}}{(2\pi)^2} e^{i\mathbf{p}\cdot\mathbf{r}} G(\mathbf{p}, \mathbf{R}) \quad (4.30)$$

as shown in Fig. 4.1: $\int d\mathbf{p}/(2\pi)^2$ is first rewritten as an integral over the energy calculated from the Fermi level, $\epsilon(\mathbf{p}) - \mu$, and over the constant-energy surfaces \mathcal{S}

$$\int \frac{d\mathbf{p}}{(2\pi)^2} = \iint \frac{d[\epsilon(\mathbf{p}) - \mu]d\mathcal{S}}{(2\pi)^2 |\nabla_{\mathbf{p}}\epsilon(\mathbf{p})|}. \quad (4.31)$$

Then the fast modes of $G(\mathbf{p}, \mathbf{R})$, which carry the information about its peak, ensure that the dominant contribution to the $d[\epsilon(\mathbf{p}) - \mu]$ integration comes from the Fermi surface. When moving around it the exponential $e^{i\mathbf{p}\cdot\mathbf{r}} \approx e^{i\mathbf{p}_F\cdot\mathbf{r}}$ oscillates quickly – the quasiclassical condition implies $p_F r \gg 1$ – and as a consequence the surface integral $d\mathcal{S}_F$ can be evaluated in the stationary phase approximation.

The steps outlined here are the *leitmotiv* of the Section and need now be made explicit. For a number of details we refer to [78] and to Appendix F.

For clarity's sake we will first go through some calculations regarding the retarded component of the Green's function. Let us start by considering its space dependence in the case of free electrons in the absence of spin-orbit coupling

$$G^R(\mathbf{x}_1, \mathbf{x}_2) = \sum_{\mathbf{p}} \frac{e^{i\mathbf{p}\cdot\mathbf{r}}}{\omega - \xi + i0^+}, \quad \mathbf{r} = \mathbf{x}_1 - \mathbf{x}_2. \quad (4.32)$$

The stationary point of the exponential is given by the condition $\partial_{\mathbf{p}}\epsilon(\mathbf{p}) \propto \mathbf{r}$, i.e. the velocity has to be parallel or antiparallel to the line connecting the two space arguments. In the case of the retarded Green's function, the important region is that with velocity parallel to \mathbf{r} . Because of the spherical symmetry of the problem polar coordinates are the natural choice, with φ the angle between \mathbf{p} and \mathbf{r} . We then get

$$\begin{aligned} G^R(\mathbf{x}_1, \mathbf{x}_2) &= \int \frac{d\xi N(\xi)d\varphi}{2\pi} \frac{e^{i\mathbf{p}\cdot\mathbf{r}}}{\omega - \xi + i0^+} \\ &= -ie^{i(p_F + \omega/v_F)r} N_0 \int d\varphi e^{-i\varphi^2(p_F r)/2} \\ &= -\sqrt{\frac{2\pi i}{p_F r}} N_0 e^{i(p_F + \omega/v_F)r}, \end{aligned} \quad (4.33)$$

where the integration over the angle φ plays the role of that over the Fermi surface in the present case. One sees how the Green's function is factorized in a rapidly varying term $\sim e^{ip_F r} / \sqrt{p_F r}$, and a slow one, $e^{i(\omega/v_F)r}$. This suggests to write quite generally – now in Wigner coordinates

$$\begin{aligned} G^R(\mathbf{r}, \mathbf{R}) &= -\sqrt{\frac{2\pi i}{p_F r}} N_0 e^{ip_F r} \gamma^R(\mathbf{r}, \mathbf{R}) \\ &= G_0^R(\mathbf{r}, \omega = 0) \gamma^R(\mathbf{r}, \mathbf{R}) \end{aligned} \quad (4.34)$$

where G_0^R indicates the free Green's function and $\gamma^R(\mathbf{r}, \mathbf{R})$ is slowly varying. We will now see how the latter is related to the quasiclassical Green's function $g^R(\hat{\mathbf{p}}, \mathbf{R})$. We first go back to Eq. (4.34) and write

$$\begin{aligned} G^R(\mathbf{r}, \mathbf{R}) &= \int \frac{d\mathbf{p}}{(2\pi)^2} e^{i\mathbf{p}\cdot\mathbf{r}} G^R(\mathbf{p}, \mathbf{R}) \\ &= \int \frac{d\mathbf{p}}{(2\pi)^2} e^{i\mathbf{p}\cdot\mathbf{r}} \int \frac{d\mathbf{p}'}{(2\pi)^2} G_{0,\omega=0}^R(\mathbf{p} - \mathbf{p}') \gamma^R(\mathbf{p}', \mathbf{R}). \end{aligned} \quad (4.35)$$

By construction, such an ansatz lets one exploit the arguments of Fig. 4.1, since

1. G_0^R is peaked at the Fermi surface, having a pole at $|\mathbf{p} - \mathbf{p}'| = p_F$;
2. γ^R is smooth in real space, i.e. peaked around zero in momentum space, which, together with the previous point, means that $G^R(\mathbf{p}, \mathbf{R})$ is peaked at $p \approx p_F$.

One therefore obtains

$$\begin{aligned} G^R(\mathbf{r}, \mathbf{R}) &\approx \iint \frac{d\varphi}{2\pi} d\xi N(\xi) e^{i\mathbf{p}(\xi)\cdot\mathbf{r}} G^R(\xi, \varphi; \mathbf{R}) \\ &= N_0 \int \frac{d\varphi}{2\pi} e^{i\mathbf{p}_F(\varphi)\cdot\mathbf{r}} \int d\xi e^{i[\mathbf{p}(\xi,\varphi) - \mathbf{p}_F(\varphi)]\cdot\mathbf{r}} G^R(\xi, \varphi; \mathbf{R}) \\ &\approx N_0 \int \frac{d\varphi}{2\pi} e^{i\mathbf{p}_F(\varphi)\cdot\mathbf{r}} \Big|_s \int d\xi e^{i[\mathbf{p}(\xi,s) - \mathbf{p}_F(s)]\cdot\mathbf{r}} G^R(\xi, s; \mathbf{R}), \end{aligned} \quad (4.36)$$

where in the first line we rewrote the momentum integration according to Eq. (4.31) – polar coordinates as in Eq. (4.33) are chosen –, in the second we exploited the peak of $G^R(\xi, \varphi, \mathbf{R})$ at $\xi = 0$ and set $N \rightarrow N_0$, and in the third we fixed all quantities at the stationary point s , i.e. for $\hat{\mathbf{p}} = \hat{\mathbf{r}}$ or equivalently $\varphi = 0$. Calculating the Gaussian integral around s one obtains

$$G^R(\mathbf{r}, \mathbf{R}) \approx G_{0,\omega=0}^R \frac{i}{2\pi} \int d\xi e^{i(p-p_F)r} G^R(\mathbf{p}, \mathbf{R}) \Big|_{\hat{\mathbf{p}}=\hat{\mathbf{r}}}, \quad (4.37)$$

and by comparison with Eq. (4.34)

$$\gamma^R(\mathbf{r}, \mathbf{R}) = \frac{i}{2\pi} \int d\xi e^{i(p-p_F)r} G^R(\mathbf{p}, \mathbf{R}) \Big|_{\hat{\mathbf{p}}=\hat{\mathbf{r}}} . \quad (4.38)$$

As Shelankov shows [78], the quasiclassical Green's function $g^R(\hat{\mathbf{p}}, \mathbf{R})$ can be constructed by taking the limit $r \rightarrow 0$ of the ansatz function $\gamma^R(\mathbf{r}, \mathbf{R})$, and is in the end given by the symmetrized expression

$$\begin{aligned} g^R(\hat{\mathbf{p}}; \mathbf{x}) &= \lim_{r \rightarrow 0} [\gamma^R(\mathbf{r}, \mathbf{R}) \Big|_{\hat{\mathbf{p}}=\hat{\mathbf{r}}} + \gamma^R(\mathbf{r}, \mathbf{R}) \Big|_{\hat{\mathbf{p}}=-\hat{\mathbf{r}}}] \\ &= \lim_{r \rightarrow 0} \frac{i}{\pi} \int d\xi \cos\left(\frac{\xi r}{v_F}\right) G^R(\mathbf{p}, \mathbf{R}). \end{aligned} \quad (4.39)$$

For the advanced Green's function one can go through the same steps with the difference that the integral is dominated by the extremum corresponding to a velocity antiparallel to \mathbf{r} , i.e. the stationary point is now given by $\hat{\mathbf{p}} = -\hat{\mathbf{r}}$. The Keldysh component, on the other hand, has poles on both sides of the real axis, and as a consequence it “sees” both stationary points $\hat{\mathbf{p}} = \pm\hat{\mathbf{r}}$. With

$$G_0^A(\mathbf{r}, \omega = 0) = \sqrt{\frac{2\pi i}{p_F r}} e^{-ip_F r} \quad (4.40)$$

the complete Green's function can then be written as

$$\begin{aligned} \check{G}(\mathbf{r}, \mathbf{R}) &\approx G_{0,\omega=0}^R \check{\gamma}(\mathbf{r}, \mathbf{R}) \Big|_{\hat{\mathbf{p}}=\hat{\mathbf{r}}} + G_{0,\omega=0}^A \check{\gamma}(\mathbf{r}, \mathbf{R}) \Big|_{\hat{\mathbf{p}}=-\hat{\mathbf{r}}} \\ &= G_{0,\omega=0}^R \frac{i}{2\pi} \int d\xi e^{i(p-p_F)r} \check{G}(\mathbf{p}, \mathbf{R}) \Big|_{\hat{\mathbf{p}}=\hat{\mathbf{r}}} + \\ &\quad + G_{0,\omega=0}^A \frac{i}{2\pi} \int d\xi e^{-i(p-p_F)r} \check{G}(\mathbf{p}, \mathbf{R}) \Big|_{\hat{\mathbf{p}}=-\hat{\mathbf{r}}}, \end{aligned} \quad (4.41)$$

with

$$\check{\gamma}(\mathbf{r}, \mathbf{R}) \Big|_{\hat{\mathbf{p}}=\pm\hat{\mathbf{r}}} = \frac{i}{2\pi} \int d\xi e^{\pm i(p-p_F)r} \check{G}(\mathbf{p}, \mathbf{R}) \Big|_{\hat{\mathbf{p}}=\pm\hat{\mathbf{r}}} \quad (4.42)$$

and

$$\begin{aligned} \check{g}(\hat{\mathbf{p}}; \mathbf{R}) &= \lim_{r \rightarrow 0} [\check{\gamma}(\mathbf{r}, \mathbf{R}) \Big|_{\hat{\mathbf{p}}=\hat{\mathbf{r}}} + \check{\gamma}(\mathbf{r}, \mathbf{R}) \Big|_{\hat{\mathbf{p}}=-\hat{\mathbf{r}}}] \\ &= \lim_{r \rightarrow 0} \frac{i}{\pi} \int d\xi \cos\left(\frac{\xi r}{v_F}\right) \check{G}(\mathbf{p}, \mathbf{R}). \end{aligned} \quad (4.43)$$

Eq. (4.43) is not just a trivial extension of Eq. (4.39), as it rests on the *a priori* not obvious result valid for the Keldysh component [78]

$$\lim_{r \rightarrow 0} \gamma^K(\mathbf{r}, \mathbf{R}) \big|_{\hat{\mathbf{p}}=\hat{\mathbf{r}}} = \lim_{r \rightarrow 0} \gamma^K(\mathbf{r}, \mathbf{R}) \big|_{\hat{\mathbf{p}}=-\hat{\mathbf{r}}}. \quad (4.44)$$

When spin-orbit coupling is present the Green's function becomes a matrix in spin space and the Fermi surface splits into two branches

$$\epsilon_{\pm}(\mathbf{p}) = \frac{p^2}{2m} \pm |\mathbf{b}|. \quad (4.45)$$

As remarked in Section 4.1, we always take this splitting to be small compared to the Fermi energy, i.e. $|\mathbf{b}|/\epsilon_F \ll 1$, and moreover assume that the Fermi surface be smooth – that is, almost spherical. This statement is made quantitative in Appendix F. We recall that the Fermi momenta and density of states are now such that

$$p_{\pm} = p_F \mp \frac{|\mathbf{b}_0|}{v_F} = p_F \mp \delta p, \quad (4.46)$$

$$N_{\pm} = N_0 \left(1 \mp \frac{|\mathbf{b}_0|}{2\epsilon_F} \right) = N_0 (1 \mp \partial_{\xi} |\mathbf{b}_0|), \quad (4.47)$$

all equalities being valid to first order in $|\mathbf{b}|/\epsilon_F$.

The Green's function has now two peaks, one for each branch of the Fermi surface, and we want an ansatz capable of catching this feature. Starting again from the retarded component, we write

$$G^R(\mathbf{p}, \mathbf{R}) = \sum_{\nu=\pm} G_{\nu}^R(\mathbf{p}, \mathbf{R}) \quad (4.48)$$

where each of the two terms $G_{\nu}^R(\mathbf{p}, \mathbf{R})$ is peaked at the respective $\nu = \pm$ fold of the Fermi surface defined by

$$\xi_{\nu} = \xi + \nu |\mathbf{b}| = 0. \quad (4.49)$$

By using this property we can once more appeal to the stationary phase argument for each branch: the momentum integration, $\int d\mathbf{p}/(2\pi)^2$, is divided in an integral over ξ_{ν} and one over the constant energy surfaces $\xi_{\nu} = \text{const.}$; the peaks of $G_{\nu}^R(\mathbf{p}, \mathbf{R})$ ensure that the dominant ones are $\xi_{\nu} = 0$; when moving along these two – the standard quasiclassical assumption $p_{\nu} r \gg 1$ holds – the relevant region is the

one around the stationary points of the exponential $e^{i\mathbf{p}\cdot\mathbf{r}}$. These need not be given by the condition $\hat{\mathbf{p}} = \hat{\mathbf{r}}$, since now Eq. (4.49) does not in general define spherical constant energy surfaces. For simplicity we however make such an assumption, and refer to Appendix F for a discussion of the more general case.

By going through the above steps we can write

$$\begin{aligned} G^R(\mathbf{r}, \mathbf{R}) &= \sum_{\nu=\pm} \int \frac{d\mathbf{p}}{(2\pi)^2} e^{i\mathbf{p}\cdot\mathbf{r}} G_\nu^R(\mathbf{p}, \mathbf{R}) \\ &\approx \sum_{\nu=\pm} \left[G_{0,\nu}^R(\mathbf{r}) \frac{N_0}{N_\nu} \right] \gamma_\nu^R(\mathbf{r}, \mathbf{R}), \end{aligned} \quad (4.50)$$

with

$$G_{0,\nu}^R(\mathbf{r}) = -\sqrt{\frac{2\pi i}{p_\nu r}} N_\nu e^{ip_\nu r} \quad (4.51)$$

and having defined

$$\gamma_\nu^R(\mathbf{r}, \mathbf{R}) \equiv \frac{i}{2\pi} \int d\xi e^{i(p-p_\nu)r} G_\nu^R(\mathbf{p}, \mathbf{R}) \Big|_{\hat{\mathbf{p}}=\hat{\mathbf{r}}} . \quad (4.52)$$

The result (4.41) can then be generalized to

$$\begin{aligned} \check{G}(\mathbf{r}, \mathbf{R}) &\approx \sum_{\nu=\pm} \left(\left[G_{0,\nu}^R \frac{N_0}{N_\nu} \right] \check{\gamma}_\nu(\mathbf{r}, \mathbf{R}) \Big|_{\hat{\mathbf{p}}=\hat{\mathbf{r}}} + \left[G_{0,\nu}^A \frac{N_0}{N_\nu} \right] \check{\gamma}_\nu(\mathbf{r}, \mathbf{R}) \Big|_{\hat{\mathbf{p}}=-\hat{\mathbf{r}}} \right) \\ &= \sum_{\nu=\pm} \left(\left[G_{0,\nu}^R \frac{N_0}{N_\nu} \right] \frac{i}{2\pi} \int d\xi e^{i(p-p_\nu)r} \check{G}_\nu(\mathbf{p}, \mathbf{R}) \Big|_{\hat{\mathbf{p}}=\hat{\mathbf{r}}} + \right. \\ &\quad \left. + \left[G_{0,\nu}^A \frac{N_0}{N_\nu} \right] \frac{i}{2\pi} \int d\xi e^{-i(p-p_\nu)r} \check{G}_\nu(\mathbf{p}, \mathbf{R}) \Big|_{\hat{\mathbf{p}}=-\hat{\mathbf{r}}} \right). \end{aligned} \quad (4.53)$$

To establish a connection with the Eilenberger equation obtained in Section 4.1, Eq. (4.13), we further specify our ansatz function by saying¹

$$\check{\gamma}_\nu(\mathbf{r}, \mathbf{R}) \Big|_{\hat{\mathbf{p}}=\pm\hat{\mathbf{r}}} \equiv \frac{1}{2} \{ |\nu\rangle\langle\nu|_0, \check{\gamma}(\mathbf{r}, \mathbf{R}) \Big|_{\hat{\mathbf{p}}=\pm\hat{\mathbf{r}}} \}, \quad (4.54)$$

with the projectors $|\nu\rangle\langle\nu|$ [see Eq. (4.3)] evaluated at the Fermi surface in the absence of spin orbit. This is sensible in the spirit of our approximation, i.e. as long as $|\mathbf{b}|/\epsilon_F \ll 1$, and since

$$\sum_{\nu=\pm} |\nu\rangle\langle\nu|_0 = 1, \quad (4.55)$$

¹Note that in the following $\nu = \pm$ stands for the band index, whereas an explicit “ \pm ” in the formulas is used to specify the stationary point $\hat{\mathbf{p}} = \pm\hat{\mathbf{r}}$.

one has

$$\begin{aligned} \sum_{\nu=\pm} \check{\gamma}_\nu(\mathbf{r}, \mathbf{R}) |_{\hat{\mathbf{p}}=\pm\hat{\mathbf{r}}} &= \frac{1}{2} \sum_{\nu} \{ |\nu\rangle \langle \nu|_0, \check{\gamma}(\mathbf{r}, \mathbf{R}) |_{\hat{\mathbf{p}}=\pm\hat{\mathbf{r}}} \} \\ &= \check{\gamma}(\mathbf{r}, \mathbf{R}) |_{\hat{\mathbf{p}}=\pm\hat{\mathbf{r}}} . \end{aligned} \quad (4.56)$$

In the limit $r \rightarrow 0$ the function $\check{\gamma}(\mathbf{r}, \mathbf{R}) |_{\hat{\mathbf{p}}=\pm\hat{\mathbf{r}}}$ will be connected to $\check{g}(\hat{\mathbf{p}}, \mathbf{R})$ just as in Eq. (4.43). This can already be guessed, since in the limit $\delta pr \ll 1$ – which is reached when sending $r \rightarrow 0$ – from the general definition of $\check{\gamma}_\nu$ given in Eq. (4.53) there follows

$$\begin{aligned} \lim_{\delta pr \ll 1} \sum_{\nu=\pm} \check{\gamma}_\nu(\mathbf{r}, \mathbf{R}) |_{\hat{\mathbf{p}}=\pm\hat{\mathbf{r}}} &= \lim_{\delta pr \ll 1} \sum_{\nu=\pm} \frac{i}{2\pi} \int d\xi e^{\pm i(p-p_\nu)r} \check{G}_\nu(\mathbf{p}, \mathbf{R}) |_{\hat{\mathbf{p}}=\pm\hat{\mathbf{r}}} \\ &= \frac{i}{2\pi} \int d\xi e^{\pm i(p-p_F)r} \sum_{\nu=\pm} \check{G}_\nu(\mathbf{p}, \mathbf{R}) |_{\hat{\mathbf{p}}=\pm\hat{\mathbf{r}}} \\ &= \frac{i}{2\pi} \int d\xi e^{\pm i(p-p_F)r} \check{G}(\mathbf{p}, \mathbf{R}) |_{\hat{\mathbf{p}}=\pm\hat{\mathbf{r}}} \\ &= \check{\gamma}(\mathbf{r}, \mathbf{R}) |_{\hat{\mathbf{p}}=\pm\hat{\mathbf{r}}} \end{aligned} \quad (4.57)$$

and the last two lines show that $\check{\gamma}(\mathbf{r}, \mathbf{R})$ has the familiar expression (4.42).

To obtain the equation of motion for $\check{\gamma}$ one needs to

1. substitute Eq. (4.53) into the “left-right subtracted” Dyson equation (2.44). Since the right-going ($\hat{\mathbf{p}} = \hat{\mathbf{r}}$) and left-going ($\hat{\mathbf{p}} = -\hat{\mathbf{r}}$) modes are independent, this yields two equations, one for $\check{\gamma} |_{\mathbf{p}=\hat{\mathbf{r}}}$ and one for $\check{\gamma} |_{\mathbf{p}=-\hat{\mathbf{r}}}$, both with identical structure;
2. move to Wigner coordinates and perform a gradient expansion, justified by the slowly varying character of $\check{\gamma}_\nu(\mathbf{r}, \mathbf{R})$. This means at most gradient terms $\propto \nabla_{\mathbf{R}} \check{\gamma}_\nu(\mathbf{r}, \mathbf{R})$ are kept;
3. take the limit $\delta pr \ll 1$.

In formulas, picking for definiteness the $\hat{\mathbf{p}} = \hat{\mathbf{r}}$ stationary point²

$$1. \Rightarrow \left[\left(i\partial_{t_1} - \frac{(-i\nabla_{\mathbf{x}_1})^2}{2m} + \mathbf{b}(-i\nabla_{\mathbf{x}_1}) \cdot \boldsymbol{\sigma} + \mu \right) \delta(1-2) + \check{\Sigma}(1,2) \otimes \sum_{\nu=\pm} \left[G_{0,\nu}^R(\mathbf{r}) \frac{N_0}{N_\nu} \right] \check{\gamma}_\nu(1,2) \right] = 0; \quad (4.58)$$

$$2. \Rightarrow \sum_{\nu=\pm} \left(G_{0,\nu}^R \frac{N_0}{N_\nu} \right) \left(\partial_T \check{\gamma}_\nu + \frac{1}{2} \left\{ \frac{\mathbf{p}_\nu}{m} - \nabla_{\mathbf{p}}(\mathbf{b}_\nu \cdot \boldsymbol{\sigma}), \nabla_{\mathbf{R}} \check{\gamma}_\nu \right\} - i[\mathbf{b}_\nu \cdot \boldsymbol{\sigma}, \check{\gamma}_\nu] \right) = -i \sum_{\nu=\pm} \left(G_{0,\nu}^R \frac{N_0}{N_\nu} \right) [\check{\Sigma}, \check{\gamma}_\nu]; \quad (4.59)$$

$$3. \Rightarrow \left(G_{0,\nu}^R \frac{N_0}{N_\nu} \right) \rightarrow -\sqrt{\frac{2\pi i}{p_F r}} e^{ip_F r} N_0. \quad (4.60)$$

Eqs. (4.60) implies that – in the $\delta pr \ll 1$ limit – the prefactors drop from Eq. (4.59) and one is left with

$$\begin{aligned} & \sum_{\nu=\pm} \left(\partial_T \check{\gamma}_\nu + \frac{1}{2} \left\{ \frac{\mathbf{p}_\nu}{m} - \nabla_{\mathbf{p}}(\mathbf{b}_\nu \cdot \boldsymbol{\sigma}), \nabla_{\mathbf{R}} \check{\gamma}_\nu \right\} - i[\mathbf{b}_\nu \cdot \boldsymbol{\sigma}, \check{\gamma}_\nu] \right) \\ & = -i [\check{\Sigma}, \check{\gamma}], \end{aligned} \quad (4.61)$$

which is the Eilenberger equation previously obtained, Eq. (4.13). It follows that $\lim_{r \rightarrow 0} \check{\gamma} |_{\hat{\mathbf{p}}=\pm\hat{\mathbf{r}}}$ differs from the quasiclassical Green's function only up to a multiplicative constant, which is given by the normalization condition. This is fixed to the result of Section 4.1 [Eqs. (4.14), (4.16)] by taking the symmetrized expression, Eq. (4.43) – in other words, the linear combination of $\check{\gamma}$'s in Eq. (4.43) is a solution of Eq. (4.61) with the normalization given by Eq. (4.16).

It should by now be clear that there is some freedom in the choice of an ansatz for the Green's function \check{G} , since its fast and slow modes can be factorized in terms of different fast and slow functions. Indeed, the momentum space ansatz used in Section 4.1, Eq. (4.4), corresponds to the following choice – compare with Eqs. (4.54)-(4.56)

$$\check{\gamma}(\mathbf{r}, \mathbf{R}) = \sum_{\nu=\pm} \frac{N_\nu}{2N_0} \{ |\nu\rangle \langle \nu|_\nu, \check{\gamma}(\mathbf{r}, \mathbf{R}) \}, \quad (4.62)$$

²Taking the other one, $\hat{\mathbf{p}} = -\hat{\mathbf{r}}$, requires only the substitution $G_{0,\nu}^R \rightarrow G_{0,\nu}^A$. The final result is however identical.

where $\check{\gamma}$ and $\check{\check{\gamma}}$ coincide in the absence of spin-orbit coupling, since in that case $N_\nu = N_0$.

4.3 Particle-hole symmetry

In Chapter 2 we have seen that in standard quasiclassics the Eilenberger equation reads

$$[\partial_T + v_F \hat{\mathbf{p}} \cdot (\nabla_{\mathbf{R}} - e \mathbf{E} \partial_\epsilon)] \check{g}^K(\epsilon, \varphi; X) + i [\check{\Sigma}(X, \epsilon, \hat{\mathbf{p}}, p_F), \check{g}(X, \epsilon, \hat{\mathbf{p}})] = 0, \quad (4.63)$$

having considered a self-energy with a slow ϵ -dependence. Such a result has been obtained by the integration procedure defined in Eq. (2.55). This in fact relies on the assumption of perfect particle-hole symmetry, since the density of states is fixed at the Fermi surface, $N(\xi) \rightarrow N_0$. Formally, the generalized Eilenberger equation (4.13) requires one to take into account some of the ξ dependence of $N(\xi)$. Indeed, the difference between N_+ and N_- is necessary if one is to “see” the spin-orbit physics that couples the charge and spin degrees of freedom. In this sense particle-hole symmetry is broken. It is a point which requires further study, and might very well prove to be fundamental for the understanding of many spin-orbit-related effects. We shall briefly return to it in Section 5.1.1.

Chapter 5

Spin-charge coupled dynamics

We now discuss some applications of the formalism developed in Chapter 4. Original results from [71, 79–81] are presented.

5.1 The spin Hall effect

As briefly mentioned in Chapter 1, the spin Hall effect describes the flow of a spin current in the direction orthogonal to an applied electric field, *in the absence* of magnetic fields (see Fig.1.1). Belonging to the same category of physical phenomena are the so-called inverse spin Hall effect, in which an electric current is induced by a spin one – and both are flowing perpendicular to each other –, the anomalous Hall effect, which is a Hall effect proportional to the magnetization but not due to the magnetic field that the latter produces, and the voltage (or current) induced spin polarization, whose name is self-explanatory.¹ They are usually classified as *intrinsic* or *extrinsic*, depending on whether they arise because of intrinsic properties of the system, i.e. the band structure, or extrinsic ones, i.e. impurities. All are due to spin-orbit coupling, and appear as potential electric field-controlled handles on the spin degrees of freedom of carriers.

As an officially-named phenomenon the spin Hall effect was born very recently, since Murakami et al. proposed it for the two-dimensional hole gas (2DHG) in 2003 [20], while a little later came Sinova and collaborators' proposal for

¹Lately effects due to topologically protected edge states have started to draw attention, but they are beyond the scope of this work. See [82–84] for more.

the two-dimensional electron gas (2DEG) [21]. The physics behind this and the other closely related phenomena is however older, sometimes *quite* older [37, 38, 85–87]. A quantity of central importance in its treatment, both in the theory and in experiments, is the spin Hall conductivity tensor σ_{sH}^{ij} relating the i -component of the spin current to the electric field in the orthogonal j -direction

$$j_{s_k}^i = \sigma_{sH}^{ij} \mathcal{E}^j, \quad i, j, k = x, y, z. \quad (5.1)$$

By using the definition of the spin current (4.19), the spin Hall conductivity has the dimensions of a conductivity divided by a charge, $\sigma_{sH} \sim \sigma/e$. This is simply a convention, the dominant one among theorists and the one we employ.²

There exists an already vast amount of theoretical literature on the subject, as well as a modest but growing experimental one, concerning both semiconducting and metallic systems. Our focus will now be on the former ones, though the formalism of the preceding Chapters is independent of this choice. An excellent review of the field is given in [40], where most further references can be found.

5.1.1 Experiments

For semiconductors, it is in two-dimensional and quasi-two-dimensional systems of the kind described in Chapter 3 that the spin Hall effect and its related phenomena were observed. All experiments were based on optical methods. In [88, 89] Kerr microscopy was used to observe, in the second case even at room temperature, the extrinsic spin Hall effect in thin layers ($1 \div 2 \mu\text{m}$ thick) of n-GaAs and n-ZnSe. An extrinsic effect was also reported in a 2DEG [90]. The intrinsic spin Hall effect was instead seen in a 2DHG [51]. Also, the first time-resolved experiment has been recently performed by the Awschalom group [91].

In metals, thin films and nanowires with typical thicknesses of $4 \div 40 \text{ nm}$ are the systems considered, and observations relied on electrical rather than optical methods. The inverse spin Hall effect was detected in Al strips [11, 12], and its direct counterpart in Pt wires [13]. Finally, both effects, direct and inverse, were reported in Pt [14] and Au [15]. It is not yet very clear if the phenomena in metals are extrinsic in nature, as suggested in [14, 15], or intrinsic, as Guo et al. put

²Experimentalists find it often more convenient to introduce a factor e into the definition of the spin current to make the electrical and spin Hall conductivities have the same dimensions.

forward in a recent theoretical analysis concerning Pt systems [92]. Whatever the case, they appear to be quite relevant, as spin Hall conductivities of the order of $10^4/e\Omega m$, i.e. four orders of magnitude larger than in semiconductors, were reported. On the other hand Duckheim and Loss noted that the mesoscopic fluctuations of spin-electric phenomena in a 2DEG are much larger than the macroscopic average [93], suggesting it might be possible to achieve sizeable effects in semiconductors too. The physics behind this is still relatively unclear. In our present understanding the smallness of spin-electric effects in degenerate systems is related to the almost exact particle-hole symmetry, i.e. the fact that the density of states and the velocity of quasiparticles are almost energy independent close to the Fermi surface. Degenerate bands near the Fermi energy, as in Pt, or disorder – which causes mesoscopic fluctuations of the density of states and the diffusion constant – break this symmetry so that large spin-electric effects are possible.

5.1.2 Bulk dynamics: the direct spin Hall effect

Unless explicitly pointed out, we focus on the direct spin Hall effect in the Rashba model following mainly Refs. [72, 94].

When a static and homogeneous electric field $\mathcal{E} = \mathcal{E}\hat{x}$ is applied to a Rashba 2DEG the spin current polarized out of plane, i.e. along \hat{z} , and flowing along \hat{y} is given by³

$$j_{s_z}^y = \sigma_{sH}^{yx} \mathcal{E}^x, \quad (5.2)$$

where σ_{sH}^{yx} is the spin Hall conductivity and the object of our study. In the original paper by Sinova et al. [21] it was proposed that in the bulk of a clean system, that is in the absence of impurities of sort, the universal equation

$$\sigma_{sH}^{yx} = \frac{e}{8\pi} \quad (5.3)$$

should hold. After a short but rather intense debate it was however found how *any* kind of non-magnetic elastic disorder, no matter its strength or specific nature, would actually lead to the equally universal and substantially less spectacular result

$$\sigma_{sH}^{yx} = 0. \quad (5.4)$$

³This arbitrary geometrical choice is made for definiteness only.

More precisely, it is now well established that Eq. (5.4) is valid in general for linear-in-momentum spin-orbit couplings like $\mathbf{b}_R(\mathbf{p})$, $\mathbf{b}_D(\mathbf{p})$ [73–76]. This can be understood by looking at the peculiar form of the continuity equation for the spin, which we take from Chapter 4 in the case $\mathbf{b}(\mathbf{p}) = \mathbf{b}_R(\mathbf{p})$ as given in Eq. (3.19). From Eqs. (4.21) and (4.22) one has

$$\partial_t s_x + \nabla \cdot \mathbf{j}_{s_x} = -2m\alpha j_{s_z}^x, \quad (5.5)$$

$$\partial_t s_y + \nabla \cdot \mathbf{j}_{s_y} = -2m\alpha j_{s_z}^y. \quad (5.6)$$

Under stationary conditions in a homogeneous bulk the l.h.s. of both equations vanishes, and so must the spin current⁴

$$\mathbf{j}_{s_z} = 0. \quad (5.7)$$

In order to have a finite effect time dependent or inhomogeneous conditions are needed, or the continuity equation has to be modified. In the following we start by discussing a specific time dependent situation, and see how to draw from it some general conclusions which give additional insights into the universal result (5.3). Later we will go back to considering steady state conditions and will discuss possible modifications of the continuity equation.

Spin Hall currents in collisionless systems

Following [71], we study the linear response of a clean 2DEG to a spatially homogeneous but time dependent electric field. For a realistic system with at least weak disorder this study still gives reliable results on short time scales, $t \ll \tau$. The Eilenberger equation is solved in the limit $\tau \rightarrow \infty$, and the electric field included via the substitution $\nabla \rightarrow -|e|\mathcal{E}\partial_\epsilon$. We do not limit our discussion to the Rashba model, but consider a generic field $\mathbf{b}(\mathbf{p}) = \mathbf{b}_{ext} + \mathbf{b}(\mathbf{p})_{int}$. The Keldysh component of the linearized Eilenberger equation becomes

$$\sum_{\nu=\pm} \left(\partial_t g_\nu^K - \frac{|e|}{m} \boldsymbol{\mathcal{E}} \cdot \mathbf{p}_\nu \partial_\epsilon g_\nu^{K,eq} \right. \\ \left. + \frac{|e|}{2} \{ (\boldsymbol{\mathcal{E}} \cdot \partial_{\mathbf{p}})(\mathbf{b}_\nu \cdot \boldsymbol{\sigma}), \partial_\epsilon g_\nu^{K,eq} \} - i[\mathbf{b}_\nu \cdot \boldsymbol{\sigma}, g_\nu^K] \right) = 0. \quad (5.8)$$

⁴The same result can be obtained looking at the operator form of the equation of motion for the spin [95–97]. Moreover, it also holds when $\mathbf{b}(\mathbf{p}) = \mathbf{b}_R(\mathbf{p}) + \mathbf{b}_D(\mathbf{p})$ [71].

We focus on the spin components of the equation. Explicitly one has

$$\begin{aligned} \partial_t g_x^K &= -2b_{y,0}g_z^K \\ &\quad -|e|\boldsymbol{\mathcal{E}} \cdot \left[\mathbf{P}\hat{b}_{x,0} - \mathbf{v}_F\partial_\xi b_{x,0} + \partial_{\mathbf{p}}b_{x,0} \right] F_\epsilon, \end{aligned} \quad (5.9)$$

$$\begin{aligned} \partial_t g_y^K &= 2b_{x,0}g_z^K \\ &\quad -|e|\boldsymbol{\mathcal{E}} \cdot \left[\mathbf{P}\hat{b}_{y,0} - \mathbf{v}_F\partial_\xi b_{y,0} + \partial_{\mathbf{p}}b_{y,0} \right] F_\epsilon, \end{aligned} \quad (5.10)$$

$$\begin{aligned} \partial_t g_z^K &= 2(b_{y,0}g_x^K - b_{x,0}g_y^K) \\ &\quad + 2(b_{x,0}\partial_\xi b_{y,0} - b_{y,0}\partial_\xi b_{x,0})g_0. \end{aligned} \quad (5.11)$$

where for the sake of brevity $\mathbf{P} = \sum_\nu \nu \mathbf{p}_\nu / 2m$ and $F_\epsilon = 2\partial_\epsilon \tanh(\epsilon/2T)$. For the g_z^K component one obtains

$$\frac{d^2 g_z^K}{dt^2} + 4b_0^2 g_z^K = 2F_\epsilon |e| [b_{x,0}(\boldsymbol{\mathcal{E}} \cdot \partial_{\mathbf{p}})b_{y,0} - b_{y,0}(\boldsymbol{\mathcal{E}} \cdot \partial_{\mathbf{p}})b_{x,0}]. \quad (5.12)$$

Notice that only the second of the two terms involving the electric field in Eq.(5.8) remains in the equation for the g_z^K component. The solution of this differential equation is the sum of an oscillating and a time independent term. Due to the (undamped) oscillations it is clear that a stationary solution is never reached so the arguments leading to a vanishing spin Hall current do not apply. We will come back to this in Section 5.1.4 (see Fig. 5.7). The time independent solution of the differential equation is related to a zero-frequency spin current given by

$$\mathbf{j}_{s_z} = -\frac{|e|}{4\pi} \langle \mathbf{p}_F (\boldsymbol{\mathcal{E}} \cdot \partial_{\mathbf{p}}) \Psi \rangle, \quad \tan \Psi = b_{y,0}/b_{x,0}. \quad (5.13)$$

Notice that the spin current does not depend on the magnitude of the field \mathbf{b} , but only on the variation of its direction when going around the Fermi surface. An even more explicit result is obtained when the spin Hall conductivity tensor is antisymmetric

$$\sigma_{sH} = \frac{1}{2} (\sigma_{sH}^{yx} - \sigma_{sH}^{xy}) \quad (5.14)$$

$$= -\frac{|e|}{8\pi} \langle (p_{Fy}\partial_{p_x} - p_{Fx}\partial_{p_y}) \Psi \rangle \quad (5.15)$$

$$= \frac{|e|}{8\pi} \oint \frac{d\mathbf{p}}{2\pi} \cdot \partial_{\mathbf{p}} \Psi, \quad (5.16)$$

i.e. the spin Hall conductivity is the universal number $|e|/8\pi$ times the winding number of the internal field \mathbf{b} when going once around the Fermi surface.

We notice that Eq. (5.13) is consistent with [98–100] where the spin-Hall conductivity ignoring disorder was calculated using the Kubo formula for a Rashba-Dresselhaus system in the presence of an in-plane magnetic field. Eq. (5.16), which relates the spin-Hall conductivity with a winding number – i.e. the Berry phase in momentum space – generalizes the equivalent result of [101], where it was assumed that the modulus of \mathbf{b} is constant on the Fermi surface. As an example, if $\mathbf{b}(\mathbf{p}) = \mathbf{b}_R(\mathbf{p}) + \mathbf{b}_D(\mathbf{p})$ one has [99]

$$\sigma_{sH} = \begin{cases} |e|/8\pi, & \mathbf{b}_R(\mathbf{p}) > \mathbf{b}_D(\mathbf{p}) \\ 0, & \mathbf{b}_R(\mathbf{p}) = \mathbf{b}_D(\mathbf{p}) \\ -|e|/8\pi, & \mathbf{b}_R(\mathbf{p}) < \mathbf{b}_D(\mathbf{p}) \end{cases}, \quad (5.17)$$

of which the result (5.3) is seen to be a subcase.

Bulk dynamics in the presence of magnetic couplings

We now go back to a steady state situation in the Rashba model and consider two ways of modifying the continuity equation (5.6): the introduction of magnetic impurities or of an applied in-plane magnetic field [72, 79, 94]. This translates into the two Hamiltonians

$$H_1 = \frac{p^2}{2m} - \mathbf{b}_R \cdot \boldsymbol{\sigma} + V_{\text{nm}}(\mathbf{x}) + V_{\text{m}}(\mathbf{x}), \quad (5.18)$$

$$H_2 = \frac{p^2}{2m} - \mathbf{b}_R \cdot \boldsymbol{\sigma} - \omega_s \hat{\mathbf{x}} + V_{\text{nm}}(\mathbf{x}), \quad (5.19)$$

where $V_{\text{nm}}(\mathbf{x})$ and $V_{\text{m}}(\mathbf{x})$ describe respectively angle-dependent (long-range) non-magnetic scattering and s -wave (short-range) magnetic disorder, whereas $\mathbf{b}_{\text{ext}} = (g\mu_B/2)\mathbf{B}_{\text{ext}} = \omega_s \hat{\mathbf{x}}$. The impurity average leads to the self-energies Σ_{nm} and Σ_{m} given in Appendix D.

From (5.18) and (5.19) the following continuity equations for the s_y spin component are obtained

$$H_1 : \partial_t s_y + \nabla \cdot \mathbf{j}_{s_y} = -2m\alpha j_{s_z}^y - \frac{4}{3\tau_{sf}} s_y, \quad (5.20)$$

$$H_2 : \partial_t s_y + \nabla \cdot \mathbf{j}_{s_y} = -2m\alpha j_{s_z}^y + 2\omega_s s_z. \quad (5.21)$$

The second term on the r.h.s. of Eq. (5.20) is due to magnetic impurities, τ_{sf} being the spin-flip time which stems from the potential $V_m(\mathbf{x})$. Under stationary and uniform conditions the above imply

$$j_{s_z}^y = -\frac{2}{3m\alpha\tau_{sf}}s_y, \quad (5.22)$$

$$j_{s_z}^y = \frac{\omega_s}{m\alpha}s_z. \quad (5.23)$$

The spin current is seen to be directly related to the spin polarizations s_y, s_z . These are in their own right interesting objects. First, an in-plane electric field induces non-vanishing polarizations s_x, s_y . Second, these are non-trivially influenced by the nature of V_{nm} – s -wave or angle-dependent – so that an additional in-plane magnetic field will tilt them out of plane and produce an s_z polarization, though only if the disorder scattering is long-range. To get a better understanding of these phenomena we use simple physical arguments to explain how an in-plane polarization can be generated by an applied voltage [37, 79, 102]. Since the Fermi surface is shifted by an amount proportional to the applied electric field (say along the x -direction), as shown in Figs. 5.1 (a) and (b), there will be more occupied states with spin up – along y – than with spin down. In the case of short-range disorder, the total in-plane polarization can be estimated to be proportional to the density of states times the shift in momentum, $s_y \sim N\delta p \sim N|e|\mathcal{E}\tau$. Since in the present situation we are dealing with the two Fermi surfaces corresponding to the two helicity bands $\epsilon_{\pm} = p^2/2m \pm \alpha p$, obtained from the Hamiltonian (5.18), one expects $s_y \sim (N_+ - N_-)\delta p$, where, for the Rashba interaction, one has $N_{\pm} = N_0(1 \mp \alpha/v_F)$, $N_0 = m/2\pi$. Explicit calculations agree with this simple picture and lead to the result due to Edelstein [37], $s_y = -N_0\alpha|e|\mathcal{E}\tau$. When long-range disorder is considered, a reasonable guess could be to substitute for τ the transport time τ_{tr}

$$\tau \rightarrow \tau_{tr}, \quad \frac{1}{\tau_{tr}} = \int d\theta W(\theta)(1 - \cos(\theta)), \quad (5.24)$$

$W(\theta)$ being the angle-dependent scattering probability, so that $s_y = -N_0\alpha|e|\mathcal{E}\tau_{tr}$. This was proposed in [103], however the picture is too simplistic, and therefore the guess is wrong. As discussed in [94] – see also Appendix D for details – , the proper s_y polarization is given by $s_y = -N_0\alpha|e|\mathcal{E}\tilde{\tau}_{tr}$, with

$$\tau \rightarrow \tilde{\tau}_{tr}, \quad \frac{1}{\tilde{\tau}_{tr}} = \int d\theta W(\theta)(1 - \cos(2\theta)). \quad (5.25)$$

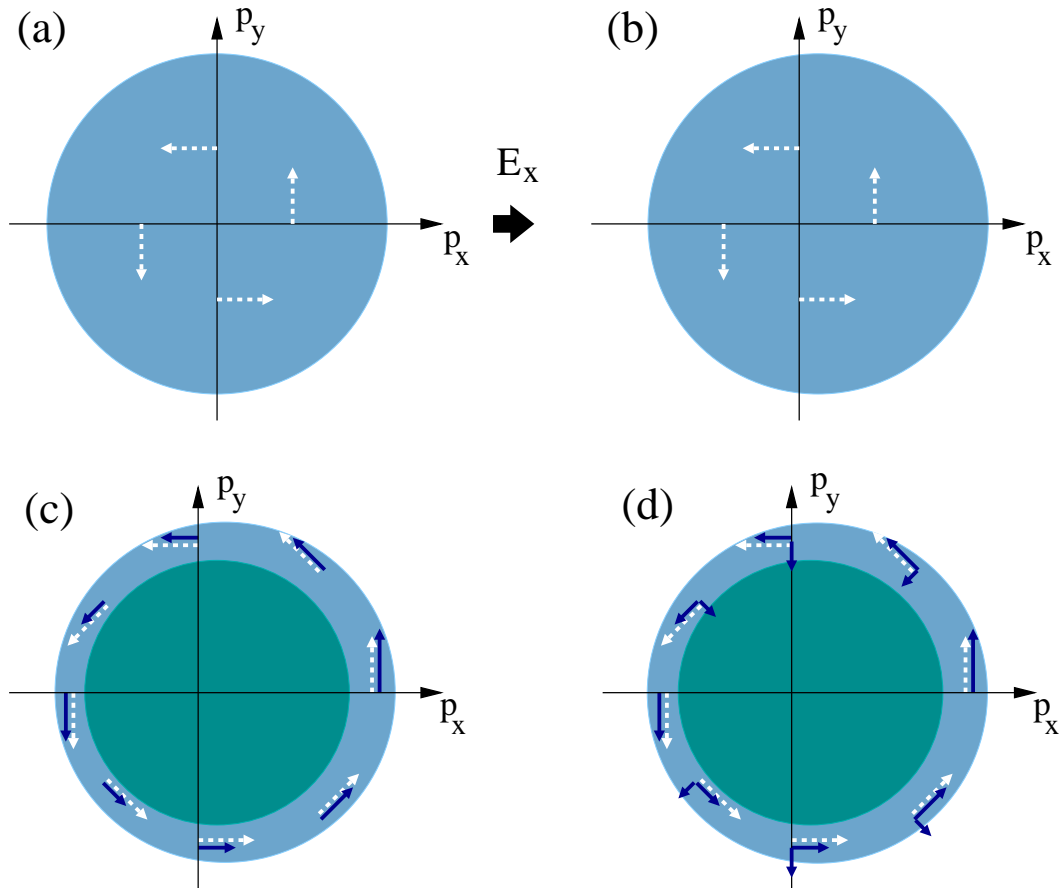


Figure 5.1: (a), (b) – The Fermi surface shift, $\delta p = |e|\mathcal{E}\tau$, due to an applied electric field along the x -direction. The white arrows show the direction of the internal field \mathbf{b} . (c), (d) Shifted bands and spin polarization in stationary conditions. (c) Asymmetric shift of the two bands when angle dependent scattering is present. The long dark (blue) arrows show the contributions to the spin polarization arising from a sector $d\varphi$ of phase space. (d) When magnetic disorder is turned on, additional contributions orthogonal to the internal field \mathbf{b} appear, here shown by the short inward and outward pointing (blue) arrows. Out-of-plane contributions are also present, but for the sake of simplicity not shown.

This particular time $\tilde{\tau}_{tr}$ arises from the asymmetric shift of the two Fermi surfaces, as depicted in Fig. 5.1 (c), due to different transport times in the two bands. It shows that contributions from both forward ($\theta = 0$) and backward ($\theta = \pi$) scattering are suppressed. The next step is to consider what happens when magnetic impurities are included. Relying once again on the simple picture of the shifted Fermi surface, one could argue that these have a rather small impact on the spin polarization, since the spin-flip scattering time usually makes a small contribution to the total transport time. However, even when this is the case, magnetic disorder does not simply modify the total transport time, but has an additional non-trivial effect. In its presence the spins do not align themselves along the internal \mathbf{b} field, since they acquire non-vanishing components in the plane orthogonal to it – see Fig. 5.1 (d). It is these components who give rise to a finite spin Hall conductivity. In this respect, magnetic disorder has an effect similar to that of an in-plane magnetic field: it affects the spin quantization axis and tilts the spins out of their expected stationary direction. We now make these arguments quantitative.

The starting point is the Keldysh component of the Eilenberger equation (4.13) for a homogeneous Rashba 2DEG in linear response to a homogeneous and time dependent applied electric field (introduced via the quasiclassical minimal substitution $\nabla \rightarrow -|e|\mathcal{E}\partial_\epsilon$)

$$\begin{aligned} \partial_t g^K &= \mathbf{v}_F \cdot \mathcal{E} |e| \partial_\epsilon g_{eq}^K + \frac{1}{2} \left\{ \frac{1}{p_F} \partial_\varphi \mathbf{b} \cdot \boldsymbol{\sigma}, \hat{\boldsymbol{\varphi}} \cdot \mathcal{E} |e| \partial_\epsilon g_{eq}^K \right\} \\ &\quad - i [\mathbf{b} \cdot \boldsymbol{\sigma}, g^K] - i [\tilde{\Sigma}, \tilde{g}]^K, \end{aligned} \quad (5.26)$$

where $\Sigma = \Sigma_{nm} + \Sigma_m$, and the “K” superscript will from now on be implicitly assumed and thus omitted. The angle φ is defined by the direction of the momentum, $\hat{\mathbf{p}} = (\cos \varphi, \sin \varphi)$, $\hat{\boldsymbol{\varphi}} = (-\sin \varphi, \cos \varphi)$. In order to solve Eq. (5.26), it is convenient to write g as a 4-vector

$$g = g_0 \sigma_0 + \mathbf{g} \cdot \boldsymbol{\sigma}, \quad (g_\mu) = (g_0, \mathbf{g}) \quad (5.27)$$

and turn it into matrix form. Details are shown in Appendix G. Taking the electric field to be along $\hat{\mathbf{x}}$, the expressions for the spin current $j_{s_z}^y$, the spin polarization s_y and the frequency dependent spin Hall conductivity $\sigma_{sH}^{yx}(\omega)$ are obtained. They read

$$j_{s_z}^y = \left[-\frac{\frac{4}{3\tau_{sf}} - i\omega}{2m\alpha} \right] s_y, \quad (5.28)$$

i.e. the continuity equation result, Eq. (5.20), under homogeneous conditions,

$$\begin{aligned}
 s_y &= -N_0\alpha|e|\mathcal{E} \left[2(\alpha p_F)^2 \right] \\
 &\times \left[\left(\frac{1}{\tau_{tr}} - i\omega \right) \left(\frac{1}{\tilde{\tau}_{tr}} - i\omega \right) \left(\frac{4}{3\tau_{sf}} - i\omega \right) + \right. \\
 &\left. + 2(\alpha p_F)^2 \left(\frac{1}{\tilde{\tau}_{tr}} + \frac{4}{3\tau_{sf}} - 2i\omega \right) \right]^{-1}, \tag{5.29}
 \end{aligned}$$

and as a consequence

$$\begin{aligned}
 \sigma_{sH}(\omega) &= \frac{|e|}{4\pi} \left(\frac{4}{3\tau_{sf}} - i\omega \right) \left[2(\alpha p_F)^2 \right] \\
 &\times \left[\left(\frac{1}{\tau_{tr}} - i\omega \right) \left(\frac{1}{\tilde{\tau}_{tr}} - i\omega \right) \left(\frac{4}{3\tau_{sf}} - i\omega \right) + \right. \\
 &\left. + 2(\alpha p_F)^2 \left(\frac{1}{\tilde{\tau}_{tr}} + \frac{4}{3\tau_{sf}} - 2i\omega \right) \right]^{-1}. \tag{5.30}
 \end{aligned}$$

Besides $1/\tau_{sf}$, there appear in the above two other different time scales

$$\frac{1}{\tau_{tr}} \equiv \frac{1}{\tau}(1 - K_1) + \frac{1}{\tau_{sf}}, \quad \frac{1}{\tilde{\tau}_{tr}} \equiv \frac{1}{\tau}(1 - K_2) + \frac{1}{\tau_{sf}}. \tag{5.31}$$

The first, τ_{tr} , is the total transport time. The second, $\tilde{\tau}_{tr}$, is the generalization of the characteristic time related to the s_y spin polarization introduced in (5.25). K_1 and K_2 are the coefficients of the first and second harmonics of the scattering kernel $K(\varphi - \varphi')$ from Appendix D.

The real part of the spin Hall conductivity is displayed in Fig. 5.2 for different values of the disorder parameter⁵ $\alpha p_F \tau$. In the limit $\omega \rightarrow 0$, its magnitude depends on the value of $\alpha p_F \tau$ as well as on the ratio τ/τ_{sf} . In the absence of magnetic impurities one has the known result $\sigma_{sH} = 0$. As spin flip scattering grows, the conductivity reaches values of the order of the ‘‘universal’’ $|e|/8\pi$. This was noted in [104], where, however, angle dependent scattering was not considered.⁶ Large values of $\alpha p_F \tau$ can be achieved both in III-V and II-VI semiconducting

⁵See Eqs. (4.17) and (4.18).

⁶In addition, a discrepancy in the expression of the static spin Hall conductivity arises, which in the limit of weak magnetic scattering does not agree with the continuity equation (5.20). In the opposite limit there is on the other hand agreement with the results from [105], where only magnetic impurities were considered.

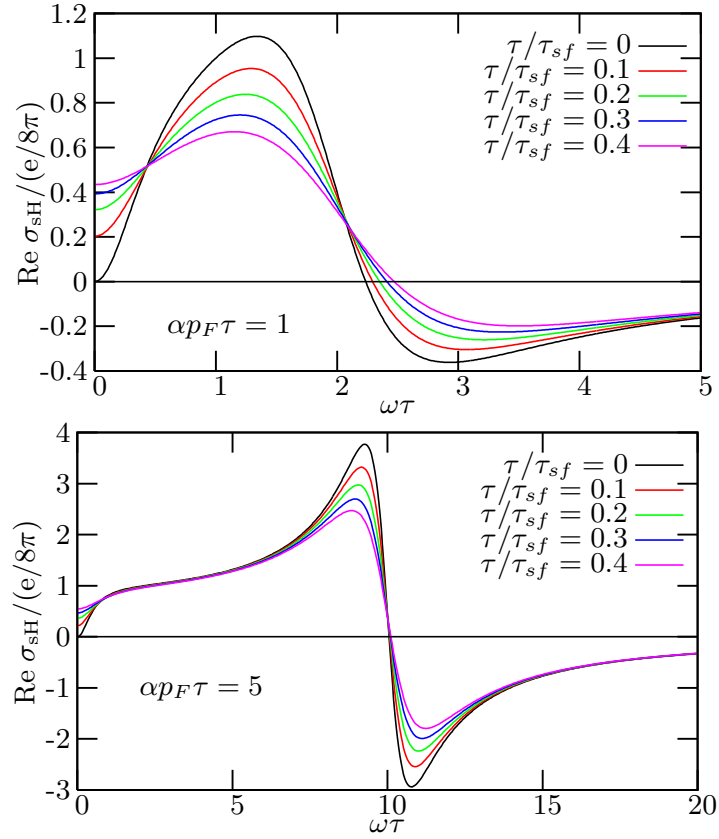


Figure 5.2: Real part of the frequency dependent spin Hall conductivity in units of the universal value $|e|/8\pi$ for $\alpha p_F \tau = 1$ (top) and $\alpha p_F \tau = 5$ (bottom). The different curves correspond to different values of the ratio $\tau/\tau_{sf} = 0, 0.1, 0.2, 0.3, 0.4$ (from top to bottom at the maximum of $\text{Re } \sigma_{sH}$).

materials. Doping the latter with Mn allows to control the spin-flip time τ_{sf} while only weakly affecting the electrons mobility [106–108], even though it is not perfectly clear whether these can appropriately be described in terms of the linear Rashba model.⁷ Additionally, for certain frequencies one can see crossing points [$\omega\tau \approx 0.5$ and $\omega\tau \approx 2$ in Fig. 5.2 (top)] at which magnetic disorder has no effect on the spin Hall response. Such points are well defined only when $\alpha p_F \tau \approx 1$. For clean ($\alpha p_F \tau \gg 1$) or dirty ($\alpha p_F \tau \ll 1$) samples the different curves cross each other over a progressively wider range of frequencies.

In the case of the Hamiltonian (5.19) similar calculations let one obtain the expressions for s_z and $\sigma_{sH}^{yx}(\omega = 0)$ to leading order in the magnetic field [94]

$$s_z = -\frac{1}{2}|e|\mathcal{E} \frac{\omega_s}{\alpha p_F} \frac{N_0}{p_F} \frac{\tau_{tr} - \tilde{\tau}_{tr}}{\tau_{tr}} \quad (5.32)$$

$$\sigma_{sH}^{yx} = -\frac{|e|}{4\pi} \left(\frac{\omega_s}{\alpha p_F} \right)^2 \frac{\tau_{tr} - \tilde{\tau}_{tr}}{\tau_{tr}}. \quad (5.33)$$

From the above it is apparent that the out-of-plane polarization s_z , and thus the spin Hall conductivity, will be non-vanishing only if both τ_{tr} and $\tilde{\tau}_{tr}$ are considered.

5.1.3 Confined geometries

Up to now only bulk phenomena have been studied. As already mentioned (see Fig. 1.1) the usual experimental signature of the direct spin Hall effect, at least in semiconductors, is the measure of spin accumulation at the boundaries of a 2DEG sample caused by the spin current flowing in its bulk [51, 88–90]. Hence, the understanding of the spin Hall physics involves the description of boundaries. Moreover, these become relevant if one is to study relaxation processes in mesoscopic systems, which in time are of fundamental importance for the typical spintronic device. For these reasons we now specialize to samples of finite size with the geometry shown in Fig. 5.3. Our main references will be [71, 80, 81].

The derivation of the boundary conditions for the quasiclassical Green's function is a delicate matter, since typically the boundary potential $U_b(\mathbf{x})$ varies on

⁷More precisely, the Rashba Hamiltonian is appropriate for narrow quantum wells (width $\lesssim 6$ nm), but most likely not for wider structures, in which the so-called inverted-band structure manifests itself.

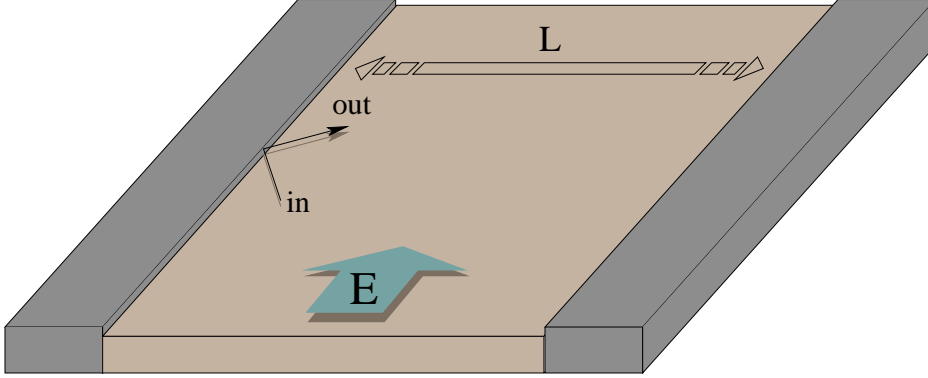


Figure 5.3: Geometry under consideration. The 2DEG is a narrow wire of finite width L along \hat{y} . Along \hat{x} , which is the direction parallel to the applied electric field, it can either be infinite or smoothly contacted to reservoirs. Scattering at the boundaries is assumed elastic, though not necessarily spin-conserving.

the microscopic scale of the Fermi wavelength λ_F , that is, beyond the quasiclassical resolution $l_{qc} \gg \lambda_F$. Following Ref. [109], in general one has that the linear matching conditions for the wavefunctions on the opposite sides of $U_b(\mathbf{x})$ become nonlinear relations between the quasiclassical amplitudes. In the case of a perfectly reflecting barrier – i.e. if no transmission across the boundary is possible – and when an ingoing trajectory is scattered into one outgoing direction, things simplify considerably and the boundary condition reads

$$g(\hat{\mathbf{p}}_{\text{out}}) = Sg(\hat{\mathbf{p}}_{\text{in}})S^\dagger. \quad (5.34)$$

A general treatment which takes into account beam splitting – i.e. inter-band transitions – at the barrier is still lacking and currently being pursued. Here S is the unitary 2×2 surface scattering matrix. Using the decomposition (5.27), Eq. (5.34) can be rewritten as

$$g_0^{\text{out}} = g_0^{\text{in}}, \quad \mathbf{g}^{\text{out}} = R\mathbf{g}^{\text{in}}, \quad (5.35)$$

with the orthogonal matrix R that rotates the spin at the barrier, and where $g(\hat{\mathbf{p}}_{\text{in,out}}) \equiv g^{\text{in,out}}$. Charge conservation implies that no current flows through the boundary

$$\langle \mathbf{n} \cdot \mathbf{v}_F g_0 \rangle \propto \mathbf{n} \cdot \mathbf{j}_c = 0, \quad (5.36)$$

where \mathbf{n} is a vector normal to the boundary. For a spin conserving boundary ($R = 1$) all components α of the spin current perpendicular to the surface are zero too,

$$\langle \mathbf{n} \cdot \mathbf{v}_F g_\alpha \rangle \propto \mathbf{n} \cdot \mathbf{j}_{s_\alpha} = 0. \quad (5.37)$$

For the general case, $R \neq 1$, Eq. (5.37) is not valid.

5.1.4 Voltage induced spin polarizations and the spin Hall effect in finite systems

Numerical results concerning voltage induced spin polarizations and the spin Hall effect in finite systems are now shown and discussed. We focus on the Rashba model, $\mathbf{b}(\mathbf{p}) = \mathbf{b}_R(\mathbf{p})$. The geometry of Fig. 5.3 is further specified by considering a sample finite along $\hat{\mathbf{x}}$ and in contact with two reservoirs at $x = 0$ and $x = L_x$. These are kept in thermal equilibrium and assumed to be made of the same material as the two-dimensional sample – that is, there is no Fermi surface mismatch. For directions $\hat{\mathbf{p}} = \hat{\mathbf{p}}_{\text{in}}$ pointing from the reservoirs into the system the quasiclassical Green's function reads (we briefly reintroduce the Keldysh superscript “ K ”)

$$\begin{aligned} (g^K)^{\text{in}}|_{x=0, L_x} &= (g^K)_{\text{eq}}^{\text{in}}|_{\mathbf{x} \text{ in the reservoir}} \\ &= \tanh\left(\frac{\epsilon \pm |e|V/2}{2T}\right) (g^R - g^A), \end{aligned} \quad (5.38)$$

with V the gate voltage.

We assume the scattering at the boundaries to be adiabatic, i.e. an incoming wave in an eigenstate $|\mathbf{p}_{\text{in}} \pm\rangle$ of the Hamiltonian $p^2/2m - \mathbf{b} \cdot \boldsymbol{\sigma}$ is scattered into the same band,

$$|\mathbf{p}_{\text{in}} \pm\rangle \rightarrow e^{\pm i\vartheta} |\mathbf{p}_{\text{out}} \pm\rangle, \quad (5.39)$$

as it is expected for a smooth confining potential [110–112]. Such a scattering does not generate inter-band transitions and Eq. (5.34) can be used. The S matrix reads

$$S = \begin{pmatrix} e^{2i\varphi} \cos \theta & -\sin \vartheta \\ \sin \vartheta & \cos \vartheta \end{pmatrix}, \quad (5.40)$$

where φ is as usual the momentum angle, while the relative phase shift θ is assumed negligible, i.e. $\vartheta = 0$. This describes an in-plane spin rotation of 2φ . In

the Pauli matrices space defined by the decomposition (5.27), this is represented by the 4×4 matrix \mathbf{R}

$$\mathbf{R} = \begin{pmatrix} 1 & 0 & 0 & 0 \\ 0 & \cos(2\varphi) & \sin(2\varphi) & 0 \\ 0 & -\sin(2\varphi) & \cos(2\varphi) & 0 \\ 0 & 0 & 0 & 1 \end{pmatrix}. \quad (5.41)$$

In the language of Eq. (5.35) the 3×3 orthogonal matrix is

$$R = \begin{pmatrix} \cos(2\varphi) & \sin(2\varphi) & 0 \\ -\sin(2\varphi) & \cos(2\varphi) & 0 \\ 0 & 0 & 1 \end{pmatrix}. \quad (5.42)$$

To integrate the equation of motion numerically we have to discretize the space coordinate \mathbf{x} and the Fermi surface. In dirty systems $g(\hat{\mathbf{p}})$ is nearly isotropic, so it is clear that a few discrete points $\hat{\mathbf{p}}_i$ on the Fermi surface are sufficient. In clean systems this is not *a priori* evident, but numerical tests show that even in this case convergence is reached quickly. Typically we describe the Fermi surface with a set of twenty to forty $\hat{\mathbf{p}}_i$.

First we show numerical results for the spin polarization in the stationary limit. Fig. 5.4 depicts the voltage induced spin polarization for $L_x = 20l$, $L_y = 10l$ and $\alpha p_F \tau = 2$; due to the linearity of the underlying equations, all our results are linear in the applied voltage. In the bulk, only the s_y component is nonzero, and given by the Edelstein result $s_0 = -N_0 \alpha |e| \mathcal{E} \tau$ [37]. A spin Hall effect induced spin polarization is found in the corners, as it is expected in [74]. It is however not purely in the z -direction, having x -components too.

Fig. 5.5 shows $s_y(x, y = L_y/2)$ for various disorder strengths. In the diffusive limit and assuming the spin polarization to be vanishing at the interface with the leads, it was predicted that [74]

$$s_y(x) = s_0 \left(1 - \frac{\cosh[(x - L_x/2)/L_s]}{\cosh(L_x/2L_s)} \right), \quad (5.43)$$

where L_s is the spin relaxation length. With our choice of boundary condition a spin polarization still exists near $x = 0, L_x$, in particular in the clean limit. Some mean free paths away from the interface on the other hand the data can be well fitted with an exponential increase or decrease, both in the clean and dirty limit.

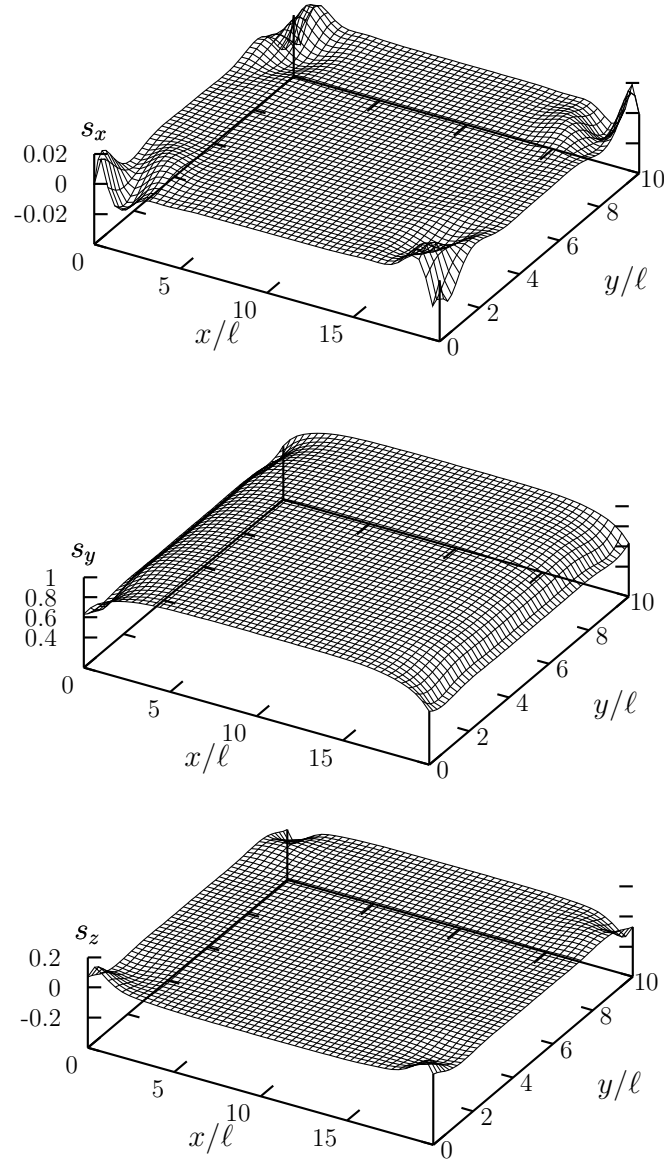


Figure 5.4: Spin polarization in the presence of an electrical current flowing in x -direction for a strip of length $L_x = 20l$ and $L_y = 10l$. The spin-orbit coupling strength is $\alpha = 10^{-3}v_F$ and the elastic scattering rate is $1/\tau = \alpha p_F/2$. The spin polarization is given in units of the bulk Edelstein value, $s_0 = -N_0\alpha|e|\mathcal{E}\tau$.

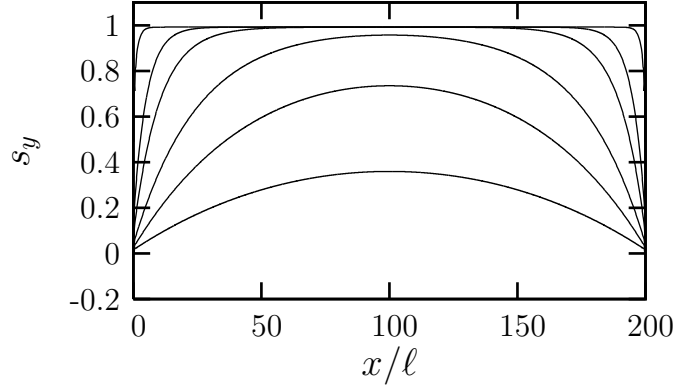


Figure 5.5: s_y in units of s_0 as a function of x for $L_x = 200l$, $L_y = 100l$ and $\alpha p_F \tau = 0.005, 0.01, 0.02, 0.05, 0.1, 1$ (from bottom to top).

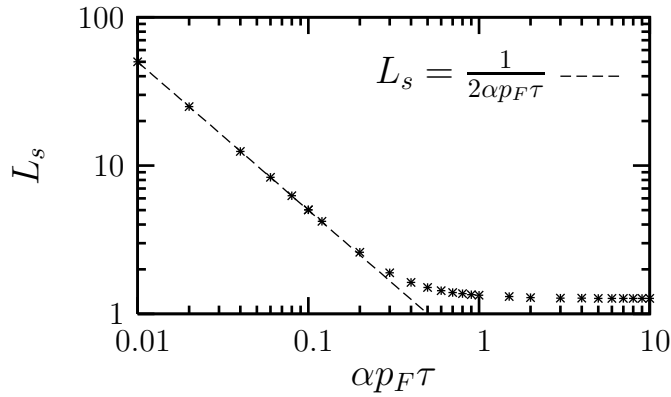


Figure 5.6: Spin relaxation length L_s in units of l as a function of disorder, obtained by fitting the spatial dependence of the electric field induced spin polarization (shown in Fig. 5.5) using $s_y = a + b[\exp(-x/L_s) + \exp(-(L_x - x)/L_s)]$. The diffusive limit expression is shown as a dashed line.

As a result we obtain the spin relaxation length as a function of disorder, shown in Fig. 5.6. In the dirty limit, $\alpha p_F \tau \ll 1$, our numerical result agrees with what is expected from the diffusion equation, $L_s = \sqrt{D\tau_s} = l/2\alpha p_F \tau$. In the clean limit, for which we are not aware of any quantitative predictions, the spin relaxation length is of the order of the mean free path, $L_s \approx 1.27l$.

We will now consider a non-static situation and study the time evolution of the spin polarization and current. The system starts in thermal equilibrium, then a voltage is switched on and the relaxation of the system into its stationary non-equilibrium state is observed. It is a nontrivial problem to describe such a situation theoretically. One might be tempted to allow a time dependent voltage in the boundary condition, Eq. (5.38), and then to follow the time evolution. In this case the charge density becomes time dependent and inhomogeneous. This procedure makes sense for non-interacting electrons, not for interacting ones where the long range Coulomb interaction enforces charge neutrality. In principle the interaction can be included into the quasiclassical formalism explicitly, see e.g. [26]. This is beyond our scope. Instead, we assume in the following that a voltage difference across the leads instantly results in a homogeneous electric field in the sample. One has thus to solve Eq. (4.13) with the initial condition $g(\mathbf{p}, \epsilon; \mathbf{x}, t = 0) = \tanh(\epsilon/2T)(g^R - g^A)$ and taking into account the electric field via the usual substitution $\nabla \rightarrow \nabla - |e|\mathcal{E}\partial_\epsilon$. In the numerics it is however more convenient to work in a scalar gauge, since then the (static) electric field disappears from the equation of motion and is present in the initial and boundary conditions only. In the end we have to solve Eq. (4.13) with the boundary condition (5.38) and the initial condition

$$g^K(\hat{\mathbf{p}}, \epsilon; \mathbf{x}, t = 0) = \tanh\left(\frac{\epsilon + |e|\phi(x)}{2T}\right)(g^R - g^A), \quad (5.44)$$

where $\phi(x)$ interpolates linearly between the two leads, $\phi(x) = V(L_x/2 - x)/L_x$.

In Fig. (5.7) we show the spin current $j_{s_z}^y$ as a function of time in the bulk and at the interface with the leads of a rather clean system ($\alpha p_F \tau = 2$). On short time scales the bulk current agrees with what is found ignoring disorder (see Section 5.1.2): the spin current oscillates as a function of time with frequency $2\alpha p_F$, and the time average is given by the universal spin Hall conductivity. In the bulk, for the weakly disordered system we are considering, the time dependent

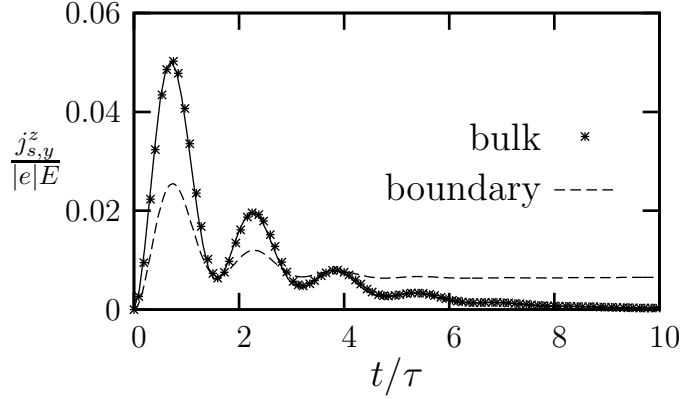


Figure 5.7: Time evolution of the spin Hall current at the interface with the leads and in the bulk. In the bulk we compare our numerical result (data points) with the analytical result (full line) of Eq. (5.45). Near the leads, only numerical data are available (dashed curve). $j_{s_z}^y$ is evaluated at $y = L_y/2$, $x = 0$ (boundary) and $x = L_x/2$ (bulk) for $L_x = 20l$, $L_y = 10l$ and $\alpha p_F \tau = 2$.

spin current is given by

$$j_{s_z}^y = \frac{|e|E}{8\pi} \left[e^{-t/2\tau} - e^{-3t/4\tau} \cos(2\alpha p_F t) \right], \quad (5.45)$$

which can be obtained from the frequency dependent spin Hall conductivity (5.30) when only s -wave non-magnetic scatterers are present. On the time scale of the spin relaxation time, here given by the scattering time τ , the bulk spin current becomes exponentially suppressed and goes to zero in the stationary limit. Near the leads, on the other hand, the situation is somewhat different, since a finite spin current remains in the stationary limit. An important question is whether the spin current polarizes the electron system at the edges. In Fig. 5.8 we show the spin polarization in the z -direction across the system at $x = L_x/2$ as a function of time. Since in the early time evolution a spin current flows in the bulk, spins accumulate near the edges. When the spin current disappears the polarization vanishes too. The spin polarization at the edges is seen to oscillate as expected with frequency $2\alpha p_F$. In the cleaner systems oscillations are of course faster. Remarkably, the maximum oscillation amplitude relative to the bulk value is larger in the dirty system ($\alpha p_F \tau = 0.25$), where it is almost of the order of one. This can be understood as follows: a rough estimate of the spin polarization at the edge is

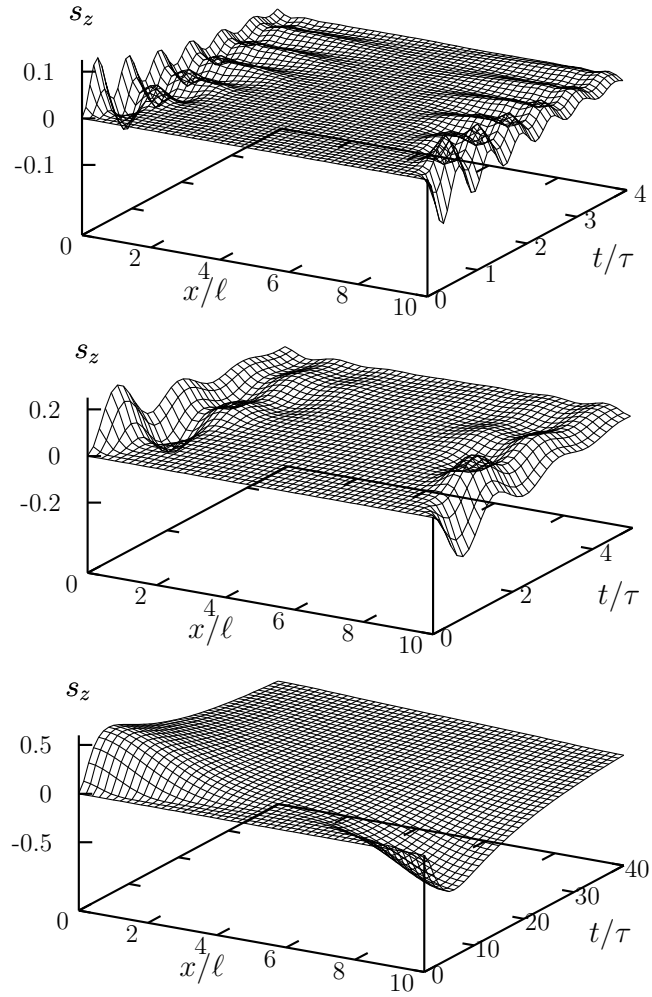


Figure 5.8: Spin Hall effect induced spin polarization s_z in units of s_0 as a function of y and t at $x = L_x/2$ for $L_x = 20l$, $L_y = 10l$ and $\alpha p_F \tau = 0.25, 2, 5$ (from bottom to top).

$s_z \sim \tau_s j_{s_z}^y / L_s$. With

$$\tau_s \sim \tau / (\alpha p_F \tau)^2 \quad (5.46)$$

$$j_{s_z}^y \sim e \mathcal{E} (\alpha p_F \tau)^2 \quad (5.47)$$

$$L_s \sim l / (\alpha p_F \tau) \quad (5.48)$$

the result is indeed $s_z \sim s_0 = -N_0 \alpha |e| \mathcal{E} \tau$. In the clean limit, on the other hand, the typical time and length scales are $\tau_s \sim \tau$ and $L_s \sim l$, from which we estimate $s_z \sim s_0 / (\alpha p_F \tau)$, in agreement with the numerical findings.

It is worthwhile bringing the attention to one additional point. In a diffusive sample, $\alpha p_F \tau \ll 1$, the Eilenberger equation (4.13) leads to the following spin diffusion equations

$$(\partial_t - D \nabla^2) s_x = -\frac{1}{\tau_s} s_x + 2C \nabla_x s_z \quad (5.49)$$

$$(\partial_t - D \nabla^2) s_y = -\frac{1}{\tau_s} (s_y - s_0) + 2C \nabla_y s_z \quad (5.50)$$

$$(\partial_t - D \nabla^2) s_z = -\frac{1}{\tau_s} s_z - 2C (\nabla_x s_x + \nabla_y s_y), \quad (5.51)$$

where $D = v_F^2 \tau / 2$ is the diffusion constant, $1/\tau_s = (2\alpha p_F \tau)^2 / (2\tau)$ the Dyakonov-Perel spin relaxation rate, $C = v_F \alpha p_F \tau$ and $s_0 = -N_0 \alpha |e| \mathcal{E} \tau$ is the usual Edelstein result. As shown in Appendix G, adiabatic scattering at the boundaries, Eq. (5.39), translates into the following boundary conditions for the s_x and s_y spin components

$$s_x = 0, \quad s_y = s_0. \quad (5.52)$$

Eqs. (5.50) and (5.52) tell an interesting story: in the bulk of a diffusive system the time scale of the spin dynamics is set by the spin relaxation time τ_s , whereas at the edges of the sample the boundary condition plays the major role. While in clean systems ($\alpha p_F \tau \gg 1$) τ_s is comparable to τ , ideally identical in the limit $\alpha p_F \tau \rightarrow \infty$, it becomes progressively larger than the latter in increasingly dirtier ones ($\alpha p_F \tau \ll 1$). In the second case, assuming adiabatic (spin active) boundaries, this implies that the s_y spin polarization approaches the stationary value $s_0 = -N_0 \alpha |e| \mathcal{E} \tau$ on a much faster time scale than τ_s when close to the boundary. This is shown in Fig. 5.9. Very recently such a phenomenon was indeed observed in a GaAs-based channel [91].

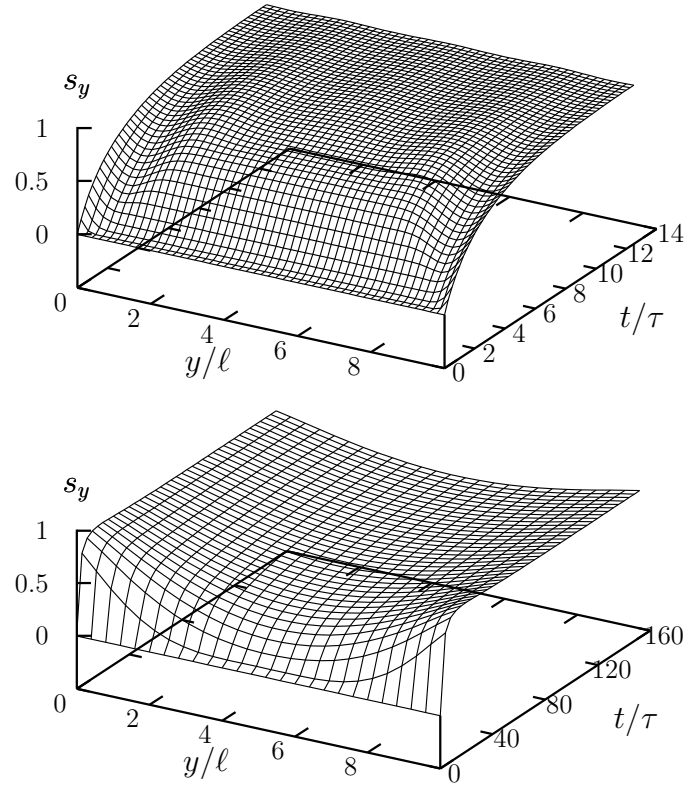


Figure 5.9: Voltage induced spin polarization as a function of y and t at $x = L_x/2$ on a strip of length $L_x = 20l$ and width $L_y = 10l$. The upper figures are obtained for $\alpha p_F \tau = 1$, which implies $\tau_s \approx \tau$, whereas in the lower figures $\alpha p_F \tau = 0.1$ and thus $\tau_s \gg \tau$. As a consequence in the second case s_y reaches s_0 on a much shorter time scale at the boundaries than in the bulk.

5.2 Spin relaxation in narrow wires

In this Section we concentrate on the specific problem of the size dependence of the spin relaxation rate in narrow samples. Concerning this matter, the recent experimental observations of Ref. [113] in a n -InGaAs wire provided the motivation for the present analysis. Indeed, they produced an unexpected result. The relaxation time showed first an increase with decreasing sample width, in accordance with a number of previous theoretical works [114–118], and then an abrupt decrease at the smallest wire widths. Such nonmonotonic behaviour set in as $L \approx L_s$, with $L_s = \sqrt{D\tau_s}$ the spin relaxation length, when the relaxation time reached its maximum and then sharply dropped. We will now see how spin-active boundaries ($R \neq 1$), not considered in the above theoretical references, radically change the size dependence of the spin relaxation time for narrower samples and provide a useful point of view as far as the interpretation of the experiment is concerned. The geometry is the usual one (see Fig. 5.3).

The starting point are the bulk spin diffusion equations, Eqs. (5.49)–(5.51). Since we are interested in the spin dynamics only, the sub-leading $\mathcal{O}(\alpha/v_F)$ spin-charge coupling terms are neglected – this means the Edelstein s_0 term is dropped

$$(\partial_t - D\nabla^2) s_x = -\frac{1}{\tau_s} s_x + 2C\nabla_x s_z, \quad (5.53)$$

$$(\partial_t - D\nabla^2) s_y = -\frac{1}{\tau_s} s_y + 2C\nabla_y s_z, \quad (5.54)$$

$$(\partial_t - D\nabla^2) s_z = -\frac{1}{\tau_s} s_z - 2C(\nabla_x s_x + \nabla_y s_y). \quad (5.55)$$

Alternatively, one could have dropped the $\mathcal{O}(\alpha/v_F)$ terms directly from Eq. (4.13) and considered the diffusive limit of the simplified equation

$$\partial_t g + \mathbf{v}_F \cdot \nabla g - i[\mathbf{b} \cdot \boldsymbol{\sigma}, g] = -\frac{1}{\tau} (g - \langle g \rangle). \quad (5.56)$$

In standard charge diffusion the longest living mode is homogeneous. Due to the coupling between the various spin components this is not anymore the case.⁸

Let us consider two types of boundaries (see Appendix G for some details). First a spin-conserving one, where

$$|\mathbf{p}_{\text{in}} s\rangle \rightarrow |\mathbf{p}_{\text{out}} s\rangle, \quad (5.57)$$

⁸See [80] for more. As a noteworthy example, when $\mathbf{b} = \mathbf{b}_R + \mathbf{b}_D$ with $\alpha = \beta$ there exists an infinite living mode with wavevector $q = 4m\alpha$ [119].

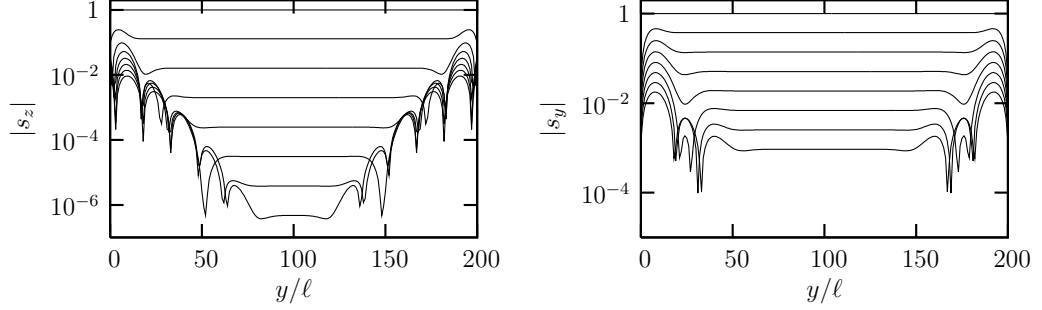


Figure 5.10: Time evolution of the spin polarization in a wide channel ($L = 200l \approx 40L_s$, $\alpha p_F \tau = 0.1$) with conserving (left) and adiabatic (right) boundary conditions. The curves from top to bottom correspond to different times, with $\Delta t = 50\tau \approx \tau_s$. The polarizations change sign at various positions where a steep drop of $|s_z|$, $|s_y|$ is visible in the figure.

such that S and \mathbf{R} are identity matrices. Then the adiabatic boundary of Eq. (5.39), with the matrices S and \mathbf{R} given by Eqs. (5.40) and (5.41), respectively.

In the first case – for the Rashba model – using the expression for the charge and spin current in the diffusive limit, one gets (see also [115, 120])

$$-D\nabla_y s_y - C s_z = \mathbf{n} \cdot \mathbf{j}_y = 0, \quad (5.58)$$

$$-D\nabla_y s_x = \mathbf{n} \cdot \mathbf{j}_x = 0, \quad (5.59)$$

$$-D\nabla_x s_z + C s_x = \mathbf{n} \cdot \mathbf{j}_z = 0, \quad (5.60)$$

where \mathbf{n} is in the y -direction. For adiabatic boundary conditions, in contrast

$$s_x = 0, \quad s_y = 0, \quad (5.61)$$

while the z -component of the spin is still conserved and therefore Eq. (5.60) remains valid. Fig. 5.10 shows the time evolution of the spin profile for a long wire of width $L = 200l$, where $l = v_F \tau$ is the elastic mean free path. In the left panel the spin is initially homogeneously polarized in the z -direction and conserving boundary conditions are assumed, $S = 1$. The results were obtained from the Eilenberger equation with $\alpha p_F \tau = 0.1$. Inside the wire one observes a homogeneous decay of the spin polarization, with the time constant $\tau_s/2$. At the boundaries long living modes show up which dominate the spin profile in the long

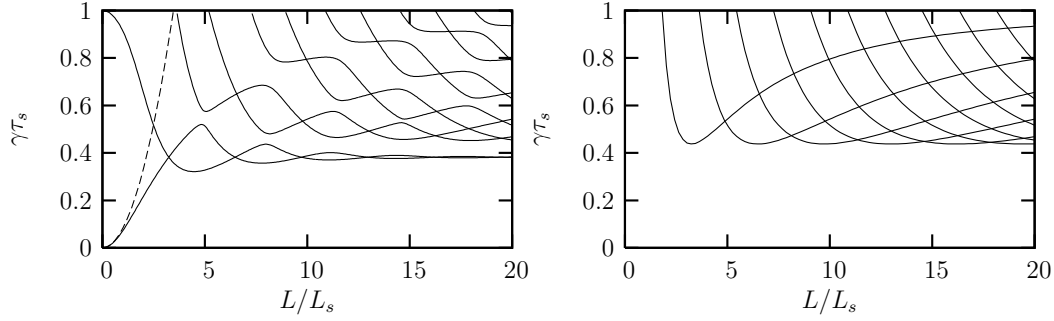


Figure 5.11: Lowest eigenvalues of the spin-diffusion operator for the Rashba model with conserving (left) and adiabatic (right) boundary conditions. On the left there appear modes with $\gamma < 7/16\tau_s$. These have a complex wave vector and can therefore exist only at the edges of the wire. The dashed curve in the left panel is $\gamma\tau_s = (L/L_s)^2/12$ obtained in Ref. [115] for very narrow wires. On the right this long-living mode is absent.

time limit. For further investigation of these modes we write the spin diffusion equations, Eqs. (5.53)–(5.55), as $\partial_t \mathbf{s} + \hat{\gamma} \mathbf{s} = 0$, and determine the eigenvalues and eigenmodes of the operator $\hat{\gamma}$. The eigenmodes are superpositions of plane waves. The low frequency spectrum of $\hat{\gamma}$ is shown in Fig. 5.11 as a function of the wire width. Recall that the smallest eigenvalue for a bulk system is $\gamma_0 = 7/16\tau_s$ [80]. The modes with smaller decay rate have a complex wave vector and are thus localized near the edges of the wire. For a wide system we find a continuum of eigenvalues above γ_0 , and two localized modes at $\gamma \approx 0.382/\tau_s$.

For a narrow wire most strikingly one eigenvalue goes to zero with decreasing width, asymptotically as

$$\gamma\tau_s \simeq \frac{1}{12} \left(\frac{L}{L_s} \right)^2. \quad (5.62)$$

This corresponds to the suppression of spin-relaxation in small systems reported earlier by other authors [114–118]. This effect can be traced back to the specific form of the spin-orbit field in the Rashba Hamiltonian – being proportional to the velocity [116]. Here we formulate the argument for a system including both the Rashba and the linear Dresselhaus term – Eqs. (3.19) and (3.22) – within the spin diffusion equation approach. For a spin profile that is homogeneous along $\hat{\mathbf{x}}$ the

angular averaged Eilenberger equation, Eq. (5.56), yields

$$\partial_t s_x + \nabla_y j_{s_x}^y = -2m\alpha j_{s_z}^x - 2m\beta j_{s_z}^y, \quad (5.63)$$

$$\partial_t s_y + \nabla_y j_{s_y}^y = -2m\alpha j_{s_z}^y - 2m\beta j_{s_z}^x, \quad (5.64)$$

$$\partial_t s_z + \nabla_y j_{s_z}^y = 2m\alpha(j_{s_x}^x + j_{s_y}^y) + 2m\beta(j_{s_x}^y + j_{s_y}^x). \quad (5.65)$$

In the diffusive limit the spin current densities are given by

$$j_{s_\alpha}^\beta = -D\partial_\beta s_\alpha + 2\tau\langle v_F^\beta(\mathbf{b} \times \mathbf{s})_\alpha \rangle, \quad (5.66)$$

which allows to reproduce the spin diffusion equation, Eqs. (5.53)–(5.55). In narrow systems the slow modes have a smooth density profile, such that to leading order in the system size the current can be considered constant in space. For a quantum dot, i.e. a system that is confined in all spatial directions, the vanishing of the spin current through the boundaries then immediately implies that $\partial_t s = 0$. For a narrow wire the situation becomes slightly more complicated since only currents flowing into the boundary are zero, which after some algebra leads to

$$\partial_t \mathbf{s} = -\frac{1}{\tau_s} \frac{1}{\alpha^2} \begin{pmatrix} \alpha^2 & \alpha\beta & 0 \\ \alpha\beta & \beta^2 & 0 \\ 0 & 0 & \alpha^2 + \beta^2 \end{pmatrix} \begin{pmatrix} s_x \\ s_y \\ s_z \end{pmatrix}. \quad (5.67)$$

In the absence of the Dresselhaus term ($\beta = 0$) this means that $\partial_t s_y = 0$, and $\partial_t s_x = -s_x/\tau_s$, $\partial_t s_z = -s_z/\tau_s$, which in time implies that the long-living mode in Fig. 5.11 is polarized in the y -direction. In the presence of both a Rashba and a Dresselhaus term, the spin is still conserved for one direction which depends on the relative strength of the two terms: perpendicular to the boundary when the first one dominates, parallel when the latter is larger, and somewhere in between (but always in-plane) when the two are comparable in size.

The above results change considerably when different boundary conditions are applied, and agree with what experimentally observed in [113]. The right panel of Fig. 5.10 shows the time evolution of a spin polarization using adiabatic boundary conditions, Eq. (5.61). Here the spin has been prepared in the y -direction, i.e. perpendicular to the boundary. In this case the boundary mode is absent, and the asymptotic decay of the spin polarization is ruled by an inhomogeneous but extended mode. The boundary condition implies that the eigenmodes are $s_{x,y} \propto$

$\sin(qx)$, $s_z \propto \cos(qx)$ with $q = n\pi/L$; the eigenvalues are given by

$$\gamma(q) = Dq^2 + \frac{3}{2\tau_s} \pm \frac{1}{2\tau_s} \sqrt{1 + 16L_s^2 q^2}. \quad (5.68)$$

By inserting the allowed q -values the spectrum shown in the right panel of Fig. 5.11 is reproduced. In contrast to the previous case of a spin-conserving boundary, here all the diffusion modes $s_{x,y}$ show an increasing spin relaxation rate at the smallest wire widths, and in particular a non monotonous behaviour as a function of the wire width with a minimum at $L/L_s = (4\pi/\sqrt{15}) n \approx 3 n$, where n is the mode index. When $L < L_s$ they all relax fast. On the other hand one should note the different behaviour of the s_z modes – for which, for example, a homogeneous mode with $\gamma\tau_s = 1$ exists. This is not surprising. Indeed, as already pointed out, the adiabatic boundary conserves the s_z spin component, in contrast to the $s_{x,y}$ ones.

Chapter 6

Epilogue

Understanding spin-charge coupled dynamics in low dimensional systems is of paramount importance to one of the main goals of spintronics: the manipulation of the spin degrees of freedom of carriers by purely electrical means. Quasiclassical equations are a powerful and versatile tool in this sense, very much at ease in the realm of mesoscopic physics. In Chapter 4 we have shown how to generalize them so as to handle systems with spin-orbit coupling, whereas in Chapter 5 we have applied the theory to some particular problems of interest. Namely, we have extensively discussed the direct spin Hall effect in various situations, e.g.

- in the bulk of a clean system, where it is possible to relate it to a Berry phase in momentum space;
- in both non-magnetically and magnetically disordered samples, possibly in the presence of an external magnetic field;
- in steady state as well as under time dependent conditions;
- in confined geometries.

We have also investigated the relation between spin Hall currents and voltage induced spin polarizations, and additionally spent some effort studying the latter in their own right. Finally, motivated by a recent experiment, we have focused on the problem of spin relaxation in narrow two-dimensional strips and have seen how this is heavily influenced by the choice of boundary conditions.

As for the open questions in the field, their number is rather large, and ranges from the fundamental to the more practical kind. In the case of spintronics proper, most are nicely summarized in the review from Awschalom [4]. We here recall a few others, some of which were mentioned at various points in the course of the previous Chapters.

1. Effects due to topologically protected edge states are attracting attention – the so-called quantum spin Hall effect, with a first round of theoretical and experimental results available.
2. The magnitude of the spin-electric effects considered is apparently directly related to the energy dependence of the density of states and the velocity near the Fermi surface. In a certain sense, to the breaking of particle-hole symmetry. How general is such a statement? And can it be formulated more precisely?
3. Mesoscopic fluctuations could definitely prove to play a major role in all of the phenomena analyzed. However, up to now almost nothing has been done in this direction.
4. In general terms, quantum corrections can be relevant in low-dimensional disordered systems such as the ones considered. Once again though, this point has been mainly overlooked, the only reference we are aware of being [97].
5. A complete generalization of the boundary conditions for the quasiclassical Green's function in the presence of spin-orbit coupling is still missing.
6. How exactly do intrinsic and extrinsic effects influence one another? Is there a clear physical picture? This is actually an old problem [121] which has more recently received new attention [122, 123] – though no clear answer has been given.
7. Is there a way to formulate quasiclassics in a $SU(2)$ -covariant form? This would let one treat all linear-in-momentum spin-orbit couplings, possibly due to both intrinsic and extrinsic mechanisms, in a unified way. Indeed, these can be introduced in the Hamiltonian $H = p^2/2m$ through a $SU(2)$

gauge transformation [77, 124], much in the same way as the electromagnetic field is introduced via the $U(1)$ gauge. It then becomes a matter of generalizing the procedure of Section 2.2.1 from the simple $U(1)$ algebra to the more complex non-commuting $SU(2)$ one.

The last three points have been the subject of recent work, which however has not yet been finalized.

Appendix A

Time-evolution operators

We discuss in some detail the structure of the unitary time-evolution operator $\mathcal{U}(t, t_0)$ generated by the Hamiltonian $\mathcal{H}(t)$

$$\mathcal{H}(t) = H + H^{ext}(t), \quad H = H_0 + H^i, \quad H^{ext}(t) = 0 \text{ for } t < t_0, \quad (\text{A.1})$$

$$\mathcal{U}(t, t_0) \equiv T \left\{ \exp \left(-i \int_{t_i}^{t_f} dt' \mathcal{H}(t') \right) \right\}, \quad (\text{A.2})$$

with $T \{ \dots \}$ the time-ordering operator. The time-ordered exponential is defined by [45]

$$T \left\{ \exp \left(-i \int_{t_i}^{t_f} dt' \mathcal{H}(t') \right) \right\} \equiv \lim_{M \rightarrow \infty} e^{-\epsilon \mathcal{H}(t_M)} e^{-\epsilon \mathcal{H}(t_{M-1})} \dots e^{-\epsilon \mathcal{H}(t_1)} e^{-\epsilon \mathcal{H}(t_0)},$$

with $\epsilon = \frac{t_f - t_i}{M}$ and $t_n = t_i + n\epsilon$. In this limit, i.e. $M \rightarrow \infty, \epsilon \rightarrow 0, M\epsilon$ finite, the exponential of operators decompose as that of c -numbers. Indeed, for any two noncommuting operators A, B , according to the Baker-Hausdorff formula

$$e^{\epsilon(A+B)} = e^{\epsilon A} e^{\epsilon B} + O(\epsilon^2). \quad (\text{A.3})$$

We will use Eq. (A.3) shortly. For convenience we rename $t_f = t, t_i = t_0$ and decompose $\mathcal{U}(t, t_0)$

$$\begin{aligned} \mathcal{U}(t, t_0) &= \mathcal{U}_0(t, t_0) \mathcal{S}(t, t_0) \\ &= e^{-iH_0(t-t_0)} \mathcal{S}(t, t_0). \end{aligned} \quad (\text{A.4})$$

We use Eq. (A.4) in the equation of motion for $\mathcal{U}(t, t_0)$

$$\begin{aligned}
i\partial_t \mathcal{U}(t, t_0) &= \mathcal{H}(t) \mathcal{U}(t, t_0) \\
&= H_0 \mathcal{U}_0(t, t_0) \mathcal{S}(t, t_0) + [H^i + H^{ext}(t)] \mathcal{U}_0(t, t_0) \mathcal{S}(t, t_0) \\
&= i\partial_t [\mathcal{U}_0(t, t_0) \mathcal{S}(t, t_0)] \\
&= H_0 \mathcal{U}_0(t, t_0) \mathcal{S}(t, t_0) + \mathcal{U}_0(t, t_0) i\partial_t \mathcal{S}(t, t_0)
\end{aligned} \tag{A.5}$$

so that, thanks to Eq. (A.3)

$$\begin{aligned}
\mathcal{S}(t, t_0) &= T \left\{ \exp \left[-i \int_{t_0}^t dt' \mathcal{U}^\dagger(t', t_0) (H^i + H^{ext}(t')) \mathcal{U}(t', t_0) \right] \right\} \\
&= T \left\{ \exp \left[-i \int_{t_0}^t dt' (H_{H_0}^i(t') + H_{H_0}^{ext}(t')) \right] \right\} \\
&= T \left\{ \exp \left[-i \int_{t_0}^t dt' H_{H_0}^i(t') \right] \right\} T \left\{ \exp \left[-i \int_{t_0}^t dt' H_{H_0}^{ext}(t') \right] \right\} \\
&= \mathcal{S}^i(t, t_0) \mathcal{S}^{ext}(t, t_0).
\end{aligned} \tag{A.6}$$

Appendix B

Equilibrium distribution

Denoting by $\langle \dots \rangle$ the grand-canonical ensemble average, in thermal equilibrium at the temperature $T = 1/\beta$ the Kubo-Martin-Schwinger boundary condition

$$\langle \psi^\dagger(\mathbf{x}', t') \psi(\mathbf{x}, t) \rangle = \langle \psi(\mathbf{x}, t) \psi^\dagger(\mathbf{x}', t' + i\beta) \rangle \quad (\text{B.1})$$

can be reformulated as a boundary condition for the Green's function

$$G_0^<(1, 1')|_{t_1=0} = \pm e^{-\beta\mu} G_0^>(1, 1')|_{t_1=-i\beta}, \quad (\text{B.2})$$

with μ the chemical potential. This is done simply by using the definition of $G^{<,>}$ and the cyclic property of the trace. The \pm sign corresponds to bosons or fermions. We will now consider fermions.

An equilibrium state is invariant under time translations. Assuming it to be translationally invariant in space too, Eq. (B.2) may be rewritten in Fourier space as $[p = (\epsilon, \mathbf{p})]$

$$\begin{aligned} G_0^<(p) &= -e^{-\beta(\epsilon-\mu)} G_0^>(p) \\ &\rightarrow -e^{-\beta\epsilon} G_0^>(p), \end{aligned} \quad (\text{B.3})$$

where in the second line the energy has been rescaled to be evaluated from the chemical potential. According to Section 2.1.2 one has

$$G^K(1, 1') = G^>(1, 1') + G^<(1, 1') \quad (\text{B.4})$$

$$G^R(1, 1') - G^A(1, 1') = G^>(1, 1') - G^<(1, 1'). \quad (\text{B.5})$$

In equilibrium Eqs. (B.3), (B.4) and (B.5) imply

$$G_0^K = [G_0^R - G_0^A] \tanh\left(\frac{\beta\epsilon}{2}\right). \quad (\text{B.6})$$

For $G_0^{-1} = \epsilon - \frac{\mathbf{p}^2}{2m} + \mu$, as given in Section 2.2, if the spectral weight has a delta-like profile, $G_0^R - G_0^A = -2i\pi\delta(\epsilon - \xi)$, then for the distribution function introduced in Eq. (2.48)

$$f(X, \mathbf{p}) \equiv \frac{1}{2} \left(1 + \int \frac{d\epsilon}{2\pi i} G^K(X, p) \right) \quad (\text{B.7})$$

in equilibrium one has

$$\begin{aligned} f_0(X, \mathbf{p}) &= \frac{1}{2} \left[1 + \int \frac{d\epsilon}{2\pi i} G_0^K(X, p) \right] \\ &= \frac{1}{2} \left[1 - \tanh\left(\frac{\beta\epsilon}{2}\right) \right], \end{aligned} \quad (\text{B.8})$$

that is, the Fermi distribution.

Appendix C

On gauge invariant Green's functions

For our calculations we rely on the following definitions and conventions.

1. Wigner coordinates and metric, as well as the Fourier-transform, are as defined in Section 2.2, see Eqs. (2.39)–(2.42).
2. The $U(1)$ gauge transformations for the field operators $\hat{\psi}$ and the connection A read

$$\begin{aligned}\hat{\psi}'(1) &= e^{i\chi(1)}\hat{\psi}(1), \\ eA'(1) &= eA(1) - \partial_1\chi(1), \text{ with } A(1) = (\Phi(1), \mathbf{A}(1)), e = |e|.\end{aligned}$$

From this it follows that \check{G} transforms according to

$$\check{G}'(1, 2) = e^{i\chi(1)}\check{G}(1, 2)e^{-i\chi(2)}. \quad (\text{C.1})$$

An exactly gauge invariant Green's function can thus be defined

$$\check{\check{G}}(X + x/2, X - x/2) \equiv \exp \left[-ie \int_{X+x/2}^{X-x/2} \mathbf{d}1' A(1') \right] \check{G}(X + x/2, X - x/2). \quad (\text{C.2})$$

In the gradient approximation one assumes $A(1')$ to vary slowly on the scale of $|\mathbf{x}_1| \sim 1/p_F, t_1 \sim 1/\epsilon_F$, i.e. to be roughly constant between $X + x/2$ and $X - x/2$, so that Eq. (C.2) becomes

$$\check{\check{G}}(X + x/2, X - x/2) \approx \exp [ieA(X)x] \check{G}(X + x/2, X - x/2). \quad (\text{C.3})$$

Fourier-transforming to the mixed representation one obtains

$$\begin{aligned}
\check{G}(X, p) &= \int dx e^{-ipx} \check{G}(X, x) \\
&\approx \int dx e^{-i[p-eA(X)]x} \check{G}(X, x) \\
&\approx \check{G}(X, p - eA(X)).
\end{aligned} \tag{C.4}$$

We emphasize that Eq. (C.4) is valid only to linear order, i.e.

$$\check{G}(X, p) = \check{G}(X, p) - e\Phi(X)\partial_\epsilon \check{G} - e\mathbf{A}(X) \cdot \nabla_{\mathbf{p}} \check{G}. \tag{C.5}$$

Note that formally, since $\check{G}(X, p)$ and $\check{G}(X, p)$ are related by a simple variable shift, the following holds

$$\begin{aligned}
\left[\partial_X \check{G}(X, p) \right]_p &= \left[\partial_X \check{G}(X, p^*) \right]_{p^*} + \\
&\quad + \left[\partial_X (p^*) \right]_p \left[\partial_{p^*} \check{G}(X, p^*) \right]_X,
\end{aligned} \tag{C.6}$$

with $p^* = p + eA(X)$, and

$$\left[\partial_p \check{G}(X, p) \right]_X = \left[\partial_{p^*} \check{G}(X, p^*) \right]_X. \tag{C.7}$$

Obviously, whereas $\check{G}(X, p) = G(X, p - eA(X))$ is a gauge invariant quantity, $\check{G}(X, p^*)$ is not, as $\check{G}(X, p^*) = G(X, p)$.

The above concept of a shift $p \rightarrow p^*$ was first used in [125], and it is safe to rely on it for the present – Abelian – case. It must however be kept in mind that the nature of the manipulations behind it is actually different and has to do with the geometrical structure of a given gauge symmetry, a fact that becomes manifest only when dealing with non-Abelian gauges. This is a topic of ongoing research we will not comment further on.

The equation of motion for $\check{G}(X, p)$ is readily obtained following the standard procedure:

1. take the Dyson equation for \check{G} , (2.67), and its adjoint;
2. subtract the two;
3. move to the mixed representation and use Eq. (2.43) to perform a gradient expansion;

4. use Eqs. (C.5)–(C.7).

The result reads

$$[\partial_T + \mathbf{v} \cdot (\nabla_{\mathbf{R}} - e\mathbf{E}\partial_\epsilon) + \mathbf{F} \cdot \nabla_{\mathbf{p}}] \tilde{G}(\epsilon, \mathbf{p}; X) = 0, \quad (\text{C.8})$$

where

$$\begin{aligned} \mathbf{v} &= \frac{\mathbf{p}}{m}, \\ \mathbf{E}(X) &= -(\nabla_{\mathbf{R}}\Phi(X) + \partial_T\mathbf{A}(X)), \\ \mathbf{B}(X) &= \nabla_{\mathbf{R}} \wedge \mathbf{A}(X), \\ \mathbf{F}(X, p) &= -e(\mathbf{E}(X) + \mathbf{v} \wedge \mathbf{B}(X)). \end{aligned} \quad (\text{C.9})$$

The ξ -integrations leads to Eq. (2.75)

$$\left[\partial_T + v_F \hat{\mathbf{p}} \cdot \nabla_{\mathbf{R}} - ev_F \mathbf{E} \cdot \hat{\mathbf{p}} \partial_\epsilon + e \frac{\mathbf{E} \cdot \hat{\mathbf{p}}}{p_F} + \frac{\mathbf{F}(p_F, \varphi) \cdot \hat{\boldsymbol{\varphi}}}{p_F} \partial_\varphi \right] \tilde{g}^K(\epsilon, \varphi; X) = 0, \quad (\text{C.10})$$

where we have used the following

$$\begin{aligned} \mathbf{F}(\xi, \varphi) &= -e\mathbf{E} - e \frac{p(\xi)}{m} \hat{\mathbf{p}} \wedge \mathbf{B}, \\ \nabla_{\mathbf{p}} &= \frac{p(\xi)}{m} \hat{\mathbf{p}} \partial_\xi + \frac{1}{p(\xi)} \hat{\boldsymbol{\varphi}} \partial_\varphi, \\ \frac{1}{m} \partial_\xi p(\xi) &= \frac{1}{p(\xi)}, \\ \hat{\mathbf{p}}(\varphi) \perp \hat{\boldsymbol{\varphi}}(\varphi), \quad \partial_\varphi \hat{\boldsymbol{\varphi}} &= -\hat{\mathbf{p}}. \end{aligned}$$

Indeed, explicitly

$$\begin{aligned} \frac{i}{\pi} \int d\xi \mathbf{F}(\xi, \varphi) \cdot \nabla_{\mathbf{p}} \tilde{G}^K &= \frac{i}{\pi} \int d\xi \mathbf{F}(\xi, \varphi) \cdot \left[\frac{p(\xi)}{m} \hat{\mathbf{p}} \partial_\xi + \frac{1}{p(\xi)} \hat{\boldsymbol{\varphi}} \partial_\varphi \right] \tilde{G}^K \\ &= \frac{i}{\pi} \int d\xi \left[-e\mathbf{E} \cdot \hat{\mathbf{p}} \frac{p(\xi)}{m} \partial_\xi + \frac{\mathbf{F}(\xi, \varphi) \cdot \hat{\boldsymbol{\varphi}}}{p(\xi)} \partial_\varphi \right] \tilde{G}^K \\ &= e\mathbf{E} \cdot \hat{\mathbf{p}} \frac{i}{\pi} \int d\xi \frac{1}{m} \partial_\xi p(\xi) \tilde{G}^K + \frac{i}{\pi} \int d\xi \frac{\mathbf{F}(\xi, \varphi) \cdot \hat{\boldsymbol{\varphi}}}{p(\xi)} \partial_\varphi \tilde{G}^K \\ &= \left[e \frac{\mathbf{E} \cdot \hat{\mathbf{p}}}{p_F} + \frac{\mathbf{F}(p_F, \varphi) \cdot \hat{\boldsymbol{\varphi}}}{p_F} \partial_\varphi \right] \tilde{g}^K(\epsilon, \varphi; X). \end{aligned} \quad (\text{C.11})$$

Integrating Eq.(C.10) over the energy and averaging over the angle must lead to the continuity equation. One has

$$\begin{aligned} \partial_T \langle \int d\epsilon \tilde{g}^K \rangle + \nabla_{\mathbf{R}} \cdot \langle \int d\epsilon v_F \hat{\mathbf{p}} \tilde{g}^K \rangle - e v_F \langle \int d\epsilon \mathbf{E} \cdot \hat{\mathbf{p}} \partial_\epsilon \tilde{g}^K \rangle + \\ + e \langle \int d\epsilon \frac{\mathbf{E} \cdot \hat{\mathbf{p}}}{p_F} \tilde{g}^K \rangle + \langle \int d\epsilon \frac{\mathbf{F}(p_F, \varphi) \cdot \hat{\varphi}}{p_F} \partial_\varphi \tilde{g}^K \rangle = 0. \end{aligned}$$

The third term is easily seen to be zero, since for $\epsilon \rightarrow \pm\infty$ \tilde{g}^K assumes its equilibrium form, which does not depend on φ . The two terms on the second line partially cancel out

$$\begin{aligned} e \langle \int d\epsilon \frac{\mathbf{E} \cdot \hat{\mathbf{p}}}{p_F} \tilde{g}^K \rangle + \langle \int d\epsilon \frac{\mathbf{F}(p_F, \phi) \cdot \hat{\varphi}}{p_F} \partial_\varphi \tilde{g}^K \rangle = \\ e \langle \int d\epsilon \frac{\mathbf{E} \cdot \hat{\mathbf{p}}}{p_F} \tilde{g}^K \rangle + \int d\epsilon \left[\frac{\mathbf{F} \cdot \hat{\varphi}}{p_F} \tilde{g}^K \Big|_0^{2\pi} - \int \frac{d\varphi}{2\pi} \partial_\varphi \frac{\mathbf{F} \cdot \hat{\varphi}}{p_F} \tilde{g}^K \right] = \\ e \langle \int d\epsilon \frac{\mathbf{E} \cdot \hat{\mathbf{p}}}{p_F} \tilde{g}^K \rangle + \int d\epsilon \frac{\mathbf{F} \cdot \hat{\varphi}}{p_F} \tilde{g}^K \Big|_0^{2\pi} - e \langle \int d\epsilon \frac{\mathbf{E} \cdot \hat{\mathbf{p}}}{p_F} \tilde{g}^K \rangle = \\ \int d\epsilon \frac{\mathbf{F} \cdot \hat{\varphi}}{p_F} \tilde{g}^K \Big|_0^{2\pi} = 0, \quad (\text{C.12}) \end{aligned}$$

where in the last line we have used that $\tilde{g}^K(\epsilon, 0; X) = \tilde{g}^K(\epsilon, 2\pi; X)$. Therefore we are left with

$$\partial_T \langle \int d\epsilon \tilde{g}^K(\epsilon, \varphi; X) \rangle + \nabla_{\mathbf{R}} \cdot \langle \int d\epsilon v_F \hat{\mathbf{p}} \tilde{g}^K(\epsilon, \varphi; X) \rangle = 0, \quad (\text{C.13})$$

i.e. the continuity equation, Eq. (2.76). Finally, from Eq. (C.5) one sees that

$$\tilde{g}(\epsilon, \hat{\mathbf{p}}) = \left[1 - e\Phi(X)\partial_\epsilon + e \frac{\mathbf{A}(X)}{p_F} (\hat{\mathbf{p}} - \hat{\varphi}\partial_\varphi) \right] g(\epsilon, \mathbf{p}), \quad (\text{C.14})$$

which then implies, using the same technique as above,

$$\rho(X) = -2N_0 \left[\frac{\pi}{2} \langle \int \frac{d\epsilon}{2\pi} g^K(\epsilon, \varphi; X) \rangle - e\Phi(X) \right] \quad (\text{C.15})$$

and

$$\mathbf{j}(X) = -N_0\pi \langle \int \frac{d\epsilon}{2\pi} \left[v_F \hat{\mathbf{p}} g^K(X, \epsilon, \hat{\mathbf{p}}) + \left(\frac{e\mathbf{A}(X) \cdot \hat{\varphi}}{m} \right) \hat{\varphi} g^K(\epsilon, \varphi; X) \right] \rangle. \quad (\text{C.16})$$

Appendix D

The self energy

We consider two kinds of disorder self energy

1. $\check{\Sigma}_{\text{nm}}$, due to non-magnetic and angle-dependent (or long-range) scattering;¹
2. $\check{\Sigma}_{\text{m}}$, arising from magnetic s -wave (or short-range) scattering.

Such scattering mechanisms are modelled by the random potentials $V_{\text{nm}}(\mathbf{x})$

$$V_{\text{nm}}(\mathbf{x}) = \sum_i U(\mathbf{x} - \mathbf{R}_i) \quad (\text{D.1})$$

and $V_{\text{m}}(\mathbf{x})$

$$V_{\text{m}}(\mathbf{x}) = \sum_i \mathbf{B} \cdot \boldsymbol{\sigma} \delta(\mathbf{x} - \mathbf{R}_i), \quad (\text{D.2})$$

which must be averaged over the impurities' positions. This operation, which we denote by a bar, is performed according to the standard technique [34]

$$\overline{V_{\text{nm}}(\mathbf{x})} = \overline{V_{\text{m}}(\mathbf{x})} = 0, \quad (\text{D.3})$$

$$\overline{V_{\text{nm}}(\mathbf{x})V_{\text{nm}}(\mathbf{x}')} = n_{\text{nm}} \sum_{\mathbf{q}} |U(\mathbf{q})|^2 e^{i\mathbf{q} \cdot (\mathbf{r} - \mathbf{r}')}, \quad (\text{D.4})$$

$$\overline{V_{\text{m}}(\mathbf{x})V_{\text{m}}(\mathbf{x}')} = n_{\text{m}} \frac{B^2}{3} \delta(\mathbf{x} - \mathbf{x}'), \quad (\text{D.5})$$

where n_{nm} and n_{m} denote the concentrations of non-magnetic and magnetic impurities, respectively.

¹Non-magnetic s -wave (or short-range) scattering is a subcase of this.

$\check{\Sigma}_{\text{nm}}$ and $\check{\Sigma}_{\text{m}}$ are evaluated in the Born approximation, i.e. diagrams with crossing impurity lines are not considered. They read

$$\check{\Sigma}_{\text{nm}}(\mathbf{p}) = n_{\text{nm}} \sum_{\mathbf{p}'} |U(\mathbf{p} - \mathbf{p}')|^2 \check{G}(\mathbf{p}') \quad (\text{D.6})$$

and

$$\check{\Sigma}_{\text{m}} = n_{\text{m}} \frac{B^2}{3} \sum_{l=1}^3 \sum_{\mathbf{p}} \sigma_l \check{G}(\mathbf{p}) \sigma_l. \quad (\text{D.7})$$

In the first case we expand the non-magnetic scattering kernel in spherical harmonics of the scattering angle and neglect its dependence on the modulus of \mathbf{p} and \mathbf{p}'

$$\begin{aligned} n_{\text{nm}} |U|^2 &= \frac{1}{2\pi N_0 \tau} (1 + 2K_1 \cos(\varphi - \varphi') + \\ &\quad 2K_2 \cos(2\varphi - 2\varphi') + \dots) \\ &\equiv \frac{1}{2\pi N_0 \tau} (1 + K(\varphi - \varphi')) \end{aligned} \quad (\text{D.8})$$

with τ the non-magnetic elastic lifetime and $N_0 = m/2\pi$ the density of states of two-dimensional electron gas. This way one has

$$\check{\Sigma}_{\text{nm}} = -\frac{i}{2\tau} \langle (1 + K) \check{g} \rangle \quad (\text{D.9})$$

where $\langle \dots \rangle = \int \frac{d\varphi}{2\pi}$. In the second instance instead we write the magnetic scattering kernel in terms of the spin-flip time τ_{sf}

$$n_{\text{m}} B^2 = \frac{1}{2\pi N_0 \tau_{sf}}, \quad (\text{D.10})$$

so that

$$\check{\Sigma}_{\text{m}} = -\frac{i}{6\tau_{sf}} \sum_{l=1}^3 \sigma_l \langle \check{g} \rangle \sigma_l. \quad (\text{D.11})$$

Given the self energy, the collision integral of the Eilenberger equation, $-i [\check{\Sigma}, \check{g}]$, can be computed. Its Keldysh component in particular reads

$$\begin{aligned} -i [\check{\Sigma}, \check{g}]^K &= -i (\Sigma^R g^K - g^K \Sigma^A + \Sigma^K g^R - g^A \Sigma^K) \\ &= -i \{ \Sigma^R, g^K \} + i \{ \Sigma^K, g^R \}, \end{aligned} \quad (\text{D.12})$$

where we have used that $g^R = -g^A$ and that $\Sigma^R = (\Sigma^A)^* = -\Sigma^A$. Substituting Eq. (D.9) or Eq. (D.11) – or the sum of the two – into the above gives the collision integral in its explicit form.

Appendix E

Effective Hamiltonians

Some details regarding the material of Chapter 3 are discussed. For an exhaustive treatment see the literature references given in the text.

E.1 The $\mathbf{k} \cdot \mathbf{p}$ expansion

We start from the Schrödinger equation (3.2) with $\hbar = c = 1$

$$\begin{aligned} H_0 \Psi_{\nu\mathbf{k}}(\mathbf{x}) &= \left[\frac{(-i\nabla)^2}{2m_0} + U(\mathbf{x}) + \frac{\hbar}{4m_0^2} \nabla U(\mathbf{x}) \wedge (-i\nabla) \cdot \boldsymbol{\sigma} \right] \Psi_{\nu\mathbf{k}}(\mathbf{r}) \\ &= \epsilon_{\nu\mathbf{k}} \Psi_{\nu\mathbf{k}}(\mathbf{x}) \end{aligned} \quad (\text{E.1})$$

and consider the expansion (3.4)

$$u_{\nu\mathbf{k}}(\mathbf{x}) = \sum_{\nu'} c_{\nu\nu'\mathbf{k}} u_{\nu'0}(\mathbf{x}) \quad (\text{E.2})$$

for the lattice-periodic part of $\Psi_{\nu\mathbf{k}}(\mathbf{x})$

$$\Psi_{\nu\mathbf{k}}(\mathbf{x}) = e^{i\mathbf{k}\cdot\mathbf{x}} u_{\nu\mathbf{k}}(\mathbf{x}). \quad (\text{E.3})$$

In ket notation

$$|\Psi_{\nu\mathbf{k}}\rangle = \sum_{\nu'} e^{i\mathbf{k}\cdot\mathbf{x}} c_{\nu\nu'\mathbf{k}} |u_{\nu'0}\rangle, \quad \langle \mathbf{x} | \Psi_{\nu\mathbf{k}} \rangle = \Psi_{\nu\mathbf{k}}(\mathbf{x}). \quad (\text{E.4})$$

Substitution into Eq. (E.1) and projection onto the state $\langle u_{\nu 0} |$ gives

$$\begin{aligned}
 \langle u_{\nu 0} | \left\{ \left[\frac{p^2}{2m_0} + U + \frac{1}{4m_0^2} \boldsymbol{\sigma} \wedge \nabla U \cdot \mathbf{p} \right] + \frac{\mathbf{k}}{m_0} \cdot \left[\mathbf{p} + \frac{1}{4m_0} \boldsymbol{\sigma} \wedge \nabla U \right] \right. \\
 \left. - \left[\epsilon_{\nu \mathbf{k}} - \frac{k^2}{2m_0} \right] \right\} | \Psi_{\nu \mathbf{k}}(\mathbf{r}) \rangle = \\
 e^{i\mathbf{k} \cdot \mathbf{x}} \sum_{\nu'} \langle u_{\nu 0} | \left\{ \epsilon_{\nu 0} + \frac{\mathbf{k}}{m_0} \cdot \left[\mathbf{p} + \frac{1}{4m_0} \boldsymbol{\sigma} \wedge \nabla U \right] + \right. \\
 \left. - \left[\epsilon_{\nu \mathbf{k}} - \frac{k^2}{2m_0} \right] \right\} | u_{\nu' 0} \rangle c_{\nu' \mathbf{k}} = \\
 e^{i\mathbf{k} \cdot \mathbf{x}} \sum_{\nu'} \left\{ \left[\epsilon_{\nu 0} - \epsilon_{\nu \mathbf{k}} + \frac{k^2}{2m_0} \right] \delta_{\nu \nu'} + \frac{1}{m_0} \mathbf{k} \cdot \boldsymbol{\pi}_{\nu \nu'} \right\} c_{\nu' \mathbf{k}} = 0
 \end{aligned} \tag{E.5}$$

with

$$\left[\frac{(-i\nabla)^2}{2m_0} + U + \frac{1}{4m_0} \nabla U \wedge (-i\nabla) \cdot \boldsymbol{\sigma} \right] u_{\nu 0}(\mathbf{x}) = \epsilon_{\nu 0} u_{\nu 0}(\mathbf{x}), \tag{E.6}$$

that is

$$\left[\frac{p^2}{2m_0} + U + \frac{1}{4m_0^2} \nabla U \wedge \mathbf{p} \cdot \boldsymbol{\sigma} \right] | u_{\nu 0} \rangle = \epsilon_{\nu 0} | u_{\nu 0} \rangle, \tag{E.7}$$

and

$$\boldsymbol{\pi}_{\nu \nu'} = \langle u_{\nu 0} | \left[\mathbf{p} + \frac{1}{4m_0} \nabla U \wedge \boldsymbol{\sigma} \right] | u_{\nu' 0} \rangle. \tag{E.8}$$

Each matrix element has to be intended as an integral over the unit cell

$$\langle u_{\nu 0} | \hat{O} | u_{\nu' 0} \rangle = \int_{\text{cell}} d\mathbf{x} u_{\nu 0}^*(\mathbf{x}) O u_{\nu' 0}(\mathbf{x}), \tag{E.9}$$

with \hat{O} a given hermitian operator.¹ $\epsilon_{\nu 0}$ is the energy offset of the ν -th band at $\mathbf{k} = 0$, since Eq. (E.6) is formally given by $H_0(\mathbf{k} = \mathbf{0})u_{\nu 0} = \epsilon_{\nu 0}u_{\nu 0}$. It is seen that \mathbf{p} denotes the atomic momentum, i.e. the fast momentum tied to the quickly oscillating lattice function $u_{\nu 0}$, whereas \mathbf{k} represents the slow crystal momentum of the electrons at the bottom of the band. Because of this one approximates

$$\boldsymbol{\pi}_{\nu \nu'} \approx \langle u_{\nu 0} | \mathbf{p} | u_{\nu' 0} \rangle, \tag{E.10}$$

¹More precisely, $\langle a | \hat{O} | b \rangle = \int \int d\mathbf{x} d\mathbf{x}' \psi_a^*(\mathbf{x}) O(\mathbf{x}, \mathbf{x}') \psi_b(\mathbf{x}')$. When \hat{O} is a function of the position operator or a power of the momentum one things simplify and Eq. (E.9) holds [126].

which amounts to neglecting the term

$$\frac{1}{4m_0^2} \mathbf{k} \cdot \nabla U \wedge \boldsymbol{\sigma} \sim kp, \quad \nabla V \sim p \quad (\text{E.11})$$

as compared to the diagonal one

$$\frac{1}{4m_0^2} \mathbf{p} \cdot \nabla U \wedge \boldsymbol{\sigma} \sim p^2. \quad (\text{E.12})$$

When an additional non-crystalline and slowly varying potential $V(\mathbf{x})$ is present, the envelope ansatz (3.9) is made

$$|\psi\rangle = \sum_{\nu} \phi_{\nu}(\mathbf{x}) |u_{\nu 0}\rangle \quad (\text{E.13})$$

and the procedure goes through as before, with the momentum $\mathbf{k} \ll \mathbf{p}$ now related to $\phi_{\nu}(\mathbf{x})$ and $V(\mathbf{x})$. That is, $\mathbf{k} \sim \nabla \phi_{\nu}(\mathbf{x}), \nabla V(\mathbf{x})$. Then, for the very same reason as before, the two additional spin-orbit terms due to V

$$\frac{1}{4m_0^2} \mathbf{k} \cdot \nabla V \wedge \boldsymbol{\sigma} \sim k^2, \quad (\text{E.14})$$

$$\frac{1}{4m_0^2} \mathbf{p} \cdot \nabla V \wedge \boldsymbol{\sigma} \sim kp, \quad (\text{E.15})$$

are neglected.

E.2 Symmetries and matrix elements

The matrix elements (3.11) are given by the selection rules determined by the symmetries of the system, whose general theory can be found in [127]. Basically, some convenient linear combinations \tilde{u}_i of the different $u_{\nu 0}$ are used as a basis, so that these will share some particular symmetries with H – for example, the total angular momentum $\mathbf{J} = \mathbf{L} + \mathbf{S}$. The \tilde{u}_i will transform according to a certain irreducible representation of the symmetry group of H , call this Γ_i , and so will a general operator \hat{O} , say Γ_O . The matrix element $\langle \tilde{u}_i | \hat{O} | \tilde{u}_j \rangle$ will transform according to the direct-product representation $\Gamma_i \times \Gamma_O \times \Gamma_j$, and it will be non-vanishing only if such a product contains the unity representation.

Concretely, when the $|J, m_J\rangle$ basis is chosen (see Table E.1) the 8×8 Kane Hamiltonian

$$H_{8 \times 8} = \begin{pmatrix} [H_c]_{2 \times 2} & [H_{cv}]_{2 \times 6} \\ [H_{cv}^\dagger]_{6 \times 2} & [H_v]_{6 \times 6} \end{pmatrix} \quad (\text{E.16})$$

reads [57]

$$[H_c]_{2 \times 2} = \begin{pmatrix} V & 0 \\ 0 & V \end{pmatrix},$$

$$[H_{cv}]_{2 \times 6} = \begin{pmatrix} \frac{-1}{\sqrt{2}}Pk_+ & \sqrt{\frac{2}{3}}Pk_z & \frac{1}{\sqrt{6}}Pk_- & 0 & \frac{-1}{\sqrt{3}}Pk_z & \frac{-1}{\sqrt{2}}Pk_- \\ 0 & \frac{-1}{\sqrt{6}}Pk_+ & \frac{2}{\sqrt{3}}Pk_z & \frac{1}{\sqrt{2}}Pk_- & \frac{-1}{\sqrt{3}}Pk_+ & \frac{1}{\sqrt{3}}Pk_z \end{pmatrix},$$

$$[H_v]_{6 \times 6} = \begin{pmatrix} [V - E_g]\hat{\mathbf{1}}_{4 \times 4} & \hat{\mathbf{0}}_{4 \times 2} \\ \hat{\mathbf{0}}_{2 \times 4} & (V - E_g - \Delta)\hat{\mathbf{1}}_{2 \times 2} \end{pmatrix},$$

where

$$P = -i \frac{1}{m_0} \langle S|p_x|X \rangle = -i \frac{1}{m_0} \langle S|p_y|Y \rangle = -i \frac{1}{m_0} \langle S|p_z|Z \rangle, \quad (\text{E.17})$$

$$\begin{aligned} \Delta &= \frac{3}{4m_0^2} \langle X | [\partial_y U \partial_x - \partial_x U \partial_y] | Y \rangle \\ &= \frac{3}{4m_0^2} \times \langle \text{any cyclic permutation} \rangle, \end{aligned} \quad (\text{E.18})$$

$k_{\pm} = k_x \pm ik_y$, and the zero of the energy has been set to the conduction band minimum, $\epsilon_{c0} = 0$. Also, U is the crystal potential and V the perturbing one. In terms of the above, the renormalized mass and g -factor, m^* and g^* , and the spin-orbit coupling constant λ that appear in Eq. (3.15) read

$$\frac{1}{2m^*} = \left(\frac{1}{E_g + \Delta} + \frac{2}{E_g} \right), \quad (\text{E.19})$$

$$g^* = \frac{2e}{\mu_B} \frac{P^2}{3} \left(\frac{1}{E_g} - \frac{1}{E_g + \Delta} \right), \quad (\text{E.20})$$

$$\lambda = \frac{P^2}{3} \left(\frac{1}{E_g^2} - \frac{1}{(E_g + \Delta)^2} \right), \quad (\text{E.21})$$

with μ_B the Bohr magneton.

E.3 The Löwdin technique

Consider the $N \times N$ problem

$$(H - E)\psi = 0 \quad (\text{E.22})$$

$$\psi = \sum_{n=1}^N c_n \chi_n \quad (\text{E.23})$$

\tilde{u}_i	Γ	$ J, m_J\rangle$	u_{J,m_J}
\tilde{u}_1	Γ_6	$ \frac{1}{2}, +\frac{1}{2}\rangle$	$i S\rangle +\frac{1}{2}\rangle$
\tilde{u}_2	Γ_6	$ \frac{1}{2}, -\frac{1}{2}\rangle$	$i S\rangle -\frac{1}{2}\rangle$
\tilde{u}_3	Γ_8	$ \frac{3}{2}, +\frac{3}{2}\rangle$	$-\frac{1}{\sqrt{2}}(X\rangle + i Y\rangle) +\frac{1}{2}\rangle$
\tilde{u}_4	Γ_8	$ \frac{3}{2}, +\frac{1}{2}\rangle$	$-\frac{1}{\sqrt{6}}(X\rangle + i Y\rangle) -\frac{1}{2}\rangle + \sqrt{\frac{2}{3}} Z\rangle +\frac{1}{2}\rangle$
\tilde{u}_5	Γ_8	$ \frac{3}{2}, -\frac{1}{2}\rangle$	$+\frac{1}{\sqrt{6}}(X\rangle - i Y\rangle) +\frac{1}{2}\rangle + \sqrt{\frac{2}{3}} Z\rangle -\frac{1}{2}\rangle$
\tilde{u}_6	Γ_8	$ \frac{3}{2}, -\frac{3}{2}\rangle$	$+\frac{1}{\sqrt{2}}(X\rangle - i Y\rangle) -\frac{1}{2}\rangle$
\tilde{u}_7	Γ_7	$ \frac{1}{2}, +\frac{1}{2}\rangle$	$-\frac{1}{\sqrt{3}}(X\rangle + i Y\rangle) -\frac{1}{2}\rangle - \frac{1}{\sqrt{3}} Z\rangle +\frac{1}{2}\rangle$
\tilde{u}_8	Γ_7	$ \frac{1}{2}, -\frac{1}{2}\rangle$	$-\frac{1}{\sqrt{3}}(X\rangle - i Y\rangle) +\frac{1}{2}\rangle + \frac{1}{\sqrt{3}} Z\rangle -\frac{1}{2}\rangle$

Table E.1: Basis of the 8×8 Kane model. $|S\rangle$ denotes an s -like orbital, $|X\rangle, |Y\rangle, |Z\rangle$ three p -like ones. $|\pm\frac{1}{2}\rangle$ is the spinor corresponding to spin up/down along the axis of quantization. Γ indicates the irreducible representation of the symmetry group of the zincblende crystal according to which each basis function transforms.

and suppose the basis $\{\chi_n\}_{n \in N}$ can be divided into two (not-overlapping) sets $A = \{\chi_n\}_{n \in A}, B = \{\chi_n\}_{n \in B}$ such that functions belonging to different sets are weakly coupled. In other words such that in the equation

$$\left[\begin{pmatrix} H_A & H_{AB} \\ H_{AB}^\dagger & H_B \end{pmatrix} - E \right] \begin{pmatrix} \psi_A \\ \psi_B \end{pmatrix} = 0 \quad (\text{E.24})$$

the off-diagonal terms H_{AB}, H_{AB}^\dagger are “small”, that is

$$H_{AB}, H_{AB}^\dagger \ll |H_A - H_B|. \quad (\text{E.25})$$

One then looks for an effective equation in A -space

$$[\mathcal{H}(E) - E] \psi_A = 0 \quad (\text{E.26})$$

which can be turned into a proper eigenvalue equation for ψ_A once $\mathcal{H}(E)$ is expanded in powers of $E/(\text{dominant energy scale})$. Obviously, such dominant energy scale is the one set by $|H_A - H_B|$. Explicitly the original $N \times N$ problem is

rewritten as

$$\sum_{n \in A} (\mathcal{U}_{mn}^A - E\delta_{mn}) c_n = 0, \quad m \in A, \quad (\text{E.27})$$

$$c_m = \sum_{n \in A} \frac{\mathcal{U}_{mn}^A}{E - H_{mm}} c_n, \quad m \in B, \quad (\text{E.28})$$

where

$$\begin{aligned} \mathcal{U}_{mn}^A = & H_{mn} + \sum_{\alpha \in B} \frac{H'_{m\alpha} H'_{\alpha n}}{E - H_{\alpha\alpha}} + \sum_{\alpha, \beta \in B} \frac{H'_{m\alpha} H'_{\alpha\beta} H'_{\beta n}}{(E - H_{\alpha\alpha})(E - H_{\beta\beta})} + \\ & + \dots, \end{aligned} \quad (\text{E.29})$$

$$H'_{mn} = H_{mn}(1 - \delta_{mn}), \quad \text{i.e. } H' = \text{off-diagonal terms of } H. \quad (\text{E.30})$$

Note that the series in Eq. (E.29) converges only if $H'/(E - H_B) \ll 1$. For $E = H_A + \delta E$, with δE a small correction, this is nothing but a rephrasing of the requirement (E.25). When the set A is a single state one obtains the expressions of standard perturbation theory, whereas if A represents a group of degenerate states, the Löwdin technique treats the problem by first tackling the effects of the perturbation, Eq. (E.29), and then removing the degeneracy in A , Eq. (E.27). For the 8×8 Kane model the two degenerate s -like levels play the role of the set A , and the six p -like states that of B . The dominant energy scale is $|H_A - H_B| \sim E_g, E_g + \Delta$.

Appendix F

The Green's function ansatz

In Section 4.2 we looked for an ansatz for the Green's function capable

1. of factorizing its fast and slow components;
2. when spin-orbit coupling appears, of distinguishing between the two poles, each belonging to a fold of the spin-split Fermi surface;
3. of making possible a connection with the quasiclassical $\check{g}(\hat{\mathbf{p}}, \mathbf{R})$.

The results are summarized by Eqs. (4.53)-(4.57), and were obtained assuming that both branches of the Fermi surface,

$$\xi_{\pm} = \xi \pm |\mathbf{b}|, \quad (\text{F.1})$$

were spherical. It was mentioned that it is possible to somewhat relax this requirement. Let us now see how and to what extent.

F.1 The stationary phase approximation

After the general change of variables

$$\int \frac{d\mathbf{p}}{(2\pi)^2} = \iint \frac{d[\epsilon(\mathbf{p}) - \mu]d\mathcal{S}}{(2\pi)^2|\nabla_{\mathbf{p}}\epsilon(\mathbf{p})|} \quad (\text{F.2})$$

the constant energy surfaces \mathcal{S}_{ϵ} need to be parameterized. We do this in terms of the angle φ between \mathbf{p} and \mathbf{r} , which is the natural choice for spherical surfaces,

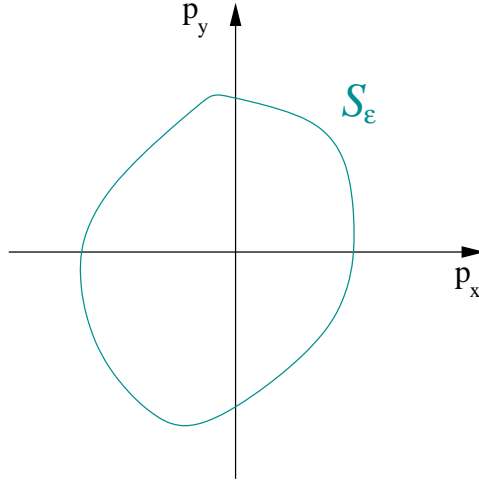


Figure F.1: A generic constant energy surface \mathcal{S}_ϵ parameterized by the angle φ , $\mathcal{S}_\epsilon = \mathbf{p}_\epsilon(\varphi)$.

and still a good one as long as the deviations from the spherically symmetric case are small. The general problem is how to determine the stationary point of $\exp\{ipr \cos(\varphi)\}$ with respect to φ at constant energy. The parameterization for $p = p(\varphi)$ [see Fig. (F.1)] is simply the one defining the profile of \mathcal{S} . The stationary condition then reads

$$\partial_\varphi [pr \cos(\varphi)] = (\partial_\varphi p(\varphi)) r \cos(\varphi) - p(\varphi) r \sin(\varphi) = 0 \quad (\text{F.3})$$

$$\iff \tan(\varphi) = \frac{p'}{p}. \quad (\text{F.4})$$

We consider two specific cases.

1. Spherical Fermi surface:

$$\implies p \text{ doesn't depend on } \varphi$$

$$\implies \tan(\varphi) = 0 \iff \sin(\varphi) = 0 \iff \varphi = 0, \pi. \quad (\text{F.5})$$

This ends the problem.

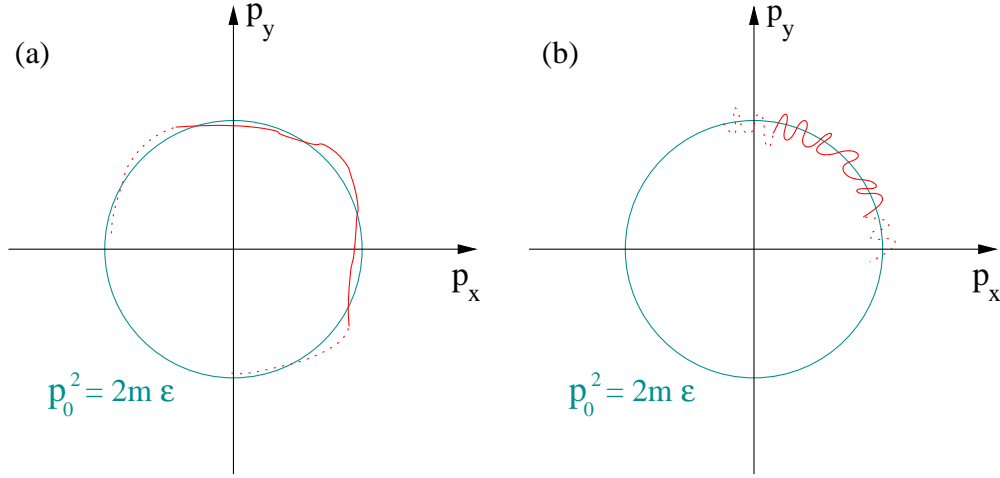


Figure F.2: Qualitative examples of an “almost spherical” Fermi surface (a) and of a non-spherical one (b). Only case (a) is tractable in our approximation.

2. “Almost spherical” Fermi surface, by which we mean a surface such that

$$\frac{|p_0 - p(\varphi)|}{p_0} \ll 1 \quad (\text{F.6})$$

and

$$\frac{|p'(\varphi)|}{p_0} \ll 1, \quad (\text{F.7})$$

where p_0 refers to the spherical Fermi surface, i.e. $p_0^2 = 2m\epsilon$ [see Fig. (F.2)]. This will anyway be defined more properly a little later. From now on we deal with this case.

The energy dispersion is taken from Eq. (4.1)

$$\epsilon(p, \varphi) = \epsilon_0(p) + b(p, \varphi) = \frac{p^2}{2m} + b(p, \varphi), \quad \frac{b}{\epsilon_F} \ll 1, \quad (\text{F.8})$$

and the constraint reads

$$\frac{p^2}{2m} + b(p, \varphi) = \epsilon_F. \quad (\text{F.9})$$

From this we want to obtain an expression for $p(\varphi, \epsilon_F)$. To first order in b/ϵ_F it reads

$$p = p_0 \left[1 - \frac{b(p_0, \varphi)}{2\epsilon_F} \right] \quad (\text{F.10})$$

and in turn we get

$$\begin{aligned}\partial_\varphi p &= -\frac{p_0}{2\epsilon_F}\partial_\varphi b(p_0, \varphi) \\ &= -\frac{\partial_\varphi b(p_0, \varphi)}{v_F}.\end{aligned}\tag{F.11}$$

If we make (F.6) and (F.7) more precise by assuming

$$|\partial_\varphi b(p, \varphi)| \lesssim b,$$

we have

$$\frac{|p'|}{p_0} \lesssim \frac{b}{\epsilon_F} \ll 1\tag{F.12}$$

or, for the stationary condition:

$$\tan(\varphi) = \frac{p'}{p} \approx \frac{p'}{p_0} \lesssim \frac{b}{\epsilon_F}.\tag{F.13}$$

In order to conclude we need one final consideration, based on the following assumptions

$$\begin{aligned}p_\pm &= p_0 \mp \delta p, \quad \frac{\delta p}{p} \sim \frac{b}{\epsilon_F}, \\ \Delta p r &\gtrsim 1, \\ \delta p r &\ll 1,\end{aligned}$$

where Δp describes the limit of resolution when relying on the stationary phase approximation. From the above we get $\delta p/\Delta p \ll 1$, that is, it is not possible to “see” small deviations in the stationary angle:

$$\tan(\varphi) \sim \frac{b}{\epsilon_F} \ll \frac{\Delta p}{p_0} \Rightarrow \tan(\varphi) = 0.\tag{F.14}$$

As long as the Fermi surface is almost spherical, in the sense specified, the stationary angle is the same we would have for an exactly spherical one. This means that the angle appearing in the ansatz for the quasiclassical Green’s function is the same in both bands, and as a consequence Eqs. (4.53)–(4.57) can still be used.

Appendix G

Matrix form of the Eilenberger equation and boundary conditions

Some useful manipulations of the Eilenberger equation, Eq. (4.13), are discussed. Its matrix form is obtained, first in the simple case of s -wave non-magnetic disorder – in order to keep the focus on the general procedure – and then under the more specific assumptions of Section 5.1.2 that lead to Eqs. (5.28)–(5.30). It is also shown how to work with the boundary conditions, Eqs. (5.39), (5.57), in the diffusive regime.

G.1 The matrix form

We start from the Keldysh component of Eq. (4.13) and take traces with respect to the various Pauli matrices. By using the decomposition (5.27)

$$g = g_0\sigma_0 + \mathbf{g} \cdot \boldsymbol{\sigma}, \quad (g_\mu) = (g_0, \mathbf{g}) \quad (\text{G.1})$$

the matrix form of the Eilenberger equation is obtained. Explicitly, with the s -wave self-energy $\Sigma = -i\langle g \rangle / 2\tau$, one has

$$(\mathbf{M}_0 + \mathbf{M}_1)g = (\mathbf{N}_0 + \mathbf{N}_1)\langle g \rangle \quad (\text{G.2})$$

where

$$\begin{aligned} \mathbf{M}_0 g &= g + \tau \partial_t g + v_F \tau \hat{\mathbf{p}} \cdot \partial_{\mathbf{x}} g \\ &\quad - i\tau [\mathbf{b}_0 \cdot \boldsymbol{\sigma}, g], \end{aligned} \quad (\text{G.3})$$

$$\begin{aligned} \mathbf{M}_1 g &= \frac{1}{2} \tau \left\{ \frac{(\mathbf{b}_0 \cdot \boldsymbol{\sigma}) \hat{\mathbf{p}}}{p_F} - \partial_{\mathbf{p}}(\mathbf{b}_0 \cdot \boldsymbol{\sigma}), \partial_{\mathbf{x}} g \right\} \\ &\quad - \frac{1}{2} i\tau [\partial_{\xi}(\mathbf{b}_0 \cdot \boldsymbol{\sigma}), \{\mathbf{b}_0 \cdot \boldsymbol{\sigma}, g\}] \\ &\quad + \frac{1}{2} \{\langle \partial_{\xi} \mathbf{b}_0 \cdot \boldsymbol{\sigma} \rangle, g\}, \end{aligned} \quad (\text{G.4})$$

$$\mathbf{N}_0 \langle g \rangle = \langle g \rangle, \quad (\text{G.5})$$

$$\mathbf{N}_1 \langle g \rangle = \frac{1}{2} \{\partial_{\xi} \mathbf{b}_0 \cdot \boldsymbol{\sigma}, \langle g \rangle\}. \quad (\text{G.6})$$

Here \mathbf{M}_1 and \mathbf{N}_1 are small in the expansion parameter $|\mathbf{b}|/\epsilon_F$. The Eilenberger equation is then rewritten as

$$g = (\mathbf{M}_0 + \mathbf{M}_1)^{-1} (\mathbf{N}_0 + \mathbf{N}_1) \langle g \rangle, \quad (\text{G.7})$$

i.e. to first order in $|\mathbf{b}|/\epsilon_F$

$$g = (\mathbf{M}_0^{-1} + \mathbf{M}_0^{-1} \mathbf{N}_1 - \mathbf{M}_0^{-1} \mathbf{M}_1 \mathbf{M}_0^{-1}) \langle g \rangle, \quad (\text{G.8})$$

from which the equation for the s -wave component of the Green function becomes

$$(1 - \langle \mathbf{M}_0^{-1} \rangle - \langle \mathbf{M}_0^{-1} \mathbf{N}_1 \rangle + \langle \mathbf{M}_0^{-1} \mathbf{M}_1 \mathbf{M}_0^{-1} \rangle) \langle g \rangle = 0. \quad (\text{G.9})$$

In the low frequency, long wavelength limit this is the generalized spin-charge coupled diffusion equation whose explicit form is obtained by evaluating the angular average of the operator product $\mathbf{M}^{-1} \mathbf{N}$.

In the Rashba model for instance, where $\mathbf{b} = \alpha \hat{\mathbf{z}} \wedge \mathbf{p}$, one finds

$$\mathbf{M}_0 = \begin{pmatrix} L & 0 & 0 & 0 \\ 0 & L & 0 & a\hat{p}_x \\ 0 & 0 & L & a\hat{p}_y \\ 0 & -a\hat{p}_x & -a\hat{p}_y & L \end{pmatrix}, \quad (\text{G.10})$$

$$\mathbf{M}_1 = \begin{pmatrix} 0 & Q_y & -Q_x & 0 \\ Q_y & 0 & 0 & 0 \\ -Q_x & 0 & 0 & 0 \\ 0 & 0 & 0 & 0 \end{pmatrix} \quad (\text{G.11})$$

with

$$L = 1 + \tau \partial_t + v_F \tau \hat{\mathbf{p}} \cdot \partial_{\mathbf{x}}, \quad (\text{G.12})$$

$$a = 2\alpha p_F \tau, \quad (\text{G.13})$$

$$Q_{x,y} = \alpha \tau (\partial_{x,y} - (\hat{\mathbf{p}} \cdot \partial_{\mathbf{x}}) \hat{p}_{x,y}) \quad (\text{G.14})$$

and

$$\mathbf{N}_0 + \mathbf{N}_1 = \begin{pmatrix} 1 & -\alpha \hat{p}_y / v_F & \alpha \hat{p}_x / v_F & 0 \\ -\alpha \hat{p}_y / v_F & 1 & 0 & 0 \\ \alpha \hat{p}_x / v_F & 0 & 1 & 0 \\ 0 & 0 & 0 & 1 \end{pmatrix}. \quad (\text{G.15})$$

Therefore in the diffusive limit, $a \ll 1$, Eq. (G.9) becomes

$$\begin{pmatrix} \partial_t - D \partial_{\mathbf{x}}^2 & -2B \partial_y & 2B \partial_x & 0 \\ -2B \partial_y & \partial_t - D \partial_{\mathbf{x}}^2 + \tau_s^{-1} & 0 & -2C \partial_x \\ 2B \partial_x & 0 & \partial_t - D \partial_{\mathbf{x}}^2 + \tau_s^{-1} & -2C \partial_y \\ 0 & 2C \partial_x & 2C \partial_y & \partial_t - D \partial_{\mathbf{x}}^2 + 2\tau_s^{-1} \end{pmatrix} \begin{pmatrix} \langle g_0 \rangle \\ \langle g_x \rangle \\ \langle g_y \rangle \\ \langle g_z \rangle \end{pmatrix} = 0 \quad (\text{G.16})$$

where $D = \frac{1}{2} v_F^2 \tau$ is the diffusion constant and

$$B = \frac{\alpha a^2}{4}, \quad C = \frac{v_F a}{2} = v_F \alpha p_F \tau, \quad \frac{1}{\tau_s} = \frac{a^2}{2\tau}. \quad (\text{G.17})$$

In a time independent situation and in the presence of an homogeneous electric field parallel to $\hat{\mathbf{x}}$, Eqs. (5.49)–(5.51) are obtained – or Eqs. (5.53)–(5.55) if the spin-charge coupling terms are neglected.

We now consider the more complicated self-energy

$$\begin{aligned} \Sigma &= \Sigma_m + \Sigma_{nm} \\ &= -\frac{i}{6\tau_{sf}} \sum_{l=1}^3 \sigma_l \langle g \rangle \sigma_l - \frac{i}{2\tau} \langle (1+K)g \rangle \end{aligned} \quad (\text{G.18})$$

arising from s -wave magnetic disorder and angle dependent non-magnetic scattering (see Appendix D), and specialize the treatment to Eq. (5.26). The Keldysh component is as usually implied. Rather than using the standard $(\sigma_x, \sigma_y, \sigma_z)$ basis, we choose to rotate to $(\sigma_{\parallel}, \sigma_{\perp}, \sigma_z)$, the subscripts \parallel and \perp indicating respectively

the directions parallel and perpendicular to the internal field \mathbf{b} . Defining the rotation matrix $\tilde{\mathbf{R}}(\varphi)$ – not to be confused with the boundary matrix \mathbf{R} from Eq. (5.41) – by

$$\begin{pmatrix} \sigma_0 \\ \sigma_x \\ \sigma_y \\ \sigma_z \end{pmatrix} = \begin{pmatrix} 1 & 0 & 0 & 0 \\ 0 & \sin \varphi & \cos \varphi & 0 \\ 0 & -\cos \varphi & \sin \varphi & 0 \\ 0 & 0 & 0 & 1 \end{pmatrix} \begin{pmatrix} \sigma_0 \\ \sigma_{\parallel} \\ \sigma_{\perp} \\ \sigma_z \end{pmatrix}, \quad (\text{G.19})$$

one has

$$g'_{\mu} = \sum_{\mu'=0}^3 \tilde{\mathbf{R}}_{\mu\mu'}^{-1}(\varphi) g_{\mu'}, \quad (g'_{\mu}) = (g_0, g_{\parallel}, g_{\perp}, g_z), \quad (\text{G.20})$$

$$\mathbf{K}_{\mu\nu}(\varphi, \varphi') = \sum_{\mu'=0}^3 \tilde{\mathbf{R}}_{\mu\mu'}^{-1}(\varphi) K(\varphi - \varphi') \tilde{\mathbf{R}}_{\mu'\nu}(\varphi'). \quad (\text{G.21})$$

Expanding in harmonics – we also drop the four-vector indices

$$\mathbf{K}(\varphi, \varphi') = \mathbf{K}^{(a)} + \cos(\varphi - \varphi') \mathbf{K}^{(b)} + \sin(\varphi - \varphi') \mathbf{K}^{(c)} + \dots \quad (\text{G.22})$$

In the above we have defined

$$\mathbf{K}^{(a)} = \begin{pmatrix} 0 & 0 & 0 & 0 \\ 0 & K_1 & 0 & 0 \\ 0 & 0 & K_1 & 0 \\ 0 & 0 & 0 & 0 \end{pmatrix}, \quad \mathbf{K}^{(b)} = \begin{pmatrix} 2K_1 & 0 & 0 & 0 \\ 0 & K_2 & 0 & 0 \\ 0 & 0 & K_2 & 0 \\ 0 & 0 & 0 & 2K_1 \end{pmatrix} \quad (\text{G.23})$$

and

$$\mathbf{K}^{(c)} = \begin{pmatrix} 0 & 0 & 0 & 0 \\ 0 & 0 & -K_2 & 0 \\ 0 & K_2 & 0 & 0 \\ 0 & 0 & 0 & 0 \end{pmatrix}. \quad (\text{G.24})$$

For the purpose of calculating polarizations and spin currents, which is our aim in Section 5.1.2, the higher harmonics play no role and are thus ignored.

By using that $g_{eq}^R = -g_{eq}^A = 1 + \partial_{\xi} \mathbf{b} \cdot \boldsymbol{\sigma}$ and performing a rotation to the new spin basis, one can write Eq. (5.26) as

$$\partial_t g' = \frac{1}{\tau^*} [-\mathbf{M}g' + (\mathbf{N}_0 + \mathbf{N}_1)\langle g' \rangle + (\mathbf{N}_2 + \mathbf{N}_3)\langle \mathbf{K}g' \rangle] + S_{\mathcal{E}}. \quad (\text{G.25})$$

The matrices appearing in Eq. (G.25) read

$$\mathbf{M} = \begin{pmatrix} 1 & -\frac{\tau^*}{\tau} \frac{\alpha}{v_F} K_1 & 0 & 0 \\ -\frac{\tau^*}{\tau} \frac{\alpha}{v_F} K_1 & 1 & 0 & 0 \\ 0 & 0 & 1 & 2\alpha p_F \tau^* \\ 0 & 0 & -2\alpha p_F \tau^* & 1 \end{pmatrix}, \quad (\text{G.26})$$

$$\mathbf{N}_0 = \begin{pmatrix} 1 & 0 & 0 & 0 \\ 0 & 1 - \frac{4\tau^*}{3\tau_{sf}} & 0 & 0 \\ 0 & 0 & 1 - \frac{4\tau^*}{3\tau_{sf}} & 0 \\ 0 & 0 & 0 & 1 - \frac{4\tau^*}{3\tau_{sf}} \end{pmatrix}, \quad (\text{G.27})$$

$$\mathbf{N}_1 = \frac{\alpha}{v_F} \begin{pmatrix} 0 & -(1 - \frac{4\tau^*}{3\tau_{sf}}) & 0 & 0 \\ -1 & 0 & 0 & 0 \\ 0 & 0 & 0 & 0 \\ 0 & 0 & 0 & 0 \end{pmatrix}, \quad (\text{G.28})$$

$$\mathbf{N}_2 = \frac{\tau^*}{\tau} \frac{\alpha}{v_F} \begin{pmatrix} 0 & -1 & 0 & 0 \\ -1 & 0 & 0 & 0 \\ 0 & 0 & 0 & 0 \\ 0 & 0 & 0 & 0 \end{pmatrix}, \quad \mathbf{N}_3 = \frac{\tau^*}{\tau} \begin{pmatrix} 1 & 0 & 0 & 0 \\ 0 & 1 & 0 & 0 \\ 0 & 0 & 1 & 0 \\ 0 & 0 & 0 & 1 \end{pmatrix} \quad (\text{G.29})$$

where τ^* is the elastic quasi-particle life time, defined as

$$\frac{1}{\tau^*} \equiv \frac{1}{\tau} + \frac{1}{\tau_{sf}}, \quad (\text{G.30})$$

which we now use for convenience of notation but which in the final result is incorporated into the proper transport time [see Eq. (5.31)]. Finally, $S_{\mathcal{E}}$ is the source term due to the electric field. As before, we take this to be along the x -direction, so that

$$S_{\mathcal{E}} \equiv |e|v_F \mathcal{E} \partial_{\epsilon} (2 \tanh(\epsilon/2T)) \begin{pmatrix} \cos \varphi \\ -\cos \varphi \frac{\alpha}{v_F} \\ -\sin \varphi \frac{\alpha}{v_F} \\ 0 \end{pmatrix}. \quad (\text{G.31})$$

Solving for the s_z spin current flowing along y Eq. (5.28) is obtained. The expression for the s_y spin polarization, Eq. (5.29), is similarly calculated, and that for the the frequency dependent spin Hall conductivity, Eq. (5.30), follows at once.

G.2 Boundary conditions

The goal is to translate the boundary conditions for the quasiclassical Green's function – i.e. Eq. (5.39) for spin-active boundaries and Eq. (5.57) for spin-conserving ones – into those for the spin polarizations and currents. We consider s -wave non-magnetic disorder in the Rashba model and assume to be in the diffusive regime. This means that Eqs. (5.49)–(5.51) hold. The geometry is as usual that determined by Fig. 5.3. The spin relaxation length $L_s = \sqrt{D\tau_s}$ sets the scale of the spatial variation of $\langle g \rangle$, i.e. the angular average of the spin components of g . Since this is much bigger than the mean free path l , $L_s \gg l$, the idea is to solve the Eilenberger equation exploiting the slow variation of $\langle g \rangle$ over $\mathcal{O}(l)$ distances. We first rewrite Eq. (G.2)

$$(\tilde{\mathbf{M}}_0 + \tilde{\mathbf{M}}_1)g = -\frac{1}{\tau}[g - (1 + \mathbf{N}_1)\langle g \rangle], \quad (\text{G.32})$$

with $\tilde{\mathbf{M}}_0 = (\mathbf{M}_0 - 1)/\tau$, $\tilde{\mathbf{M}}_1 = \mathbf{M}_1/\tau$. As the dominant energy scale is set by $1/\tau$, the bulk expression for g reads

$$\begin{aligned} g^{(0)} &= (1 + \mathbf{N}_1)\langle g \rangle + \mathcal{O}[(\alpha/v_F)^2], \\ g^{(1)} &= -(\tilde{\mathbf{M}}_0 + \tilde{\mathbf{M}}_1 + \tilde{\mathbf{M}}_0\mathbf{N}_1)\langle g \rangle + \mathcal{O}[(\alpha/v_F)^2] \\ \Rightarrow g &= (1 - \tilde{\mathbf{M}}_0 + \mathbf{N}_1 - \tilde{\mathbf{M}}_1 - \tilde{\mathbf{M}}_0\mathbf{N}_1)\langle g \rangle + \mathcal{O}[(\alpha/v_F)^2]. \end{aligned} \quad (\text{G.33})$$

At the boundary the complete g is a superposition of the incoming (g^{in}) and outgoing ($g^{\text{out}} = \mathbf{R}g^{\text{in}}$) one

$$\begin{array}{ccc} & \text{at the boundary} & \\ & \downarrow & \\ g & \stackrel{=}{=} & (1 + \mathbf{R})g^{\text{in}}. \end{array} \quad (\text{G.34})$$

Therefore

$$\langle g \rangle = \int_{\varphi_{\text{in}}} \frac{d\varphi_{\text{in}}}{2\pi} (1 + \mathbf{R})(1 - \tilde{\mathbf{M}}_0 + \mathbf{N}_1 - \tilde{\mathbf{M}}_1 - \tilde{\mathbf{M}}_0\mathbf{N}_1)\langle g \rangle, \quad \varphi_{\text{in}} \in [0, \pi). \quad (\text{G.35})$$

We focus on the spin components in the stationary limit. In the case of spin-active boundary conditions \mathbf{R} is given in Eq. (5.41), and the angular average in Eq. (G.35) yields

$$s_x = 0, \quad s_y = s_0, \quad -D\partial_y s_z + C s_x = 0, \quad (\text{G.36})$$

that is, the result (5.52). All results are intended to leading order in l/L_s and first order in α/v_F . Notice that if spin-charge coupling is neglected, as in Section 5.1.3, Eq. (G.35) simplifies to

$$\langle g \rangle = \int_{\varphi_{\text{in}}} \frac{d\varphi_{\text{in}}}{2\pi} (1 + \mathbf{R})(1 - \tilde{\mathbf{M}}_0) \langle g \rangle, \quad \varphi_{\text{in}} \in [0, \pi) \quad (\text{G.37})$$

and the boundary condition for s_y reads simply $s_y = 0$ [see Eq. (5.61)]. In Section 5.1.3 spin-conserving boundaries are considered too. In this case \mathbf{R} is just the identity, and from Eq. (G.37) the expressions (5.58)–(5.60) are obtained.

Bibliography

- [1] S. A. Wolf, D. D. Awschalom, R. A. Buhrman, J. M. Daughton, S. von Molnár, M. L. Roukes, A. Y. Chtchelkanova, and D. M. Treger. Spintronics: a spin-based electronics vision for the future. *Science*, 294:1488, 2001.
- [2] I. Žutić, J. Fabian, and S. Das Sarma. Spintronics: fundamentals and applications. *Rev. Mod. Phys.*, 76:323, 2004.
- [3] G. A. Prinz. Magnetoelectronics. *Science*, 282:1660, 1998.
- [4] D. D. Awschalom and M. E. Flatté. Challenges for semiconductor spintronics. *Nature Physics*, 3:153, 2007.
- [5] B. van Wees. Spins go their own way. *Nature Physics*, 3:147, 2007.
- [6] Y. Ohno, D. K. Young, B. Beschoten, F. Matsukara, H. Ohno, and D. D. Awschalom. Electrical spin injection in a ferromagnetic semiconductor heterostructure. *Nature*, 402:790, 1999.
- [7] R. Fiederling, M. Keim, G. Reuscher, W. Ossau, G. Schmidt, A. Waag, and L. W. Molenkamp. Injection and detection of a spin-polarized current in a light-emitting diode. *Nature*, 402:787, 1999.
- [8] V. F. Motsnyi, J. De Boeck, J. Das, W. Van Roy, G. Borghs, E. Goovaerts, and V. I. Safarov. Electrical spin injection in a ferromagnet/tunnel barrier/semiconductor heterostructure. *Appl. Phys. Lett.*, 81:265, 2002.
- [9] X. Jiang, R. Wang, R. M. Shelby, R. M. Macfarlane, S. R. Bank, J. S. Harris, and S. S. P. Parkin. Highly spin-polarized room-temperature tunnel injector for semiconductor spintronics using MgO(100). *Phys. Rev. Lett.*, 94:056601, 2005.

- [10] M. Johnson and R. H. Silsbee. Interfacial charge-spin coupling: injection and detection of spin magnetization in metals. *Phys. Rev. Lett.*, 55:1790, 1985.
- [11] S. O. Valenzuela and M. Tinkham. Direct electronic measurement of the spin Hall effect. *Nature*, 442:176, 2006.
- [12] S. O. Valenzuela and M. Tinkham. Electrical detection of spin currents: the spin-current induced Hall effect. *J. Appl. Phys.*, 101:09B103, 2007.
- [13] L. Vila, T. Kimura, and Y. Otani. Evolution of the spin Hall effect in Pt nanowires: size and temperature effects. *Phys. Rev. Lett.*, 99:226604, 2007.
- [14] T. Kimura, Y. Otani, T. Sato, S. Takahashi, and S. Maekawa. Room-temperature reversible spin Hall effect. *Phys. Rev. Lett.*, 98:156601, 2007.
- [15] T. Seki, Y. Hasegawa, S. Mitani, S. Takahashi, H. Imamura, S. Maekawa, J. Nitta, and K. Takanashi. Giant spin Hall effect in perpendicularly spin-polarized FePt/Au devices. *Nature Materials*, 7:125, 2008.
- [16] G. Schmidt, D. Ferrand, L. W. Molenkamp, A. T. Filip, and B. G. van Wees. Fundamental obstacle for electrical spin injection from a ferromagnetic metal into a diffusive semiconductor. *Phys. Rev. B*, 62:R4790, 2000.
- [17] A. T. Filip, B. H. Hoving, B. G. van Wees, B. Dutta, and S. Borghs. Experimental search for the electrical spin injection in a semiconductor. *Phys. Rev. B*, 62:9996, 2000.
- [18] B. T. Jonker, Y. D. Park, B. R. Bennet, H. D. Cheong, G. Kioseoglou, and A. Petrou. Robust electrical spin injection into a semiconductor heterostructure. *Phys. Rev. B*, 62:8180, 2000.
- [19] X. Lou, C. Adelman, S. A. Crooker, E. S. Garlid, J. Zhang, K. S. M. Reddy, S. D. Flexner, C. J. Palmstrom, and P. A. Crowell. Electrical detection of spin transport in lateral ferromagnet-semiconductor devices. *Nature Physics*, 3:197, 2007.
- [20] S. Murakami, N. Nagaosa, and S. C. Zhang. Dissipationless quantum spin current at room temperature. *Science*, 301:1348, 2003.

BIBLIOGRAPHY

- [21] J. Sinova, D. Culcer, Q. Niu, N. A. Sinitsyn, T. Jungwirth, and A. H. MacDonald. Universal intrinsic spin Hall effect. *Phys. Rev. Lett.*, 92:126603, 2004.
- [22] R. Kubo, M. Toda, and N. Hashitsume. *Statistical Physics II - Nonequilibrium Statistical Mechanics (Second Edition)*. Springer, 1995.
- [23] G. F. Mazenko. *Nonequilibrium Statistical Mechanics*. Wiley, 2006.
- [24] J. Rammer. *Quantum Field Theory of Non-equilibrium States*. Cambridge University Press, 2007.
- [25] J. Rammer and H. Smith. Quantum field-theoretical methods in transport theory of metals. *Rev. Mod. Phys.*, 58:323, 1986.
- [26] P. Schwab and R. Raimondi. Quasiclassical theory of charge transport in disordered interacting electron systems. *Ann. Phys.*, 12:471, 2003.
- [27] R. E. Prange and L. P. Kadanoff. Transport theory for electron-phonon interactions in metals. *Phys. Rev.*, 134:A566, 1964.
- [28] B. L. Altshuler, P. A. Lee, and R. A. Webb. *Mesoscopic Phenomena in Solids*. North-Holland, 1991.
- [29] S. Datta. *Electronic Transport in Mesoscopic Systems*. Cambridge University Press, 1995.
- [30] A. Kamenev. Keldysh technique and nonlinear σ -model: basic principles and applications. *arXiv:cond-mat/0901.3586*, 2009.
- [31] L. V. Keldysh. Diagram technique for nonequilibrium processes. *JETP*, 20:1018, 1965.
- [32] J. Rammer. *Quantum Transport Theory*. Perseus Books, 1998.
- [33] A. L. Fetter and J. D. Walecka. *Quantum Theory of Many-Particle Systems*. Dover Publications, 2003.
- [34] A. A. Abrikosov, L. P. Gorkov, and I. E. Dzyaloshinski. *Methods of Quantum Field Theory in Statistical Physics*. Dover Publications, 1975.

- [35] J. Schwinger. Brownian motion of a quantum particle. *J. Math. Phys.*, 2:407, 1961.
- [36] L. P. Kadanoff and G. Baym. *Green's Function Methods in Equilibrium and Nonequilibrium Problems*. Addison-Wesley Publishing Co., 1962.
- [37] V. M. Edelstein. Spin polarization of conduction electrons induced by electric current in two-dimensional asymmetric electron systems. *Solid State Commun.*, 73:233, 1990.
- [38] R. Karplus and J. M. Luttinger. Hall effect in ferromagnetics. *Phys. Rev.*, 95:1154, 1954.
- [39] M. I. Dyakonov. Magnetoresistance due to edge spin accumulation. *Phys. Rev. Lett.*, 99:126601, 2007.
- [40] H. A. Engel, E. I. Rashba, and B. I. Halperin. *Handbook of Magnetism and Advanced Magnetic Materials*, pages 2858–2877. Wiley, 2007.
- [41] F. Cooper, S. Habib, Y. Kluger, E. Mottola, J. P. Paz, and P. R. Anderson. Nonequilibrium quantum fields in the large- n expansion. *Phys. Rev. D*, 50:2848, 1994.
- [42] E. Calzetta and B. I. Hu. Closed-time-path functional formalism in curved spacetime: application to cosmological back-reaction problems. *Phys. Rev. D*, 35:495, 1987.
- [43] A. J. Niemi and G. W. Semenoff. Finite-temperature quantum field theory in minkowski space. *Ann. Phys.*, 152:105, 1984.
- [44] F. Cooper. Nonequilibrium problems in quantum field theory and schwinger's closed time path formalism. *arXiv:hep-th/9504073*, 1995.
- [45] J. W. Negele and H. Orland. *Quantum Many-Particle Systems*. Addison-Wesley Publishing Co., 1988.
- [46] A. I. Larkin and Yu. N. Ovchinnikov. Nonlinear conductivity of superconductors in the mixed state. *JETP*, 41:960, 1975.

BIBLIOGRAPHY

- [47] U. Eckern and A. Schmid. Quasiclassical green's function in the bcs pairing theory. *J. Low Temp. Phys.*, 45:137, 1981.
- [48] M. I. Dyakonov. *Spin Physics in Semiconductors*. Springer, 2008.
- [49] J. H. Davies. *The Physics of Low-dimensional Semiconductors*. Cambridge University Press, 2006.
- [50] M. J. Kelly. *Low-dimensional Semiconductors*. Oxford Science Publications, 1995.
- [51] J. Wunderlich, B. Kaestner, J. Sinova, and T. Jungwirth. Experimental observation of the spin-Hall effect in a two-dimensional spin-orbit coupled semiconductor system. *Phys. Rev. Lett.*, 94:047204, 2005.
- [52] S. Schmult, M. J. Manfra, A. M. Sergent, A. Punnoose, H. T. Chou, D. Goldhaber-Gordon, and R. J. Molnar. Quantum transport in high mobility AlGaIn/GaN 2DEGs and nanostructures. *Physica Status Solidi B*, 243:1706, 2006.
- [53] V. Umansky, R. De Picciotto, and M. Heiblum. Extremely high mobility two dimensional electron gas: evaluation of scattering mechanisms. *Appl. Phys. Lett.*, 71:683, 1997.
- [54] J. M. Luttinger and W. Kohn. Motion of electrons and holes in perturbed periodic fields. *Phys. Rev.*, 97:869, 1955.
- [55] R. Winkler. *Spin-orbit Coupling Effects in Two-dimensional Electron and Hole Systems*. Springer, 2003.
- [56] E. O. Kane. Band structure of indium antimonide. *J. Phys. Chem. Solids*, 1:249, 1957.
- [57] T. Darnhofer and U. Rössler. Effects of band structure and spin in quantum dots. *Phys. Rev. B*, 47:16020, 1993.
- [58] R. S. Calsaverini, E. Bernardes, J. C. Egues, and D. Loss. Intersubband-induced spin-orbit interaction in quantum wells. *Phys. Rev. B*, 78:155313, 2008.

- [59] R. Lassnig. $\mathbf{k} \cdot \mathbf{p}$ theory, effective-mass approach, and spin splitting for two-dimensional electrons in GaAs-GaAlAs heterostructures. *Phys. Rev. B*, 31:8076, 1985.
- [60] P. O. Löwdin. A note on the quantum-mechanical perturbation theory. *J. Chem. Phys.*, 19:1396, 1951.
- [61] G. Dresselhaus. Spin-orbit coupling effects in zinc blend structures. *Phys. Rev.*, 100:580, 1955.
- [62] S. Giglberger, L. E. Golub, V. V. Bel'kov, S. N. Danilov, D. Schuh, C. Gerl, F. Rohlfing, J. Stahl, W. Wegscheider, D. Weiss, W. Prettl, and S. D. Ganichev. Rashba and Dresselhaus spin splittings in semiconductor quantum wells measured by spin photocurrents. *Phys. Rev. B*, 75:035327, 2007.
- [63] J. Schliemann and D. Loss. Anisotropic transport in a two-dimensional electron gas in the presence of spin-orbit coupling. *Phys. Rev. B*, 68:165311, 2003.
- [64] F. E. Meijer, A. F. Morpurgo, T. M. Klapwijk, T. Koga, and J. Nitta. Competition between spin-orbit interaction and Zeeman coupling in Rashba two-dimensional electron gases. *Phys. Rev. B*, 70:201307(R), 2004.
- [65] J. Luo, H. Munekata, F. F. Fang, and P. J. Stiles. Effects of inversion asymmetry on electron energy band structures in GaSb/InAs/GaSb quantum wells. *Phys. Rev. B*, 41:7685, 1990.
- [66] Y. Sato, T. Kita, S. Gozu, and S. Yamada. Large spontaneous spin splitting in gate-controlled two-dimensional electron gases at normal In_{0.75}Ga_{0.25}As/In_{0.75}Al_{0.25}As. *J. Appl. Phys.*, 89:8017, 2001.
- [67] D. Grundler. Large Rashba splitting in InAs quantum wells due to electron wave function penetration into the barrier layers. *Phys. Rev. Lett.*, 84:6074, 2000.
- [68] J. Nitta, T. Akazaki, H. Takayanagi, and T. Enoki. Gate control of spin-orbit interaction in an inverted In_{0.53}Ga_{0.47}As/In_{0.52}Al_{0.48}As heterostructure. *Phys. Rev. Lett.*, 78:1335, 1997.

BIBLIOGRAPHY

- [69] J. P. Heida, B. J. van Wees, J. J. Kuipers, T. M. Klapwijk, G. Borghs, S. Stal-lone, and C. Eastwood. Spin-orbit interaction in a two-dimensional elec-tron gas in a InAs/AlSb quantum well with gate-controlled electron density. *Phys. Rev. B*, 57:11911, 1998.
- [70] B. Das, S. Datta, and R. Reifenberg. Zero-field spin splitting in a two-dimensional electron gas. *Phys. Rev. B*, 41:8278, 1990.
- [71] R. Raimondi, C. Gorini, P. Schwab, and M. Dzierzawa. Quasiclassical approach to the spin Hall effect in the two-dimensional electron gas. *Phys. Rev. B*, 74:035340, 2006.
- [72] C. Gorini, P. Schwab, M. Dzierzawa, and R. Raimondi. Quasiclassical approach and spin-orbit coupling. *Physica E*, 40:1078, 2008.
- [73] J. I Inoue, G. E. Bauer, and L. W. Molenkamp. Suppression of the persistent spin Hall current by defect scattering. *Phys. Rev. B*, 70:041303(R), 2004.
- [74] E. G. Mishchenko, A. V. Shytov, and B. I. Halperin. Spin current and polarization in impure two-dimensional electron systems with spin-orbit coupling. *Phys. Rev. Lett.*, 93:226602, 2004.
- [75] R. Raimondi and P. Schwab. Spin-Hall effect in a disordered two-dimensional electron system. *Phys. Rev. B*, 71:033311, 2005.
- [76] A. Khaetskii. Nonexistence of intrinsic spin currents. *Phys. Rev. Lett.*, 96:056602, 2006.
- [77] P. Q. Jin, Y. Q. Li, and F. C. Zhang. $SU(2) \times U(1)$ unified theory for charge, orbit and spin currents. *J. Phys. A: Math. Gen.*, 39:7115, 2006.
- [78] A. L. Shelankov. On the derivation of quasiclassical equations for super-conductors. *J. Low Temp. Phys.*, 60:29, 1985.
- [79] C. Gorini, P. Schwab, M. Dzierzawa, and R. Raimondi. Spin polarizations and spin Hall currents in a two-dimensional electron gas with magnetic impurities. *Phys. Rev. B*, 78:125327, 2008.

- [80] P. Schwab, M. Dzierzawa, C. Gorini, and R. Raimondi. Spin relaxation in narrow wires of a two-dimensional electron gas. *Phys. Rev. B*, 74:155316, 2006.
- [81] R. Raimondi, C. Gorini, M. Dzierzawa, and P. Schwab. Current-induced spin polarization and the spin Hall effect: a quasiclassical approach. *Solid State Communications*, 144:524, 2007.
- [82] M. Koenig, H. Buhmann, L. W. Molenkamp, T. Hughes, C. X. Liu, and S. C. Zhang. The quantum spin Hall effect: theory and experiment. *J. Phys. Soc. Jpn.*, 77:031007, 2008.
- [83] B. A. Bernevig and S. C. Zhang. Quantum spin Hall effect. *Phys. Rev. Lett.*, 96:106802, 2006.
- [84] C. L. Kane and E. J. Mele. A new spin on the insulating state. *Science*, 314:1692, 2006.
- [85] M. I. Dyakonov and V. I. Perel. Current-induced spin orientation of electrons in semiconductors. *Phys. Lett.*, 35A:459, 1971.
- [86] A. G. Aronov and Y. B. Lyanda-Geller. Nuclear electric resonance and orientation of carrier spins by an electric field. *JETP Lett.*, 50:431, 1989.
- [87] J. E. Hirsch. Spin Hall effect. *Phys. Rev. Lett.*, 83:1834, 1999.
- [88] Y. K. Kato, R. C. Myers, A. C. Gossard, and D. D. Awschalom. Observation of the spin Hall effect in semiconductors. *Science*, 306:1910, 2004.
- [89] N. P. Stern, S. Gosh, G. Xiang, M. Zhu, N. Samarth, and D. D. Awschalom. Current-induced polarization and the spin Hall effect at room temperature. *Phys. Rev. Lett.*, 97:126603, 2006.
- [90] V. Sih, R. C. Myers, Y. K. Kato, W. H. Lau, A.C. Gossard, and D. D. Awschalom. Spatial imaging of the spin Hall effect and current-induced polarization in two-dimensional electron gases. *Nature Physics*, 1:31, 2005.
- [91] N. P. Stern, D. W. Steuerman, S. Mack, A. C. Gossard, and D. D. Awschalom. Time-resolved dynamics of the spin Hall effect. *Nature Physics*, 4:843, 2008.

BIBLIOGRAPHY

- [92] G. Y. Guo, S. Murakami, T. W. Chen, and N. Nagaosa. Intrinsic spin Hall effect in platinum: first-principles calculations. *Phys. Rev. Lett.*, 100:096401, 2008.
- [93] M. Duckheim and D. Loss. Mesoscopic fluctuations in the spin-electric susceptibility due to Rashba spin-orbit interaction. *Phys. Rev. Lett.*, 101:226602, 2008.
- [94] M. Millettari, R. Raimondi, and P. Schwab. Magneto-spin Hall conductivity of a two-dimensional electron gas. *Europhys. Lett.*, 82:67005, 2008.
- [95] E. I. Rashba. Sum rules for spin Hall conductivity cancellation. *Phys. Rev. B*, 70:201309(R), 2004.
- [96] O. V. Dimitrova. Spin-Hall conductivity in a two-dimensional Rashba electron gas. *Phys. Rev. B*, 71:245327, 2005.
- [97] O. Chalaev and D. Loss. Spin-Hall conductivity due to Rashba spin-orbit interaction in disordered systems. *Phys. Rev. B*, 71:245318, 2005.
- [98] N. A. Sinitsyn, E. M. Hankiewicz, W. Teizer, and J. Sinova. Spin Hall and spin-diagonal conductivity in the presence of Rashba and Dresselhaus spin-orbit coupling. *Phys. Rev. B*, 70:081312(R), 2004.
- [99] S. Q. Shen. Spin Hall effect and Berry phase in two-dimensional electron gas. *Phys. Rev. B*, 70:081311(R), 2004.
- [100] M. C. Chang. Effect of in-plane magnetic field on the spin Hall effect in a Rashba-Dresselhaus system. *Phys. Rev. B*, 71:085315, 2005.
- [101] A. V. Shytov, E. G. Mishchenko, H. A. Engel, and B. I. Halperin. Small-angle impurity scattering and the spin Hall conductivity in two-dimensional semiconductor systems. *Phys. Rev. B*, 73:075316, 2006.
- [102] D. Culcer and R. Winkler. Generation of spin currents and spin densities in systems with reduced symmetry. *Phys. Rev. Lett.*, 99:226601, 2007.
- [103] H. A. Engel, E. I. Rashba, and B. I. Halperin. Out-of-plane spin polarization from in-plane electric and magnetic fields. *Phys. Rev. Lett.*, 98:036602, 2007.

- [104] J. I. Inoue, T. Kato, Y. Ishikawa, H. Itoh, G. E. Bauer, and L. W. Molenkamp. Vertex corrections to the anomalous Hall effect in spin-polarized two-dimensional electron gases with a Rashba spin-orbit interaction. *Phys. Rev. Lett.*, 97:046604, 2006.
- [105] P. Wang, Y. Q. Li, and X. Zhao. Nonvanishing spin Hall currents in the presence of magnetic impurities. *Phys. Rev. B*, 75:075326, 2007.
- [106] S. A. Crooker, D. A. Tulchinsky, J. Levy, D. D. Awschalom, R. Garcia, and N. Samarth. Enhanced spin interactions in digital magnetic heterostructures. *Phys. Rev. Lett.*, 75:505, 1995.
- [107] Y. S. Gui, C. R. Becker, J. Liu, V. Daumer, V. Hock, H. Buhmann, and L. W. Molenkamp. Interplay of Rashba, Zeeman and Landau splitting in a magnetic two-dimensional electron gas. *Europhys. Lett.*, 65:393, 2004.
- [108] V. Daumer, I. Golombek, M. Gbordzoe, E. G. Novik, V. Hock, C. R. Becker, H. Buhmann, and L. W. Molenkamp. Quasiballistic transport in HgTe quantum-well nanostructures. *Appl. Phys. Lett.*, 83:1376, 2003.
- [109] A. Millis, D. Rainer, and J. A. Sauls. Quasiclassical theory of superconductivity near magnetically active interfaces. *Phys. Rev. B*, 38:4504, 1998.
- [110] A. O. Govorov, A. V. Kalameitsev, and J. P. Dulka. Spin-dependent transport of electrons in the presence of a smooth lateral potential and spin-orbit interaction. *Phys. Rev. B*, 70:245310, 2004.
- [111] P. G. Silvestrov and E. G. Mishchenko. Polarized electric current in semiclassical transport with spin-orbit interaction. *Phys. Rev. B*, 64:165301, 2006.
- [112] H. Chen, J. J. Hermans, J. A. Peters, A. O. Govorov, N. Goel, S. J. Chung, and M. B. Santos. Spin-polarized reflection in a two-dimensional electron system. *Appl. Phys. Lett.*, 86:032113, 2005.
- [113] A. W. Holleitner, V. Sih, R. C. Myers, A. C. Gossard, and D. D. Awschalom. Suppression of spin relaxation in submicron InGaAs wires. *Phys. Rev. Lett.*, 97:036805, 2006.

BIBLIOGRAPHY

- [114] A. Bournel, D. Dollfus, P. Bruno, and P. Hesto. Gate-induced spin precession in an $\text{In}_{0.53}\text{Ga}_{0.47}\text{As}$ two dimensional electron gas. *Eur. Phys. J.:Appl. Phys.*, 4:1, 1998.
- [115] A. G. Mal'schukov and K. A. Chao. Waveguide diffusion modes and slowdown of D'yakonov-Perel' spin relaxation in narrow two-dimensional semiconductor channels. *Phys. Rev. B*, 61:R2413, 2000.
- [116] B. I. Halperin, A. Stern, Y. Oreg, J. N. H. J. Cremers, J. A. Folk, and C. M. Marcus. Spin-orbit effects in a GaAs quantum dot in a parallel magnetic field. *Phys. Rev. Lett.*, 86:2106, 2001.
- [117] I. L. Aleiner and V. I. Fal'ko. Spin-orbit coupling effects on quantum transport in lateral semiconductor dots. *Phys. Rev. Lett.*, 87:256801, 2001.
- [118] O. Zaitsev, D. Frustaglia, and K. Richter. Role of orbital dynamics in spin relaxation and weak antilocalization in quantum dots. *Phys. Rev. Lett.*, 94:026809, 2005.
- [119] B. A. Bernevig, J. Orenstein, and S. C. Zhang. Exact $SU(2)$ symmetry and persistent spin helix in a spin-orbit coupled system. *Phys. Rev. Lett.*, 97:236601, 2006.
- [120] V. M. Galitski, A. A. Burkov, and S. Das Sarma. Boundary conditions for spin diffusion in disordered systems. *Phys. Rev. B*, 74:115331, 2006.
- [121] P. Nozières and C. Lewiner. Small-angle impurity scattering and the spin Hall conductivity in two-dimensional semiconductor systems. *J. Phys. (Paris)*, 34:901, 1973.
- [122] W. K. Tse and S. Das Sarma. Intrinsic spin Hall effect in the presence of extrinsic spin-orbit scattering. *Phys. Rev. B*, 74:245309, 2006.
- [123] E. M. Hankiewicz and G. Vignale. Phase diagram of the spin Hall effect. *Phys. Rev. Lett.*, 100:026602, 2008.
- [124] I. V. Tokatly. Equilibrium spin currents: non-abelian gauge invariance and color diamagnetism in condensed matter. *Phys. Rev. Lett.*, 101:106601, 2008.

- [125] D. C. Langreth. Hall coefficient of Hubbard's model. *Phys. Rev.*, 148:707, 1966.
- [126] J. J. Sakurai. *Modern Quantum Mechanics*. Addison-Wesley, 1994.
- [127] L. D. Landau and E. M. Lifschitz. *Quantum Mechanics: Non-Relativistic Theory, Volume 3*. Butterworth-Heinemann.
- [128] T. Yang, T. Kimura, and Y. Otani. Giant spin-accumulation signal and pure spin-current-induced reversible magnetization switching. *Nature Physics*, 4:851, 2008.
- [129] J. Wunderlich, A. C. Irvine, J. Sinova, B. G. Park, X. L. Lu, B. Kaestner, V. Novak, and T. Jungwirth. Spin-injection Hall effect in a planar photovoltaic cell. *arXiv:cond-mat/0811.3486*, 2008.
- [130] Y. K. Kato, R. C. Myers, A. C. Gossard, and D. D. Awschalom. Current-induced spin polarization in strained semiconductors. *Phys. Rev. Lett.*, 93:176601, 2004.

Acknowledgements

I am very thankful to Priv.-Doz. Dr. Peter Schwab, Prof. Roberto Raimondi, Dr. Michael Dzierzawa and Prof. Dr. Ulrich Eckern for their continuous support during the past three years, and to Prof. Jørgen Rammer and Prof. Andrei Shelankov for instructive and stimulating discussion – regarding both physics and the collapse of capitalism. Additional thanks go to Dr. Michael Dzierzawa, who produced most of the plots&curves appearing throughout the text.

I do not wish to turn this into an emotional ramble over my family and the people with whom I have shared these years, spent between Augsburg, Munich, Rome and Florence. It would anyway be beyond me to do them justice with words. “Wovon man nicht sprechen kann, darüber muß man schweigen.”

Walking away, Dante’s Virgil would lordly say “non ragioniam di lor, ma guarda e passa”. His great admirer Benigni would more prosaically mutter ““fanculo alla maggioranza”. Inspiring examples, but I will simply say it is good to conclude here.

Curriculum Vitae

Cosimo Gorini

Born in Florence, Italy

August 2, 1979

-
- 2006/2009 Wissenschaftlicher Angestellter
 Universität Augsburg
- 2005 M.Sc. in physics
 Università degli Studi di Roma Tre
- 1998 Maturità classica (highschool degree)
 Liceo Classico Convitto Nazionale
 Vittorio Emanuele II, Rome